Identification of novel targets in prostate cancer progression

Ghotra, V.P.S.

IDENTIFICATION OF NOVEL TARGETS IN PROSTATE CANCER PROGRESSION

Veerander Paul Singh Ghotra

Veerander Paul Singh Ghotra

IDENTIFICATION OF NOVEL TARGETS IN PROSTATE CANCER PROGRESSION

Thesis, Leiden University, 2013

ISBN: 978-94-6259-006-9

Cover: High resolution imaging and surface rendering of CM-DiI-labeled PC3 tumor cell foci interacting with host vasculature of Tg (Fli:EGFP) ZF embryo

Printed by: Ipskamp Drukkers B.V., Enschede

IDENTIFICATION OF NOVEL TARGETS IN PROSTATE CANCER PROGRESSION

Proefschrift

ter verkrijging van

de graad van Doctor aan de Universiteit van Leiden,

op gezag van Rector Magnificus prof.mr. C.J.J.M. Stolker,

volgens het besluit van het College voor Promoties

te verdedigen op donderdag 19 december 2013

klokke 11:15 uur

door

Veerander Paul Singh Ghotra

geboren te Mukerian, India
in 1979

Promotie commissie

Promotor :	Prof. Dr. B. van de Water	Universiteit Leiden
Co-promotor :	Dr. E.H.J. Danen	Universiteit Leiden
Overige leden :	Prof.Dr. P.H. van der Graaf	Universiteit Leiden
	Prof. Dr. A. Ijzerman	Universiteit Leiden
	Prof. Dr. H. Spaink	Universiteit Leiden
	Prof. Dr. R. Pelger	LUMC, Leiden
	Prof. Dr. G. Jenster	Erasmus MC, Rotterdam

The studies presented in this thesis were performed in the Division of Toxicology, LACDR, Leiden University.
This research was financially supported by a grant from EU FP7 (HEALTH-F2-2008-201439).

TABLE OF CONTENTS

CHAPTER 1

GENERAL INTRODUCTION AND SCOPE OF THE THESIS

PROSTATE CANCER

Prostate cancer is a principal cause of illness and death among men in the United States and Western Europe. Autopsy series have demonstrated small prostatic carcinomas in up to 29 percent of men 30 to 40 years of age and 64 percent of men 60 to 70 years of age. Moreover, the risk of prostate cancer is 1 in 6 and the risk of death due to metastatic prostate cancer is 1 in 30 (1). Curative treatment is usually prostatectomy or radiation to remove or destroy the cancerous cells that are still confined within the prostate capsule (fig. 1). However, many patients are not cured by this form of therapy and their cancer recurs, or they are diagnosed after the cancer has spread to distant sites. Curative treatment of prostate cancer is only possible when tumor cells are predominantly confined to the prostate (1).

MECHANISM OF ANDROGEN ACTION

Why do prostate cancer cells need androgens to grow and survive (2) ? Prostate cancer growth is dependent on the ratio of proliferating cells to those dying. Androgens are considered as the main regulator of this ratio by both stimulating proliferation and inhibiting apoptosis. So it could be concluded that, prostate cancer depends on a crucial level of androgenic stimulation for growth and survival. Androgen blockage causes regression of prostate cancer because without androgen, the rate of cell proliferation is lower and the rate of cell death is increased, leading to extinction of these cells (3). Testosterone - which is the main circulating androgen — is secreted primarily by the testes, but is also synthesized by peripheral conversion of adrenal steroids (2). 90% of the free testosterone entering the prostate cells is converted to dihydrotestosterone (DHT) by the enzyme 5α-reductase (SRD5A2). DHT is the more biologically active hormone, possessing five-fold higher affinity for the androgen receptor (AR) than does testosterone. DHT binds to the androgen receptors in the cytoplasm, leading to the phosphorylation, dimerization, and subsequent translocation into the nucleus, thereby binding to the androgen-response elements within the DNA, with resultant activation of genes involved in cell growth and survival (2). Almost all metastatic prostate cancers initially require testosterone for growth, and the use of androgen deprivation as a first-line therapy for metastatic prostate cancer has been recognized for more than 60 years (4, 5). Hormone deprivation is achieved by surgical (orchiectomy) or medical (luteinizing hormone-releasing hormone agonists, anti-androgens) castration. Furthermore, simultaneous administration of therapies designed to block adrenal androgen production or the binding of residual androgens to the androgen receptor by synthetic anti-androgens has been recommended by many studies (6, 7). Androgen deprivation therapy leads to remissions lasting 2 to 3 years; however, virtually all patients progress to a clinically androgen-independent state resulting in death in 16 to 18 months (8-12).

MECHANISM OF AIPC DEVELOPMENT

Androgen-independent prostate cancer (AIPC) is a lethal form of prostate cancer that progresses and metastasizes. There are several pathways, which have been shown to be responsible for the development of AIPC. These pathways gives us deep insights into the mechanisms of androgen action and provides us a deeper understanding of the mechanisms by which cancer cells subvert normal growth control and escape attempts to treat the prostate cancer (13). Deeper understanding of these pathways is the first step towards developing new therapies against this lethal form of prostate cancer. These mechanisms are demonstrated in Fig.2 and include:

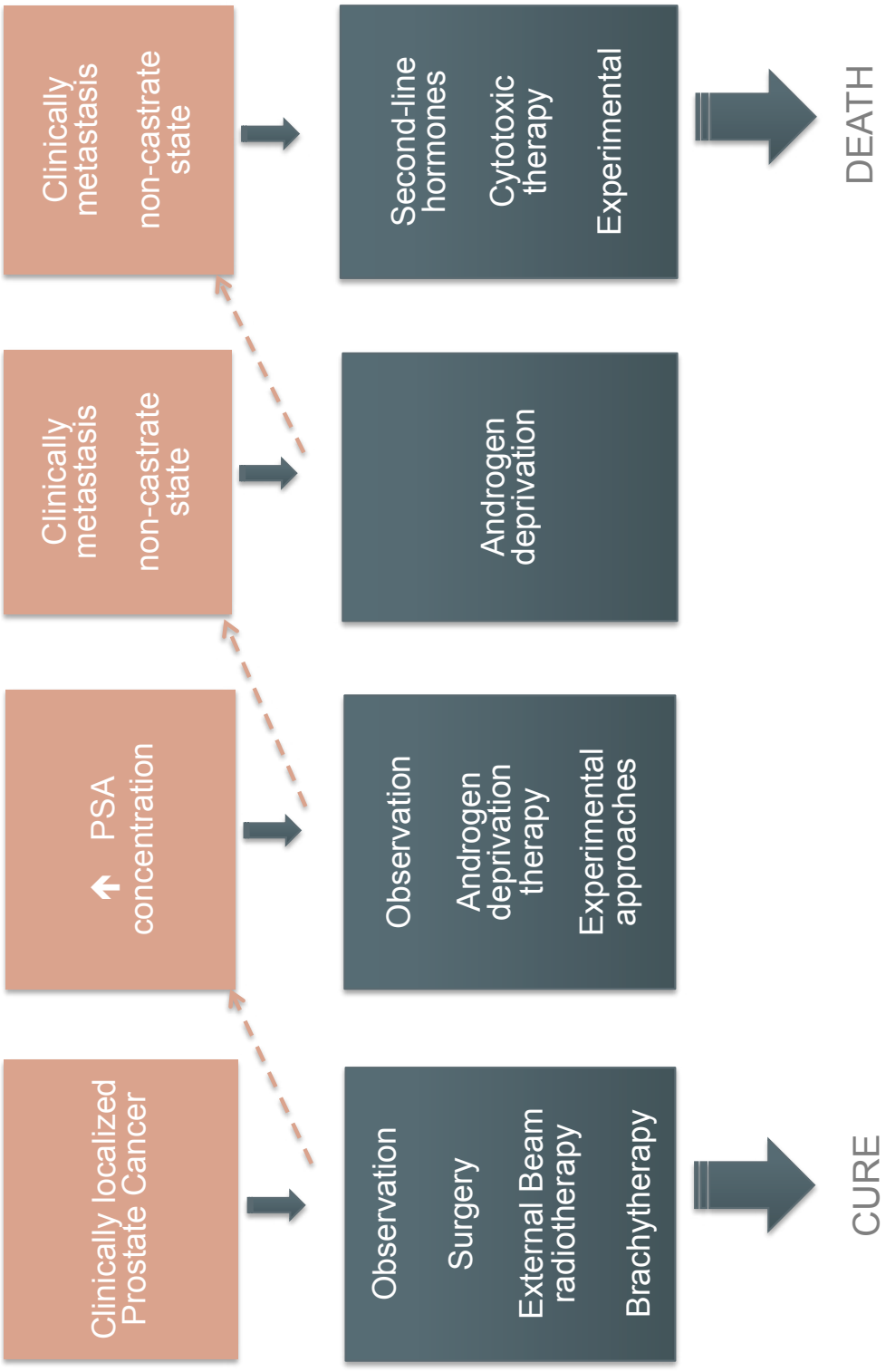

FIGURE 1. *Represents clinical states of prostate cancer*. Curative therapy is available only for the localized disease when tumor cells are confined to the prostate."Adapted from Lancet Oncol 4:407-14, 2003"

The hypersensitive pathway

One way in which prostate cancer cells surpass the effects of androgen blockade is by developing the ability to use very low levels of androgens for (14-16), which means that they do not become androgen independent in the classic sense, but rather castration independent (13).There are several mechanisms which could explain response to lower levels of androgens.

One of these responsible mechanism is enhanced expression of the androgen receptor, which eventually allows enhanced binding of ligand. The existence of this pathway is supported by various studies of hormone refractory tumors that show increased expression of androgen receptor as compared to androgen-dependent tumors (14, 17-22). Elevated production of androgen receptor is caused either due to gene amplification or mutations through selective pressure of the androgen-depleted environment, which eventually causes the cells with fewer androgen receptors to die off and leading to clonal expansion of cells expressing more androgen receptor. Chen en colleagues have shown that AR gene expression was up regulated during the progression from androgen-dependent to castration-independent growth (14). Furthermore, they also showed that androgen-independent cells require 80% lower concentrations of androgen than androgen-dependent cells for growth (14).

Increased androgen receptor sensitivity to androgens has been suggested as another important mechanism for castration resistance (15). In support of this, Gregory and colleagues have shown that recurrent prostate tumors posses high level expression of the androgen receptor, increased stability of the androgen receptor, and enhanced nuclear localization of the androgen receptor, which is associated with an increased sensitivity to the growth-enhancing effects of dihydrotestosterone (15).

A third hypersensitive mechanism considered to be important is increased local production of androgens by prostate cancer cells themselves, which most likely occurs due to increased rate of conversion of testosterone to dihydrotestosterone via an increased activity of 5-alpha-reductase (2). There are various evidences that are in support of this mechanism which includes (a) ethnic groups with higher levels of 5-alpha-reductase activity are at a higher chance of development of prostate cancer (23); (b) after the initiation of the androgen ablation therapy, serum testosterone levels decrease by 95%, but concentration of dihydrotestosterone in prostatic tissue reduces by only 60% (24); and (c) genes involved in steroid biosynthesis have been shown to be overexpressed in recurrent human prostate tumors (20).

Promiscuous Receptor

The wild-type androgen receptor is stimulated only by testosterone and dihydrotestosterone, and it has been shown that specificity of androgen receptor is broadened by mutations.The majority of mutations are found to be clustered in the ligand-binding domains leading to binding promiscuity of androgen receptor (25, 26). Due to these mutations the androgen receptor can be activated by nonandrogenic steroid molecules, which are normally present in the circulation as well as antiandrogens (2, 14, 27-32). Such mutations have been demonstrated to be more frequent in androgen-independent prostate cancer cells and it form the basis of antiandrogen withdrawal syndromes in which 10% to 30% of patients treated with long-term antiandrogens will show disease regression with drug withdrawal (33-36).

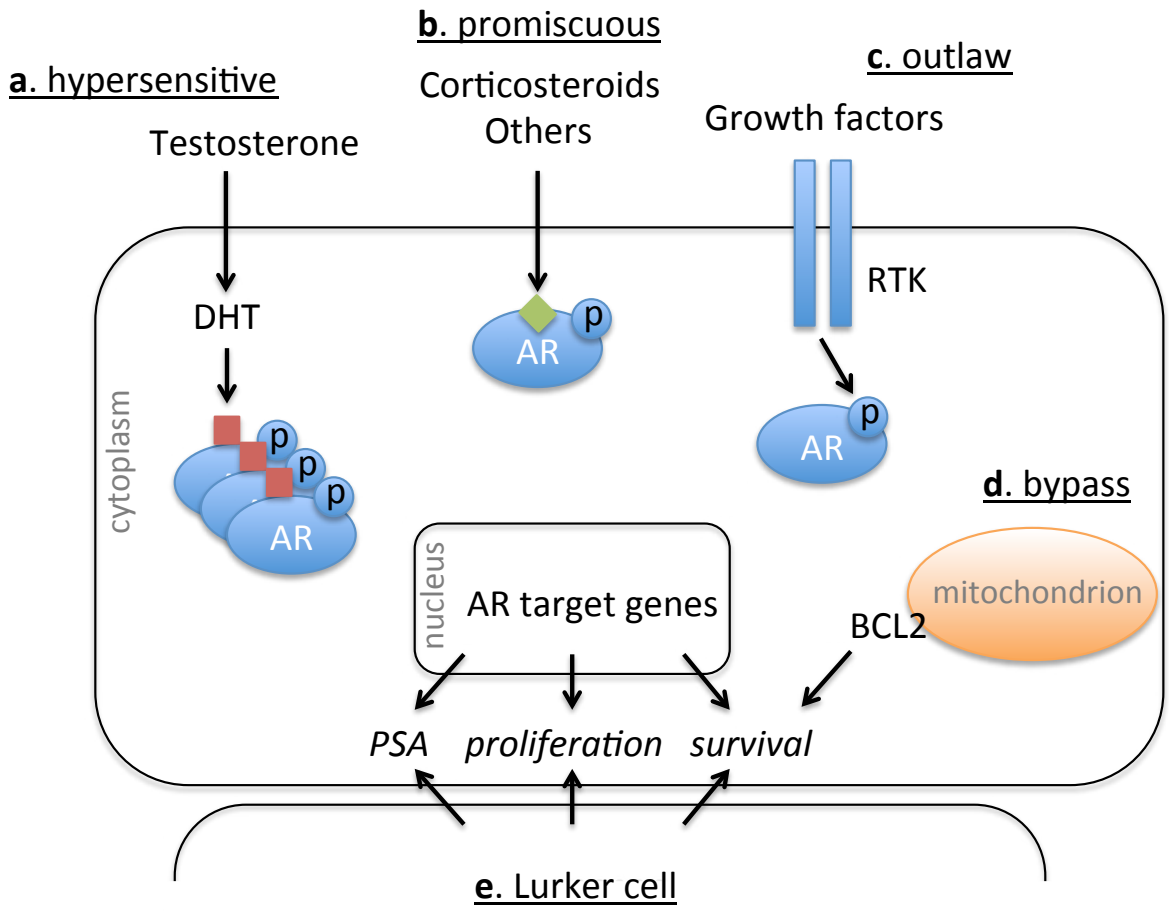

FIGURE 2. *Pathways to androgen independence.* (a) Hypersensitive pathway : Enhanced expression of the androgen receptor leading to enhanced ligand binding or enhanced conversion of testosterone to more potent dihydrotestosterone (DHT) by 5α-reductase.(b) Promiscuous pathway : AR(Androgen receptor) activated by non-androgenic molecules present in the circulation leading to the activation of AR.(c) Outlaw pathway : Activation of receptor tyrosine kinases (RTKs) leading to downstream activation of either AKT(protein kinase B) or the mitogen-activated protein kinase (MAPK), which leads to phosphorylation and activation of AR. (d) Bypass pathway : Activation of the parallel survival pathways, thus obviating the need for AR or its ligand.(e) The lurker cell pathway : Presence of prostate cancer stem cells that continually resupply the tumor cell population, despite therapy. Although these cancer stem cells remain a small percentage of the actual percentage of the tumor, they are not affected by androgen-depletion therapy. "Adapted from Nature reviews cancer 1:34-45, 2001"

Outlaw Pathway

It is known that stimulation of androgen receptor can be achieved by ligand dependent binding of nonsteroid molecules or via the activation of downstream signaling of the androgen receptor by ligand independent mechanisms. Such type of activation has been defined as outlaw activation (2, 27, 28, 37). Deregulation of growth factors, for example insulin-like growth factor, keratinocyte growth factor, and epidermal growth factor, and cytokines, including IL-6, have been shown to directly phosphorylate and stimulate the androgen receptor (38, 39). It has been shown that androgen receptor dependent genes can be activated by deregulation of signal transduction pathways (40,41). HER-2/neu receptor overexpression activates androgen receptor–dependent genes in the absence of a ligand (40,41). Furthermore, the overactivity of outlaw pathways demonstrates the potential importance of tumor-microenvironment interactions in the development of castration-independent growth (42,43). Paget in his famous theory hypothesized that a ‘‘fertile soil’’ was required for the successful growth of cancer metastases (44). The interaction of prostate cancer cells with bone stromal cells, osteoblasts, and osteoclasts and bone extracellular matrix, leads to the deregulation of multiple growth factors that the prostate cancer cells can utilize to become androgen independent (2).

Co-activators and co-repressors

A large number of co-activators and co-repressors have been identified that are involved in the regulation of androgen receptor driven transcription (45). Imbalance between co-activators and co-repressors have been shown to influence androgen receptor activation, but the precise mechanisms are unknown (2, 46-49). An increased level of co-activators has been well identified in androgen-independent disease (46, 50-52). Co-activator proteins enhances the activity of the androgen receptor to alternative ligands, thereby sensitizing the receptor to lower levels of native and nonnative ligands, leading to ligand-independent activation(46).

Activation of bypass Pathways

Androgen receptor pathway can be completely bypassed, and prostate cancer cells can develop the ability to survive independent of ligand-mediated or non-ligand-mediated androgen receptor activation. Modulation of apoptosis is the best-known bypass mechanism. In androgen-dependent prostate cancer cells, androgen receptor activation stimulates cell proliferation but depletion of androgen leads to apoptosis of these cells. Androgen-independent prostate cancer cells have been shown to possess higher levels of anti-apoptotic molecules (53-56). Inactivation of the tumor suppressor gene phosphatase and tensin homologue (PTEN) leading to subsequent activation of Akt is one of the best known way in which AIPC cells escape apoptosis in an androgen-depleted environment (28). Another suggested bypass mechanism is the neuroendocrine differentiation of prostate cancer cells (28). Neuroendocrine cells exhibits a low rate of proliferation and are more prevalent in androgen refractory prostate cancers (28). They also secrete neuropeptides, which leads to increase in the proliferation of neighboring cancer cells, ultimately leading to progression in a low-androgen environment (28).

Prostate Cancer Stem Cells

In contrast to the stochastic model of tumorigenesis, the stem cell model of cancer postulates that only a rare subset of tumor cells are tumorigenic (54). Such population of cells comprising 0.1% of prostate tumors,

have been shown to be CD44+/alpha2 beta1hi/CD133, which do not express androgen receptors, and is thought to be enriched in prostate cancer stem - or progenitor cells (57). The prostate cancer stem cells in the androgen-depleted environment continually resupply the tumor cell population, and these cancer stem cells are not effected by the androgen-depletion therapy. Differentiation of these cancer stem cells into androgen dependent and independent cells results in the formation of heterogenous androgen receptor phenotype observed in AIPC patients (12).

DEVELOPMENT OF TARGETED APPROACHES AGAINST PROSTATE CANCER METASTASIS

Several molecular abnormalities have been identified that can lead to prostate cancer progression and development of androgen independent state. Many of these targeted therapies are now under various phases of clinical development (13, 58). Although most previous work have been focused on the androgen receptor but it is likely that several other molecular targets leads to the development of prostate cancer progression and androgen independent state (13). Development of these therapies requires the recognition that some of these targets may be relevant to the entire disease spectrum of prostate cancer but others may only be relevant for specific stages of prostate cancer. Many of these hypotheses-driven therapies are undergoing preclinical and clinical testing but, still there is a clear need for a better identification and selection of the specific patient population that will experience maximum benefit from specific molecular targeted approach (58).May be in the near future, it will be possible to determine the predominant mechanism of resistance in a tumor as it progresses during treatment and then apply that knowledge for the selection of the appropriate targeted therapy , with the goal of turning prostate cancer into a chronic disease. (58)

MOLECULAR MECHANISMS IN PROSTATE CANCER INVASION

Local invasion is one of the earliest steps in metastasis. To become invasive, the malignant cell should have the ability to downregulate its cell–cell contacts and alter cell–matrix adhesive characteristics, become motile and acquire the ability to degrade the extracellular matrix (ECM) (59). As soon the malignant cell has degraded the basement membrane, then it must enter the vascular or lymphatic circulation by breaching the endothelial barriers. Then the cancer cell should have acquired the ability to migrate via the blood or lymphatic circulation and should have the ability to arrest at a secondary endothelial site before binding to the endothelium, extravasating and then transmigrate through the endothelial layer to reach the interstitium, where it could have various fates as outlined in the figure 3 (60). There are various molecular mediators that have been shown to mediate the local invasion and dissemination of these prostate cancer cells. Some of well-known mechanisms are:

Epithelial to mesenchymal transition (EMT) in prostate cancer

In the normal prostate gland, epithelial cells have restricted migratory capability because the basal cells inside the lumen attach to the basement membrane and to each other forming a layer of interconnected cells with apical-basal polarity. Cell-to-cell adhesion in this epithelial layer is maintained by several types of junctions, such as adherens- and tight junctions. These junctions are composed of protein complexes of cell adhesion molecules (CAMs), such as cadherins. EMT is a cellular process through which epithelial cells lose

their epithelial characteristics like cell polarity and cell-cell junctions. During this epithelial to mesenchymal transition cells undergo changes in cytoskeleton and shape leading to acquirement of mesenchymal characteristics resulting in gain of migratory and invasive properties (61). Disruption of the E-cadherin-catenin adhesion complex is a key step in these processes. In prostate cancer, one of the most important features of cells undergoing EMT is cadherin switching, whereby E-cadherin (expressed in normal epithelial cells) is downregulated and N-cadherin (expressed in mesenchymal cells) is upregulated. Higher gleason grade prostate cancers have lower E-cadherin and higher N-cadherin expression, as compared to prostate cancer in patients with lower gleason grade disease (62-64). Decreased catenin expression has been also shown to be associated with decreased expression of E-cadherin, and with higher grade prostate cancer (65). In prostate cancer, one important signaling axis that can support EMT (in addition to effects on proliferation) is the HGF receptor, MET. Expression of the MET receptor is associated with disease progression and MET inhibitors are actively tested in prostate cancer clinical trials (66)

Prostate cancer invasion: Roles of proteases

Matrix metalloproteinases and serine proteinases (for example urokinase- type plasminogen activator) are the most important families of proteinases that have been shown to be most associated with degradation of extracellular matrix in prostate cancer. It has been shown that primary prostate tumor tissues posses higher levels of MMP-9, and also the ratios of of MMP-2/-9 to tissue inhibitor of metalloproteinases-1 (TIMP-1) are increased as compared to normal prostate epithelium. Also, the levels of MMP-9 and the ratios of MMP-2/-9 are increased in patients with high gleason grade prostate cancer, which is associated with poorer patient survival (67-69). Furthermore, It has been shown that that loss of TIMP-1 is correlated with upregulation of MMPs in malignant human prostate cancer tissues(70). Patients with metastatic prostate cancers are observed to have high concentrations of MMP-2 and MMP- 9 in their plasma (71). MMP-12 downregulation using RNAi approach reduced the invasiveness of PC3 cells by reducing degradation of Type I collagen in the bone, which supports the fact that MMP-12 also participates in bone-tropic metastasis(72).

Adhesion signaling in prostate cancer migration

Cell migration is a dynamic process mediated by Focal adhesion (FA) signaling. Focal adhesions are the regions where integrins, in large dynamic protein complexes establish a signaling link between the ECM and actin cytoskeleton. Integrin-mediated ECM adhesion leads to activation of downstream pathways involved in gene regulation, proliferation, apoptosis, cell survival, polarity, actin dynamics and cell migration (73, 74). The predominant integrins present in normal prostate epithelial cells are alpha5 beta1, alpha6 beta1, alpha6 beta4, alpha V beta3 and alpha3 beta1 (75). Lee et al., has showed that levels of beta1 integrins and integrin-induced autophosphorylation of FAK are increased in prostate cancer cells in primary prostate cancer and lymph node metastases, which suggests that beta1 integrin activation occurs in metastatic progression of prostate cancer (76). It suggests that alterations in integrin composition and function can thus affect migration of prostate cancer cell through modulation of FAK function. Furthermore, overexpression of FAK has been observed in high-grade and metastatic prostate cancer tissues as compared to normal prostate tissues (77).

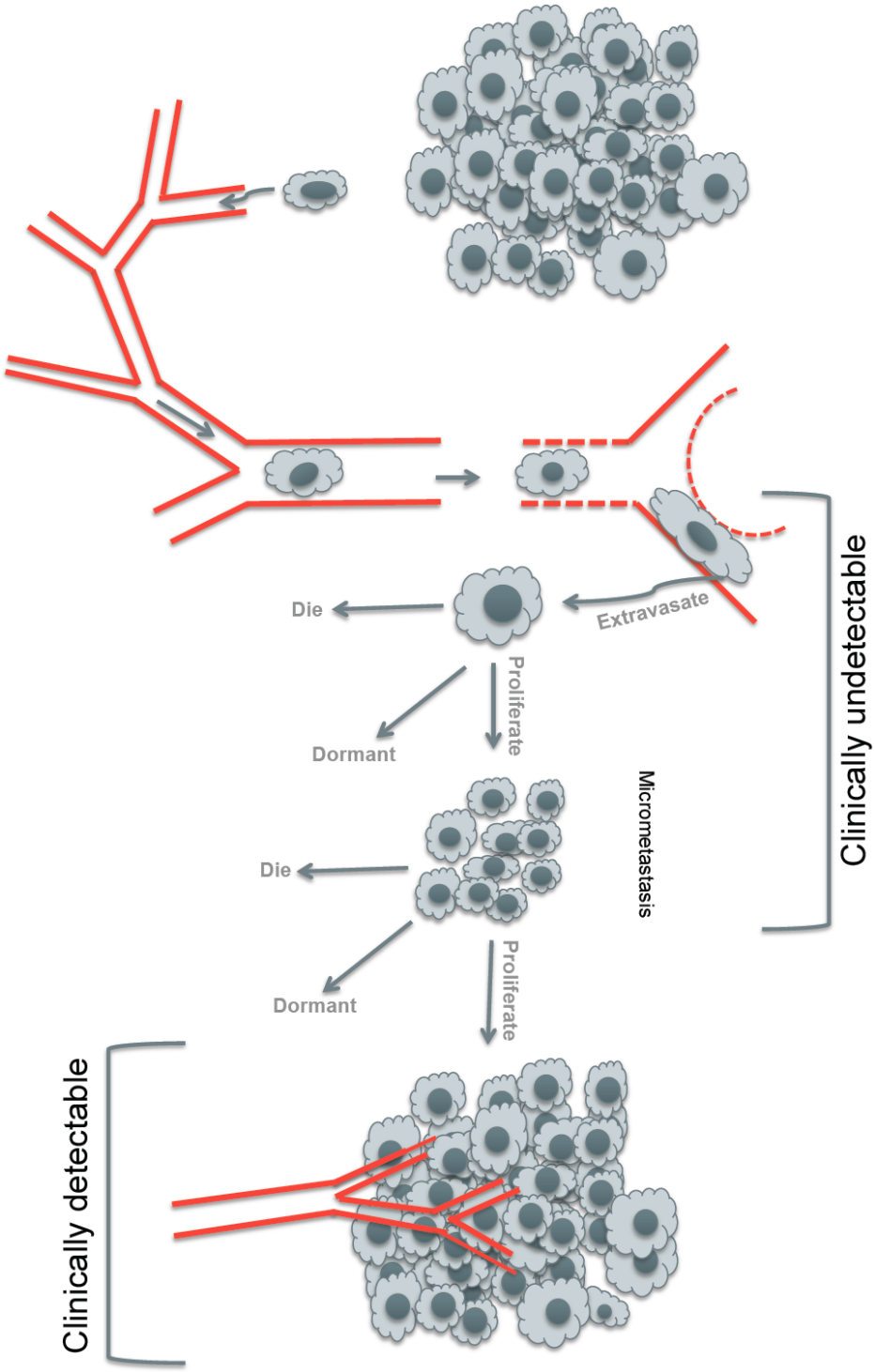

FIGURE 3. *The metastatic cascade* (a) Tumor cells escape from the primary tumor and then arrest at the secondary metastatic sites (b) Cancer cells can have various fates following their arrival at the secondary metastatic sites. At secondary sites, cancer cells can exist in various forms like solitary cells, micrometastasis and vascularized macrometastasis. The balance between the proliferation and survival governs their fate at each step. Cells, which adapt better to the foreign microenvironment (in line with Pagets seed and soil hypothesis) survive, proliferate and progresses to form vascularized macrometastasis.The cells where proliferation is balanced by apoptosis stays dormant, and those cells die where the balance tilts in favour of apoptosis. “Adapted from Nature Rev Cancer 2:563-72, 2002”

MODELS TO STUDY PROSTATE CANCER METASTASIS

As our understanding of prostate cancer becomes more comprehensive, the need for more sophisticated and accurate models increases (78). Experimental therapeutics targeting specific tumor-specific molecules must be validated in well-characterized models that enable the testing of the experimental hypothesis. By establishing models that replicate human prostate cancer progression more closely and by asking more disease specific questions with such models, animal models will continue to play an important role in validating novel cancer targets and evaluating putative cancer therapies (78). Three dimensional extracellular matrix models and animal based models, are being utilized to replicate and model the various steps of metastatic cascade. Figure 3 gives an overview of the steps involved in metastasis cascade. Basic understanding of the dynamics of metastasis cascade is the key to the development of novel models and to the development of novel anti-cancer therapies. In 3D based assays prostate cancer cells are either grown inside the matrix or plated on the top of the matrix to model the complex processes of growth, local invasion and migration. Also these 3D based models provide an ideal platform to study the complex interactions between the cancer cells and the extracellular matrix (79). In animal based models, cancer cells are injected to form a primary tumor orthotopically (in the prostate) or at other, more easily accessible sites (e.g. subcutaneous) and tumor growth as well as metastasis is monitored. Alternatively, tumor cells are injected directly into the circulation to model the later phases of the metastatic process such as extravasation and metastatic colonization. These assays are called, respectively, spontaneous or experimental metastasis assays (80, 81) and the end point of both assays is the formation of visible metastases at a secondary site. These assays have led to the identification of many molecular alterations in cancer cells that can contribute to their ability to metastasize, and selective targeting of these tumor cell specific alterations is the basis of molecular targeted approach (82-87). These models constitute the major preclinical tool required for the further development of new therapeutic strategies. Xenografts are the most commonly used models in drug development and are able to maintain several biological properties of the human tumors they are derived from, particularly when orthotopically transplanted. Osteoblastic bone metastases can also be modeled (78). Non-invasive methods of imaging have been recently developed to significantly reduce the number of mice required and have improved the follow up of tumor growth and response to therapy in these models. Genetic models are very useful for target validation, but have not yet been extensively used for drug evaluation. Finally, some models are more relevant for the study of specific pathways as androgen receptor signaling, or bone metastases development, and others are useful in developing strategies targeting prostate cancer stem cells or mechanisms of resistance to chemotherapy or radiotherapy (78).

The modern drug development technologies increase the number of candidate therapeutics and subsequently increase the costs for preclinical and clinical testing. Mouse models are time, labor, and finance intensive and current limitations have hampered the transition of scientific findings from these models to human clinical trials. Moreover, while the vast contribution of mouse models to advancing our understanding of cancer biology is indisputable, there have been ongoing concerns about the value of mouse models for predicting drug efficacy and usefulness in humans, and the predictive value of tumor xenograft models in cancer research is still a matter of debate. Thus, the development of faster and cheaper animal model systems and improvements in the ability of preclinical models to predict clinical efficacy can have a high impact by lowering the cost of drug development and by helping to prioritize compounds for clinical investigation.

AIM OF THESIS

General purpose

Metastasis is a major cause of death and morbidity in patients with neoplastic disease, but one major obstacle in the progress of prostate cancer studies has been the limited availability of relevant preclinical models (78). Current limitations of these models have hampered and delayed the transition of scientific findings to clinical trials. The ideal prostate cancer model is one that reproduces and replicates the natural history of the prostate cancer, and able to generate long-term spontaneous metastases to lymph nodes, lungs and bones. Such ideal prostate cancer model does not exist (78). However, models for investigating key steps in the metastatic cascade have been developed and can be further improved. The greatest challenge of the post genomic cancer drug discovery is to develop mechanism based agents that act on the key biological tumor specific processes and then sequentially to test the hypothesis that such tumor specific agents are indeed more potent and more specific than the current available generation of anti cancer drugs. There is lot of criticism regarding the value of two-dimensional based in vitro models in anti-cancer drug target discovery (88). Facing this criticism, the cancer researcher is continuously challenged to develop novel models that could enable us to study disease specific question in a setting that nearly recapitulates the natural history of metastatic process. The development of better anti-cancer targets continues, and it is now evident that selection of the appropriate disease models is of utmost importance during the pre-clinical drug discovery process when investigating biological processes like invasion, dissemination and metastatic colonization. One of the most important thing is to use the right models to ask the right questions about the right therapies (78).

Based on this background the ***specific aims*** were (as schematically outlined in figure 4) :

- To develop novel 3D in vitro and whole organism-based high-throughput models of (prostate) cancer progression that are suitable for both compound as well as RNA-interference screening approaches.

- To Identify/validate novel candidate genes playing a significant role in prostate cancer progression.

OUTLINE OF THESIS

The ultimate aim of this thesis is the identification and validation of novel candidate genes playing a significant role in the prostate cancer metastasis. For that purpose, we established imaging based automated in-vitro and in-vivo models to study growth, migration, invasion and dissemination of (prostate) cancer. First, we established an automated 3D in vitro assay to study growth, local invasion and migration of cancer cell spheroids in an extracellular collagen matrix. The development of this assay is described in ***chapter 2***. For prostate cancer, and most other solid cancers, it is necessary to develop whole organism based bio-imaging models to screen for novel candidate target genes which can deepen our understanding of the mechanism underlying metastatic progression. In ***chapter 3***, we developed an automated bio-imaging model of cancer progression using xenotransplantation in zebrafish embryos. In ***chapter 4,*** current state of art in prostate cancer treatment is discussed. Here, we discuss emerging new molecular targets and the potential clinical applications of combining radiotherapy with these molecular targeted agents for the treatment of prostate cancer. It will be important to find more drug targets and this is what we describe in following two chapters. In ***chapter 5***, we describe the identification of SYK as a novel candidate prostate cancer target gene derived from a RNA-interference screen exploiting the zebrafish xenotransplantation model. Next to the RNA-interference screening, focused research has been conducted on previously identified novel candidate genes. In ***chapter 6***, we describe MST1R as a dominant factor in prostate cancer progression. Finally ***chapter 7,*** provides a summary and a general discussion on the findings and implications of the work in this thesis.

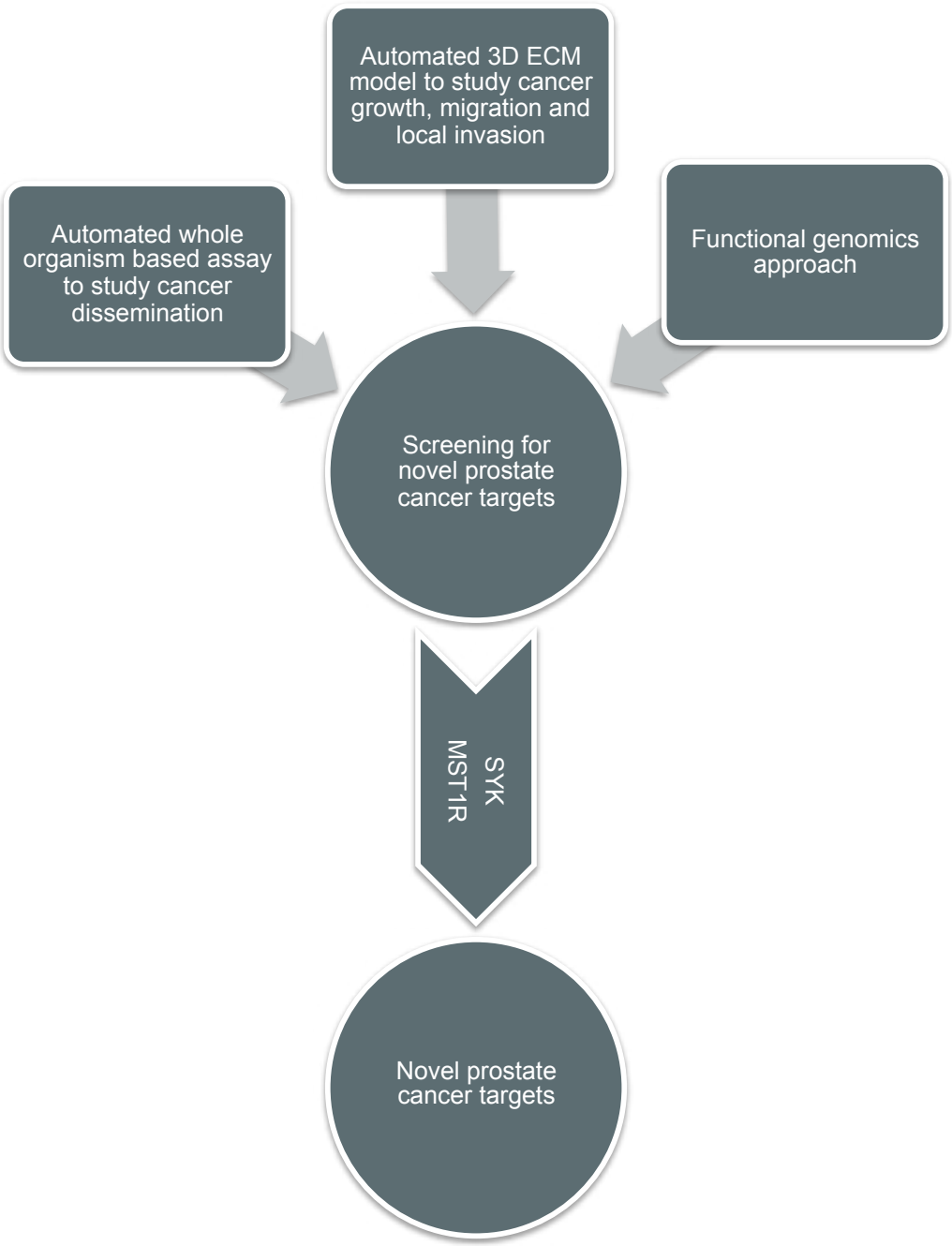

FIGURE 4. *Schematic representation of the specific aims/outcomes of the thesis.*

REFERENCES

1.Sakr WA, Grignon DJ, Crissman JD, Heilbrun LK, Cassin BJ, Pontes JJ, et al. High grade prostatic intraepithelial neoplasia (HGPIN) and prostatic adenocarcinoma between the ages of 20-69: an autopsy study of 249 cases. In Vivo. 1994;8:439-43.

2.Feldman BJ, Feldman D. The development of androgen-independent prostate cancer. Nature reviews Cancer. 2001;1:34-45.

3.Denmeade SR, Lin XS, Isaacs JT. Role of programmed (apoptotic) cell death during the progression and therapy for prostate cancer. The Prostate. 1996;28:251-65.

4.Huggins C, Hodges CV. Studies on prostatic cancer. I. The effect of castration, of estrogen and androgen injection on serum phosphatases in metastatic carcinoma of the prostate. CA: a cancer journal for clinicians. 1972;22:232-40.

5.Huggins C. Endocrine-induced regression of cancers. American journal of surgery. 1978;136:233-8.

6.Labrie F, Dupont A, Belanger A, Lacoursiere Y, Raynaud JP, Husson JM, et al. New approach in the treatment of prostate cancer: complete instead of partial withdrawal of androgens. The Prostate. 1983;4:579-94.

7.Schmitt B, Bennett C, Seidenfeld J, Samson D, Wilt T. Maximal androgen blockade for advanced prostate cancer. Cochrane Database Syst Rev. 2000:CD001526.

8.Saitoh H, Hida M, Shimbo T, Nakamura K, Yamagata J, Satoh T. Metastatic patterns of prostatic cancer. Correlation between sites and number of organs involved. Cancer. 1984;54:3078-84.

9.Grayhack JT, Keeler TC, Kozlowski JM. Carcinoma of the prostate. Hormonal therapy. Cancer. 1987;60:589-601.

10.Harada M, Iida M, Yamaguchi M, Shida K. Analysis of bone metastasis of prostatic adenocarcinoma in 137 autopsy cases. Advances in experimental medicine and biology. 1992;324:173-82.

11.Bubendorf L, Schopfer A, Wagner U, Sauter G, Moch H, Willi N, et al. Metastatic patterns of prostate cancer: an autopsy study of 1,589 patients. Human pathology. 2000;31:578-83.

12.Shah RB, Mehra R, Chinnaiyan AM, Shen R, Ghosh D, Zhou M, et al. Androgen-independent prostate cancer is a heterogeneous group of diseases: lessons from a rapid autopsy program. Cancer research. 2004;64:9209-16.

13.Pienta KJ, Bradley D. Mechanisms underlying the development of androgen-independent prostate cancer. Clinical cancer research : an official journal of the American Association for Cancer Research. 2006;12:1665-71.

14.Chen CD, Welsbie DS, Tran C, Baek SH, Chen R, Vessella R, et al. Molecular determinants of resistance to antiandrogen therapy. Nature medicine. 2004;10:33-9.

15.Gregory CW, Johnson RT, Jr., Mohler JL, French FS, Wilson EM. Androgen receptor stabilization in recurrent prostate cancer is associated with hypersensitivity to low androgen. Cancer research. 2001;61:2892-8.

16.Weber MJ, Gioeli D. Ras signaling in prostate cancer progression. Journal of cellular biochemistry. 2004;91:13-25.

17.Visakorpi T, Hyytinen E, Koivisto P, Tanner M, Keinanen R, Palmberg C, et al. In vivo amplification of the androgen receptor gene and progression of human prostate cancer. Nature genetics. 1995;9:401-6.

18.Koivisto P, Kononen J, Palmberg C, Tammela T, Hyytinen E, Isola J, et al. Androgen receptor gene amplification: a possible molecular mechanism for androgen deprivation therapy failure in prostate cancer. Cancer research. 1997;57:314-9.

19.Linja MJ, Savinainen KJ, Saramaki OR, Tammela TL, Vessella RL, Visakorpi T. Amplification and overexpression of androgen receptor gene in hormone-refractory prostate cancer. Cancer research. 2001;61:3550-5.

20.Latil A, Bieche I, Vidaud D, Lidereau R, Berthon P, Cussenot O, et al. Evaluation of androgen, estrogen (ER alpha and ER beta), and progesterone receptor expression in human prostate cancer by real-time quantitative reverse transcription-polymerase chain reaction assays. Cancer research. 2001;61:1919-26.

21.Ford OH, 3rd, Gregory CW, Kim D, Smitherman AB, Mohler JL. Androgen receptor gene amplification and protein expression in recurrent prostate cancer. The Journal of urology. 2003;170:1817-21.

22.Holzbeierlein J, Lal P, LaTulippe E, Smith A, Satagopan J, Zhang L, et al. Gene expression analysis of human prostate carcinoma during hormonal therapy identifies androgen-responsive genes and mechanisms of therapy resistance. The American journal of pathology. 2004;164:217-27.

23.Makridakis N, Ross RK, Pike MC, Chang L, Stanczyk FZ, Kolonel LN, et al. A prevalent missense substitution that modulates activity of prostatic steroid 5alpha-reductase. Cancer research. 1997;57:1020-2.

24.Labrie F, Dupont A, Belanger A, St-Arnaud R, Giguere M, Lacourciere Y, et al. Treatment of prostate cancer with gonadotropin-releasing hormone agonists. Endocrine reviews. 1986;7:67-74.

25.Gelmann EP. Molecular biology of the androgen receptor. Journal of clinical oncology : official journal of the American Society of Clinical Oncology. 2002;20:3001-15.

26.Taplin ME, Balk SP. Androgen receptor: a key molecule in the progression of prostate cancer to hormone independence. Journal of cellular biochemistry. 2004;91:483-90.

27.Nelson WG, De Marzo AM, Isaacs WB. Prostate cancer. The New England journal of medicine. 2003;349:366-81.

28.Debes JD, Tindall DJ. Mechanisms of androgen-refractory prostate cancer. The New England journal of medicine. 2004;351:1488-90.

29.Wilding G, Chen M, Gelmann EP. Aberrant response in vitro of hormone-responsive prostate cancer cells to antiandrogens. The Prostate. 1989;14:103-15.

30.Veldscholte J, Berrevoets CA, Ris-Stalpers C, Kuiper GG, Jenster G, Trapman J, et al. The androgen receptor in LNCaP cells contains a mutation in the ligand binding domain which affects steroid binding characteristics and response to antiandrogens. The Journal of steroid biochemistry and molecular biology. 1992;41:665-9.

31.Buchanan G, Greenberg NM, Scher HI, Harris JM, Marshall VR, Tilley WD. Collocation of androgen receptor gene mutations in prostate cancer. Clinical cancer research : an official journal of the American Association for Cancer Research. 2001;7:1273-81.

32.Shi XB, Ma AH, Xia L, Kung HJ, de Vere White RW. Functional analysis of 44 mutant androgen receptors from human prostate cancer. Cancer research. 2002;62:1496-502.

33.Taplin ME, Bubley GJ, Shuster TD, Frantz ME, Spooner AE, Ogata GK, et al. Mutation of the androgen-receptor gene in metastatic androgen-independent prostate cancer. The New England journal of medicine. 1995;332:1393-8.

34.Tilley WD, Buchanan G, Hickey TE, Bentel JM. Mutations in the androgen receptor gene are associated with progression of human prostate cancer to androgen independence. Clinical cancer research : an official journal of the American Association for Cancer Research. 1996;2:277-85.

35.Marcelli M, Ittmann M, Mariani S, Sutherland R, Nigam R, Murthy L, et al. Androgen receptor mutations in prostate cancer. Cancer research. 2000;60:944-9.

36.Taplin ME, Rajeshkumar B, Halabi S, Werner CP, Woda BA, Picus J, et al. Androgen receptor mutations in androgen-independent prostate cancer: Cancer and Leukemia Group B Study 9663. Journal of clinical oncology : official journal of the American Society of Clinical Oncology. 2003;21:2673-8.

37.Tindall D, Horne FM, Hruszkewycz A, Mohla S, Shuman M, Wang Z, et al. Symposium on androgen action in prostate cancer. Cancer research. 2004;64:7178-80.

38.Culig Z, Hobisch A, Cronauer MV, Radmayr C, Trapman J, Hittmair A, et al. Androgen receptor activation in prostatic tumor cell lines by insulin-like growth factor-I, keratinocyte growth factor, and epidermal growth factor. Cancer research. 1994;54:5474-8.

39.Culig Z, Steiner H, Bartsch G, Hobisch A. Interleukin-6 regulation of prostate cancer cell growth. Journal of cellular biochemistry. 2005;95:497-505.

40.Craft N, Shostak Y, Carey M, Sawyers CL. A mechanism for hormone-independent prostate cancer through modulation of androgen receptor signaling by the HER-2/neu tyrosine kinase. Nature medicine. 1999;5:280-5.

41.Gioeli D, Ficarro SB, Kwiek JJ, Aaronson D, Hancock M, Catling AD, et al. Androgen receptor phosphorylation. Regulation and identification of the phosphorylation sites. The Journal of biological chemistry. 2002;277:29304-14.

42.Pienta KJ, Loberg R. The "emigration, migration, and immigration"of prostate cancer. Clinical prostate cancer. 2005;4:24-30.

43.Loberg RD, Logothetis CJ, Keller ET, Pienta KJ. Pathogenesis and treatment of prostate cancer bone metastases: targeting the lethal phenotype. Journal of clinical oncology : official journal of the American Society of Clinical Oncology. 2005;23:8232-41.

44.Paget S. The distribution of secondary growths in cancer of the breast. 1889. Cancer metastasis reviews. 1989;8:98-101.

45.Janne OA, Moilanen AM, Poukka H, Rouleau N, Karvonen U, Kotaja N, et al. Androgen-receptor-interacting nuclear proteins. Biochemical Society transactions. 2000;28:401-5.

46.Gregory CW, He B, Johnson RT, Ford OH, Mohler JL, French FS, et al. A mechanism for androgen receptor-mediated prostate cancer recurrence after androgen deprivation therapy. Cancer research. 2001;61:4315-9.

47.Li P, Yu X, Ge K, Melamed J, Roeder RG, Wang Z. Heterogeneous expression and functions of androgen receptor co-factors in primary prostate cancer. The American journal of pathology. 2002;161:1467-74.

48.Kang Z, Janne OA, Palvimo JJ. Coregulator recruitment and histone modifications in transcriptional regulation by the androgen receptor. Mol Endocrinol. 2004;18:2633-48.

49.Wang L, Hsu CL, Chang C. Androgen receptor corepressors: an overview. The Prostate. 2005;63:117-30.

50.Fujimoto N, Yeh S, Kang HY, Inui S, Chang HC, Mizokami A, et al. Cloning and characterization of androgen receptor coactivator, ARA55, in human prostate. The Journal of biological chemistry. 1999;274:8316-21.

51.Ngan ES, Hashimoto Y, Ma ZQ, Tsai MJ, Tsai SY. Overexpression of Cdc25B, an androgen receptor coactivator, in prostate cancer. Oncogene. 2003;22:734-9.

52.Debes JD, Sebo TJ, Lohse CM, Murphy LM, Haugen DA, Tindall DJ. p300 in prostate cancer proliferation and progression. Cancer research. 2003;63:7638-40.

53.McDonnell TJ, Troncoso P, Brisbay SM, Logothetis C, Chung LW, Hsieh JT, et al. Expression of the protooncogene bcl-2 in the prostate and its association with emergence of androgen-independent prostate cancer. Cancer research. 1992;52:6940-4.

54.Colombel M, Symmans F, Gil S, O'Toole KM, Chopin D, Benson M, et al. Detection of the apoptosis-suppressing oncoprotein bc1-2 in hormone-refractory human prostate cancers. The American journal of pathology. 1993;143:390-400.

55.Raffo AJ, Perlman H, Chen MW, Day ML, Streitman JS, Buttyan R. Overexpression of bcl-2 protects prostate cancer cells from apoptosis in vitro and confers resistance to androgen depletion in vivo. Cancer research. 1995;55:4438-45.

56.Furuya Y, Krajewski S, Epstein JI, Reed JC, Isaacs JT. Expression of bcl-2 and the progression of human and rodent prostatic cancers. Clinical cancer research : an official journal of the American Association for Cancer Research. 1996;2:389-98.

57.Collins AT, Berry PA, Hyde C, Stower MJ, Maitland NJ. Prospective identification of tumorigenic prostate cancer stem cells. Cancer research. 2005;65:10946-51.

58.Attar RM, Takimoto CH, Gottardis MM. Castration-resistant prostate cancer: locking up the molecular escape routes. Clinical cancer research : an official journal of the American Association for Cancer Research. 2009;15:3251-5.

59.Arya M, Bott SR, Shergill IS, Ahmed HU, Williamson M, Patel HR. The metastatic cascade in prostate cancer. Surgical oncology. 2006;15:117-28.

60.Chambers AF, Groom AC, MacDonald IC. Dissemination and growth of cancer cells in metastatic sites. Nature reviews Cancer. 2002;2:563-72.

61.Kalluri R, Weinberg RA. The basics of epithelial-mesenchymal transition. The Journal of clinical investigation. 2009;119:1420-8.

62.Gravdal K, Halvorsen OJ, Haukaas SA, Akslen LA. A switch from E-cadherin to N-cadherin expression indicates epithelial to mesenchymal transition and is of strong and independent importance for the progress of prostate cancer. Clinical cancer research : an official journal of the American Association for Cancer Research. 2007;13:7003-11.

63.Umbas R, Schalken JA, Aalders TW, Carter BS, Karthaus HF, Schaafsma HE, et al. Expression of the cellular adhesion molecule E-cadherin is reduced or absent in high-grade prostate cancer. Cancer research. 1992;52:5104-9.

64.Umbas R, Isaacs WB, Bringuier PP, Schaafsma HE, Karthaus HF, Oosterhof GO, et al. Decreased E-cadherin expression is associated with poor prognosis in patients with prostate cancer. Cancer research. 1994;54:3929-33.

65.Jaggi M, Johansson SL, Baker JJ, Smith LM, Galich A, Balaji KC. Aberrant expression of E-cadherin and beta-catenin in human prostate cancer. Urologic oncology. 2005;23:402-6.

66.Ryan CJ, Rosenthal M, Ng S, Alumkal J, Picus J, Gravis G, et al. Targeted MET inhibition in castration-resistant prostate cancer: a randomized phase II study and biomarker analysis with rilotumumab plus mitoxantrone and prednisone. Clinical cancer research : an official journal of the American Association for Cancer Research. 2013;19:215-24.

67.Lichtinghagen R, Musholt PB, Lein M, Romer A, Rudolph B, Kristiansen G, et al. Different mRNA and protein expression of matrix metalloproteinases 2 and 9 and tissue inhibitor of metalloproteinases 1 in benign and malignant prostate tissue. European urology. 2002;42:398-406.

68.Trudel D, Fradet Y, Meyer F, Harel F, Tetu B. Significance of MMP-2 expression in prostate cancer: an immunohistochemical study. Cancer research. 2003;63:8511-5.

69.Wood M, Fudge K, Mohler JL, Frost AR, Garcia F, Wang M, et al. In situ hybridization studies of metalloproteinases 2 and 9 and TIMP-1 and TIMP-2 expression in human prostate cancer. Clinical & experimental metastasis. 1997;15:246-58.

70.Brehmer B, Biesterfeld S, Jakse G. Expression of matrix metalloproteinases (MMP-2 and -9) and their inhibitors (TIMP-1 and -2) in prostate cancer tissue. Prostate cancer and prostatic diseases. 2003;6:217-22.

71.Morgia G, Falsaperla M, Malaponte G, Madonia M, Indelicato M, Travali S, et al. Matrix metalloproteinases as diagnostic (MMP-13) and prognostic (MMP-2, MMP-9) markers of prostate cancer. Urological research. 2005;33:44-50.

72.Nabha SM, dos Santos EB, Yamamoto HA, Belizi A, Dong Z, Meng H, et al. Bone marrow stromal cells enhance prostate cancer cell invasion through type I collagen in an MMP-12 dependent manner. International journal of cancer Journal international du cancer. 2008;122:2482-90.

73.Zaidel-Bar R, Geiger B. The switchable integrin adhesome. Journal of cell science. 2010;123:1385-8.

74.Zaidel-Bar R, Itzkovitz S, Ma'ayan A, Iyengar R, Geiger B. Functional atlas of the integrin adhesome. Nature cell biology. 2007;9:858-67.

75.Mol AJ, Geldof AA, Meijer GA, van der Poel HG, van Moorselaar RJ. New experimental markers for early detection of high-risk prostate cancer: role of cell-cell adhesion and cell migration. Journal of cancer research and clinical oncology. 2007;133:687-95.

76.Lee YC, Jin JK, Cheng CJ, Huang CF, Song JH, Huang M, et al. Targeting constitutively activated beta1 integrins inhibits prostate cancer metastasis. Molecular cancer research : MCR. 2013;11:405-17.

77.Rovin JD, Frierson HF, Jr., Ledinh W, Parsons JT, Adams RB. Expression of focal adhesion kinase in normal and pathologic human prostate tissues. The Prostate. 2002;53:124-32.

78.Chauchereau A. Experimental models for the development of new medical treatments in prostate cancer. Eur J Cancer. 2011;47 Suppl 3:S200-14.

79.Nyga A, Cheema U, Loizidou M. 3D tumor models: novel in vitro approaches to cancer studies. Journal of cell communication and signaling. 2011;5:239-48.

80.Fidler IJ. Orthotopic implantation of human colon carcinomas into nude mice provides a valuable model for the biology and therapy of metastasis. Cancer metastasis reviews. 1991;10:229-43.

81.Welch DR. Technical considerations for studying cancer metastasis in vivo. Clinical & experimental metastasis. 1997;15:272-306.

82.Chambers AF, Tuck AB. Ras-responsive genes and tumor metastasis. Critical reviews in oncogenesis. 1993;4:95-114.

83.Kohn EC, Liotta LA. Molecular insights into cancer invasion: strategies for prevention and intervention. Cancer research. 1995;55:1856-62.

84.Chambers AF, Matrisian LM. Changing views of the role of matrix metalloproteinases in metastasis. Journal of the National Cancer Institute. 1997;89:1260-70.

85.Freije JM, MacDonald NJ, Steeg PS. Nm23 and tumor metastasis: basic and translational advances. Biochemical Society symposium. 1998;63:261-71.

86.Eccles SA. The role of c-erbB-2/HER2/neu in breast cancer progression and metastasis. Journal of mammary gland biology and neoplasia. 2001;6:393-406.

87.Skubitz AP. Adhesion molecules. Cancer treatment and research. 2002;107:305-29.

88.Kimlin LC, Casagrande G, Virador VM. In vitro three-dimensional (3D) models in cancer research: an update. Molecular carcinogenesis. 2013;52:167-82.

CHAPTER 2

AUTOMATED MICROINJECTION OF CELL POLYMER SUSPENSIONS IN 3D ECM SCAFFOLDS FOR HIGH-THROUGHPUT QUANTITATIVE CANCER INVASION SCREENS

Hoa H Truong[1], Jan de Sonneville[2], Veerander PS Ghotra[1], Jiangling Xiong[1], Leo Price[1], Pancras Hogendoorn[3], Herman Spaink[4], Bob van de Water[1],Erik HJ Danen[1]

Published in Biomaterials,2012 Jan;33(1):181-8

[1]Division of Toxicology, Leiden Academic Center for Drug Research, Leiden University, Einsteinweg 55,2333 CC, Leiden,The Netherlands;[2]Division of Biophysical Structural Chemistry, Leiden Institute of Chemistry, Leiden University, Einsteinweg 55, 2333 CC Leiden, the Netherlands;[3]Department of Pathology, Leiden University Medical Center, Albinusdreef 2, 2333 ZA, Leiden, The Netherlands; [4]Institute of Biology, Leiden University

ABSTRACT

Cell spheroids (CS) embedded in 3D extracellular matrix (ECM) serve as in vitro mimics for multicellular structures in vivo. Such cultures, started either from spontaneous cell aggregates or single cells dispersed in a gel are time consuming, applicable to restricted cell types only, prone to high variation, and do not allow CS formation with defined spatial distribution required for high-throughput imaging. Here, we describe a novel method where cell-polymer suspensions are microinjected as droplets into collagen gels and CS formation occurs within hours for a broad range of cell types. We have automated this method to produce CS arrays in fixed patterns with defined x-y-z spatial coordinates in 96 well plates and applied automated imaging and image analysis algorithms. Low intra- and inter-well variation of initial CS size and CS expansion indicates excellent reproducibility. Distinct cell migration patterns, including cohesive strand-like- and individual cell migration can be visualized and manipulated. A proof-of-principle chemical screen is performed identifying compounds that affect cancer cell invasion/migration. Finally, we demonstrate applicability to freshly isolated mouse and human tumor biopsy material - indicating potential for development of personalized cancer treatment strategies.

INTRODUCTION

Cells grown under classical 2D culture conditions behave differently from the same cell types grown in vivo. In addition to soluble factors produced in the in-vivo microenvironment, differences in cell shape, intercellular contacts, and connections to ECM have striking effects on gene expression, cell survival, proliferation, differentiation, cytoarchitecture, and migration. Various systems have been developed to culture cells within 3D ECM environments, aimed at more closely mimicking the in-vivo context (1,2). Several of these systems produce 3D cell aggregates in which, after compaction, depletion of oxygen, nutrients, and growth factors occurs in the core, leading to cell heterogeneity depending on the position in the resulting CS (3,4). Multistep methods are used in which aggregates are allowed to form spontaneously and, following a compaction phase, can subsequently be transferred to a 3D ECM. The best-known example of this approach is the “hanging drop assay” that was developed to create embryoid bodies from ES cells and has also been applied to cancer cell lines to produce tumor-like structures (5,6). Alternative methods involve mixing of single cell suspensions with a solidifying ECM, resulting in individual cells that eventually form spheroids randomly within a 3D ECM structure (7), or seeding polymeric scaffolds with cell/ECM suspensions (2). Cell behavior in 3D cultures is controlled by chemical (composition) and physical (rigidity, cross-linking) properties of the gel. Natural ECM proteins can be used such as collagen, fibrinogen, or the laminin-rich matrigel to represent the in-vivo ECM composition most relevant to a given cell type. More recently, synthetic polymers have been developed for 3D CS culture environments although it remains to be established how well these support a variety of cell behavioral outputs, including cell migration (8). Collagen type 1 is an abundant polymer in ECM in vivo, and it is widely used for 3D cultures. Various physical properties of the collagen gel, such as rigidity and pore size modulate stem cell differentiation, cancer growth, and cell migration (9-11). Cells can use various migration strategies in 3D environments, including mesenchymal or amoeboid individual cell migration modes or collective invasion strategies, depending on properties of the cells and of the matrix (10). Changes in matrix pore size can force cells to adopt alternative migration strategies or - if too extreme - pose a barrier to cell migration. Importantly, cells can modify the ECM by physical deformation and proteoly-

sis, to overcome such barriers (12). Chemical compound screens as well as RNAi screens for various types of cellular functions, including survival, growth, differentiation, and migration are mostly performed in 2D culture conditions. Methods to analyze cells in 3D based on the hanging-drop assay are labor and time intensive; are limited to cell types that are cohesive and aggregate spontaneously; and are prone to high variability between experiments due to variation in aggregation and compaction time and CS size. Alternative methods in which single cell suspensions are mixed with soluble ECM substrates that are subsequently allowed to form a gel are relatively easy to perform but also have several major disadvantages: formation of CS depends on the ability of a cell type to survive and proliferate as single cells in low adhesion conditions for extended periods; CS formation is time consuming; CS show a large variation in size; and CS form at random locations, which is disadvantageous for imaging purposes. To allow for CS formation that is relatively fast and easy, highly reproducible, and overcomes the disadvantages described above we have developed a novel method where cell-polymer suspensions are microinjected into multiwell plates containing a collagen gel. This method has been automated to produce CS arrays with highly reproducible properties in large quantities in 96 well plates. We use this system to visualize distinct 3D migration strategies and regulation of those strategies by ECM properties and actomyosin contractility. We demonstrate applicability in high-throughput screening platforms in a chemical screen for compounds that affect breast cancer invasion/migration. Finally, we apply the method to cell suspensions derived from fresh tumor biopsies, which opens the possibility to test therapeutic strategies on freshly isolated material from individual patients.

RESULTS

Development and characterization of the method

To design a protocol that rapidly produces CS with highly reproducible characteristics, we developed a novel method based on microinjection. For the microinjection method we mixed cells with polyvinylpyrrolidone (PVP), which is an inert (hydrophilic) water-soluble synthetic polymer, also used as emulsifier, food-additive (E1201) and as solubilizing agent for injections (13). In our application it was used to delay cell sedimentation within the capillary needle. Furthermore, in our experience cells rapidly disperse in the absence of PVP while cells injected in the presence of PVP remained localized (e.g. trapped by the polymer) at the site of injection, allowing time for aggregation and CS formation. We first compared our method to the established hanging drop assay (5). Twenty µl drops containing $5x10^3$ GEß1 cells were used to create hanging drops in an inverted 10 cm dish (Fig. 1a). The time required to form cell aggregates was 24h. These cell aggregates were transferred to agarose-coated dishes where they formed tightly packed spheroids over a period of 48h. Next, the spheroids were embedded in 2.4 mg/mL collagen solution that was subsequently allowed to solidify. For microinjection, GEß1 cells were suspended in 2% PVP, loaded into a pulled glass needle, and ~80nL droplets containing ~$1x10^4$ cells were injected directly into preformed 2.4 mg/mL collagen gels where they formed tightly packed spheroids within 1h (Fig. 1a). Microinjection-derived CS at 24h post-injection and hanging-drop-derived CS at 96h post initiation (24h in collagen) displayed similar cell migration the following days (Fig. 1b). Microinjection-derived CS were also established from 4T1 mouse breast carcinoma cells where E-cadherin staining marked cell-cell contacts within the first day post-injection that were maintained for at least 96h (Fig. 1c). CS derived by microinjection of different cancer- or non-cancerous cell types allowed analysis of various distinct motile strategies in 3D (Fig.1d). Cell types that do not typically form cell-

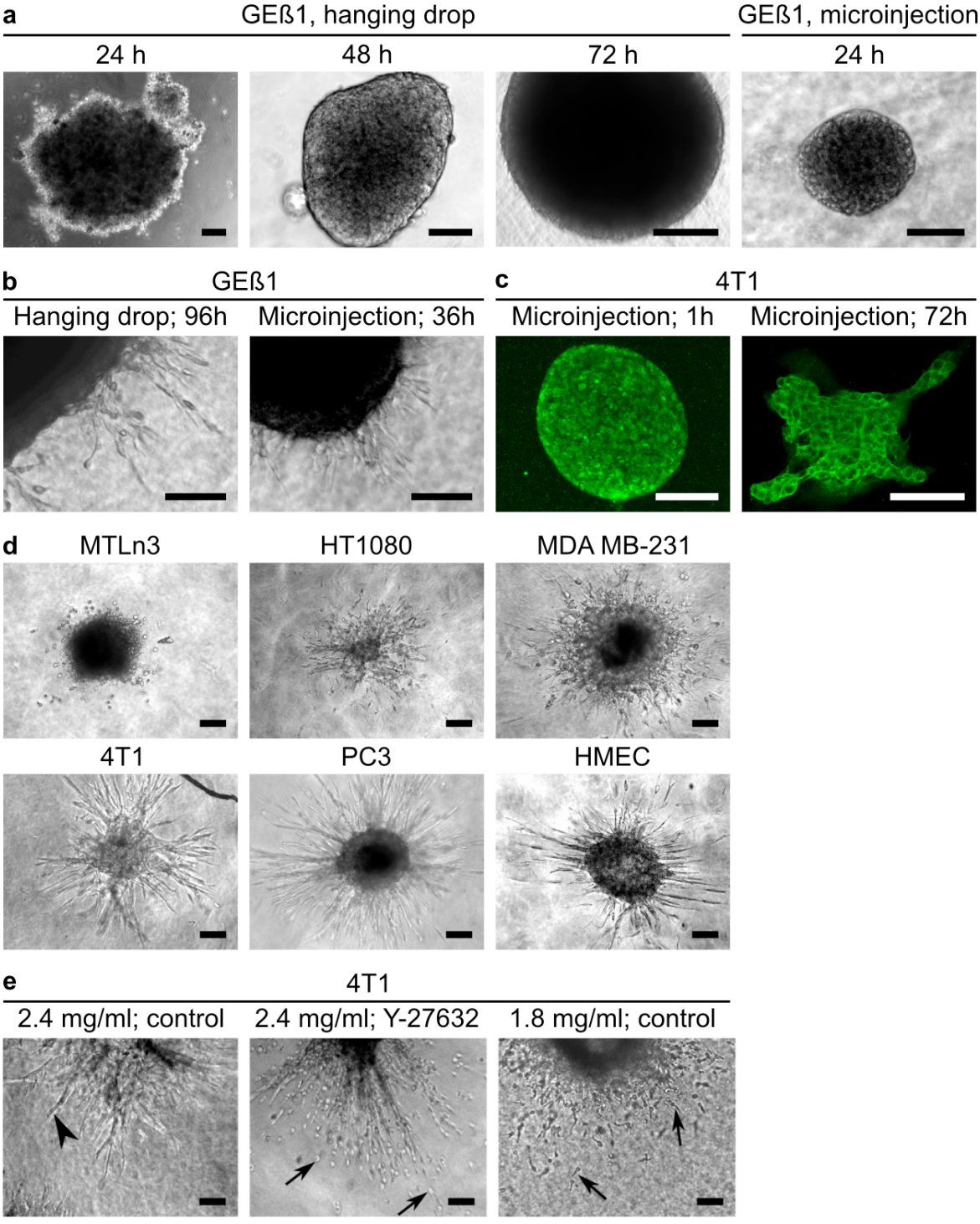

FIGURE 1.*Characteristics of microinjection-derived spheroids.* A, Comparison of hanging-drop and microinjection method for GEß1 cells. B, Migration of GEß1 cells from hanging-drop and microinjection-derived spheroids. C, E-cadherin staining in spheroids at indicated timepoints post-injection for 4T1 cells. D, Different modes of cell migration from spheroids for indicated cell types showing individual (top row) and cohesive strand migration (bottom row). E, Modulation of cell migration modes by alterations in collagen gel network (left and middle) or interfering with cytoskeletal network (right image, ROCK inhibitor). Arrowheads indicate cohesive migration strands; arrows indicate individual migrating cells. Scales, 120 µm.

cell contacts in 2D cell culture (and that are typically difficult to study in 3D using the hanging-drop-, liquid overlay-, or other assays in absence of additives like matrigel (14,15) such as MTLn3 and MDA-MB-231 breast cancer cells and HT1080 fibrosarcoma cells, displayed amoeboid (MTLn3)or mesenchymal (HT1080 and MDA-MB-231) movement of individual cells. On the other hand, 4T1 breast cancer, and human microvascular endothelial cells (HMEC) that grow as islands in 2D culture, invaded as cohesive strands into the collagen matrix.ECM rigidity influences cell behavior in 3D and the actin cytoskeleton is believed to be essential for sensing and responding to such physical ECM properties (12). We used these CS to study the effect of alterations in ECM network composition or intracellular cytoskeletal network properties on migration strategies in 3D. Lowering ECM rigidity by decreasing collagen concentration from 2.5 to 0.25 mg/mL or lowering cytoskeletal tension by application of a ROCK inhibitor, both caused a switch from cohesive strand invasion to individual cell migration in 4T1 cells (Fig. 1e). This suggests that tension exerted on cell-cell adhesion structures either from outside or inside the cell is required for cohesive 3D movement. Altogether, these results demonstrate that the microinjection method produces CS for 3D growth and migration studies rapidly (hours versus days), conveniently (one step), with a broad spectrum of cell types including those that are incompatible with previous methods, and displaying a variety of migration patterns.

Method automation

Since this method has the potential to rapidly create CS with high reproducibility for large- scale analysis in 3D ECM of cell growth and migration/invasion we set up a procedure to automate the CS formation process. For this purpose, a 96 well plate containing 60 µL collagen gel per well was placed on a motorized stage and the glass needle containing the cell/PVP suspension described above was placed vertically in a motorized micromanipulator above the stage (Fig. 2a). After calibration of needle and 96-well plate using camera vision from under the stage, a computer script was used to automate the injection process with various macros.With this set up, cell droplets were injected resulting in spheroids of ~300 µm diameter (Movie S1). To increase reproducibility, using commercial needles reduced needle tip diameter variance and gels were prepared from a single large batch of collagen isolated in-house from rat-tail. Various layouts of injection patterns were tested. A hexagonal pattern of 19 spheroids spaced at 1.2 mm started to show interaction between migration strands of CS at day 4 but a less dense hexagon pattern of 7 spheroids at 2 mm spacing provided sufficient spacing for 96h analysis of CS migration (Fig. 2b,c). Visual inspection indicated reduced CS migration on the most outer rows and columns of each plate, pointing to edge effects. We therefore chose to exclude these wells in all further experiments. We determined reproducibility in all other wells and detected no significant intra- or inter-well variation in initial CS size (ANOVA, $P>0.5$) or CS expansion over ~92h (ANOVA, $P>0.5$) (Fig.2d). These data demonstrate that the microinjection method can be automated to create with high reproducibility and predefined x-y-z coordinates CS arrays in 96 well plates. Such properties make this protocol ideal for automated imaging strategies.

Application of the method to automated drug screens

A proof of principle drug screen was performed to test the applicability of this procedure to automated high-throughput drug screening assays (HTS). 4T1 CS were generated and various previously described inhibitors, including AG1478 (EGFR), PP2 (Src), ML-7 (MLCK), Y-27632 (ROCK), NSC23766 (Rac), SB-431542 (TGFβR activin-like kinases), AG-82 (EGFR), LY-294002 (PI3K), JSI-124 (STAT3) were added one hour later

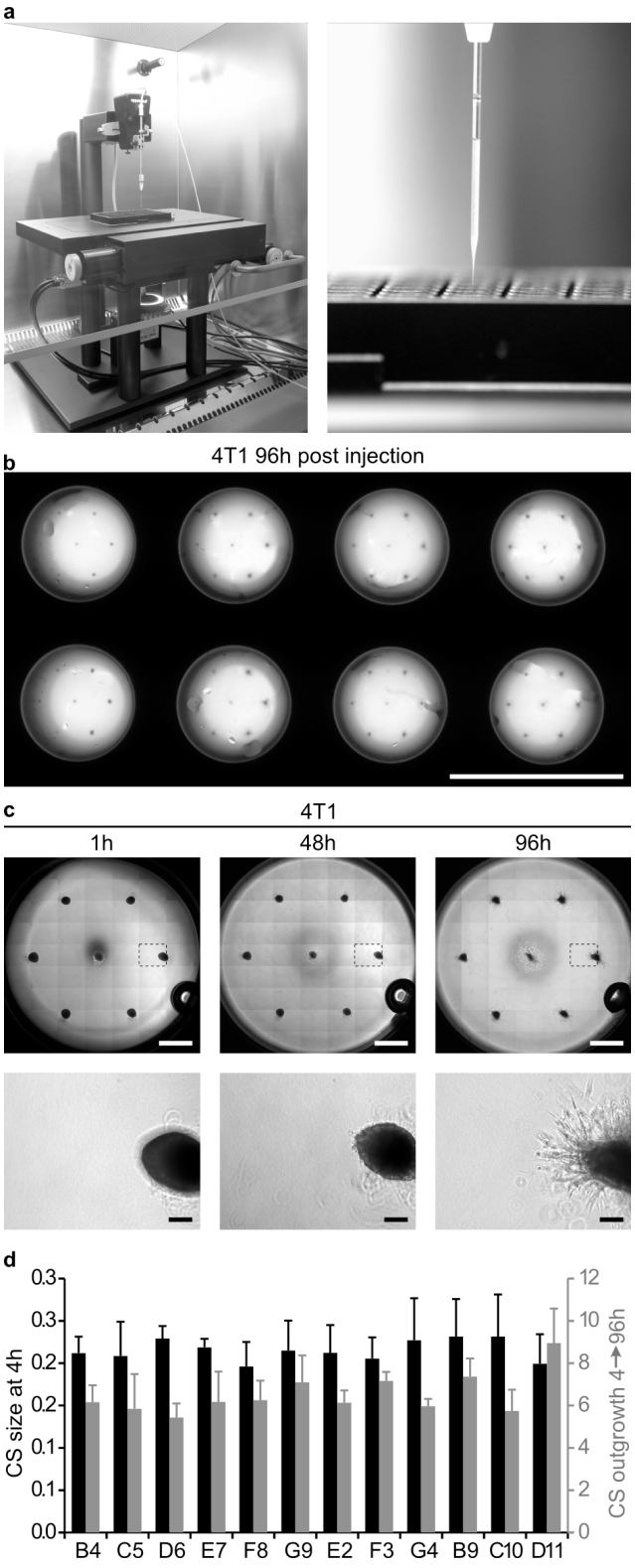

FIGURE 2. *Automated production of spheroid arrays*. A, Automated injection system (left) and cell/PVP suspension in needle during injection (right). B, Bottom view of multiple wells with 4T1 spheroid arrays 96 hours post-injection. Scale, 10mm. C, Upper row shows stitched brightfield images showing spheroid arrays at indicated timepoints. Scale, 1 mm. Bottom row shows cell migration from single bright-field images of spheroids marked by dashed rectangle in upper row. Scale, 100 µm. D, Mean and SD for initial spheroid size 4h post-injection (black bars) and CS migration over ~4 days determined from outline of migration strands (grey bars) obtained from all 7 spheroids /well for indicated wells of a 96-well plate.

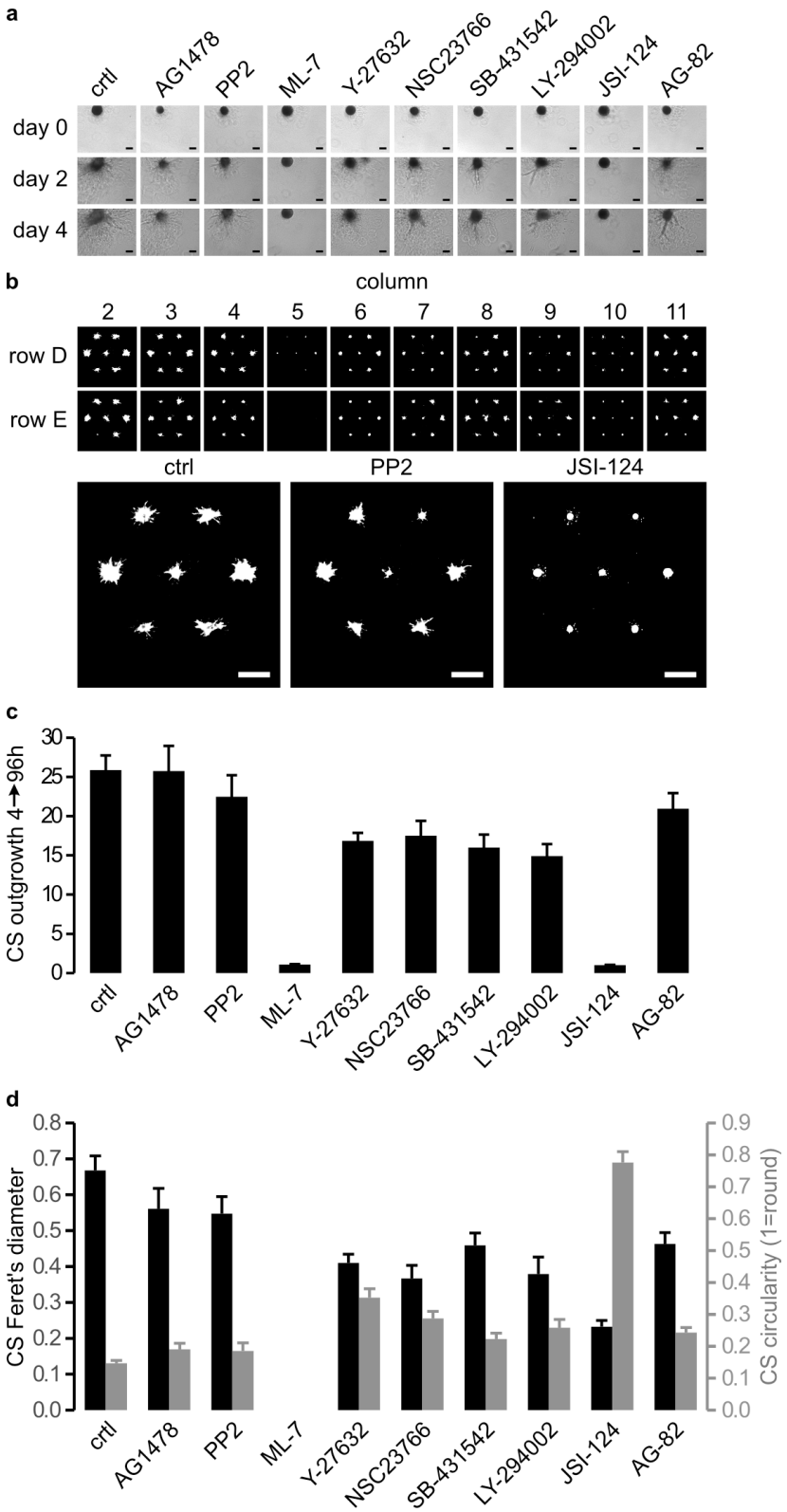

FIGURE 3. *Results from a drug screen performed on 4T1 cells in a 96 well plate.* A, DIC images showing tumor cell migration in the presence of indicated inhibitors at indicated timepoints (scale = 100 µm). B, Top 2 rows, rhodamine-phalloidin staining and thresholding for indicated wells at 4 dpi (columns correspond to treatments from A; rows represent duplicates); bottom row, zoom in on well D2 (Ctr), D4 (PP2), and D10 (JSI-124). Scale, 1 mm. C, effect of indicated inhibitors on CS migration over ~4 days determined from outline of migration strands derived from DIC images in A (mean and SD for 14 spheroids derived from 2 wells is shown). D, Quantification of data derived from automated analysis of fluorescent images shown in B (mean and SD for 14 spheroids derived from 2 wells is shown).

at different concentrations (4, 10, 20 μM) in duplicate. Effects on cell migration could be clearly observed by DIC imaging after 2 and 4 days for ML-7 and JSI-124 (Fig.3a). For automated imaging and image analysis protocols, we labeled the actin cytoskeleton at day 4 of all 10 μM treatments and controls (Fig.3b). This allowed automated capture of Z-stacks that were converted to maximum projection images, thresholded, and used for automated multiparameter analysis including Feret's diameter and circularity. Visual inspection and manual assessment of Feret's diameter from DIC images at day 0 and 4 demonstrated that initial CS size, CS expansion, and inhibition of invasion by ML-7 and JSI-124 were highly reproducible (Fig. 3a,c). Automated image analysis fitted well with these data showing that ML-7 and JSI-124 caused significantly reduced Feret's diameters ($p<0.05$) (Fig.3d). For JSI-124 this correlated with increased circularity ($p<0.05$) in agreement with inhibition of invasion and a remaining round CS. The extremely low values observed for ML-7 (Fig. 3d) despite the fact that a CS was observed by DIC (Fig.3a) can be explained by ML-7-induced loss of filamentous actin fibers causing reduced staining in this particular method. Alternative staining procedures should lead to improvement and compatibility with real-time analysis. Nevertheless, the reproducibility of the injection procedure (Fig. 2 and 3) combined with the similarity between visual inspection and automated imaging (Fig. 3c,d), demonstrates that this automated injection system can be coupled to fully automated imaging and image analysis methodology that is accurate and reproducible.

Compatibility of the method with primary biopsy material

We determined if this methodology is compatible with freshly isolated biopsy material. First, a cell suspension was generated from 4T1-GFP orthotopic breast tumors in mice using collagenase- treatment. In contrast to alternative methods, the microinjection method circumvents any 2D tissue culture steps, which may cause altered cell behavior (16-20). Following injection, these cells rapidly formed CS from which migration was analyzed after 3 days (Fig. 4a). CS were stained for actin and DNA and the near complete overlap between actin and GFP staining demonstrates that these CS consist mainly of tumor cells. Next, cell suspensions were derived by collagenase treatment of freshly isolated human osteosarcoma and chondrosarcoma tissue. Following injection, CS readily formed from these human biopsies and survival and migration could be studied for up to one week with the two tumor types showing distinct migratory behavior (Fig.4b). Osteosarcoma mainly displayed individual amoeboid movement whereas chondrosarcoma showed predominantly individual mesenchymal movement. We treated these CS with the range of compounds described above at 10 μM starting one day post-injection. Several of the chemical inhibitors effectively inhibited migration of both tumor types (Fig. 4b,c). Notably, the ROCK inhibitor Y-27632 did not affect mesenchymal movement but caused switching from amoeboid to mesenchymal movement in the osteosarcoma cells, in line with the described requirement for ROCK activity only in amoeboid single cell movement (21). Taken together, these data indicate that the automated CS injection methodology has the potential to be used for drug testing on tumor cells freshly isolated from individual patients.

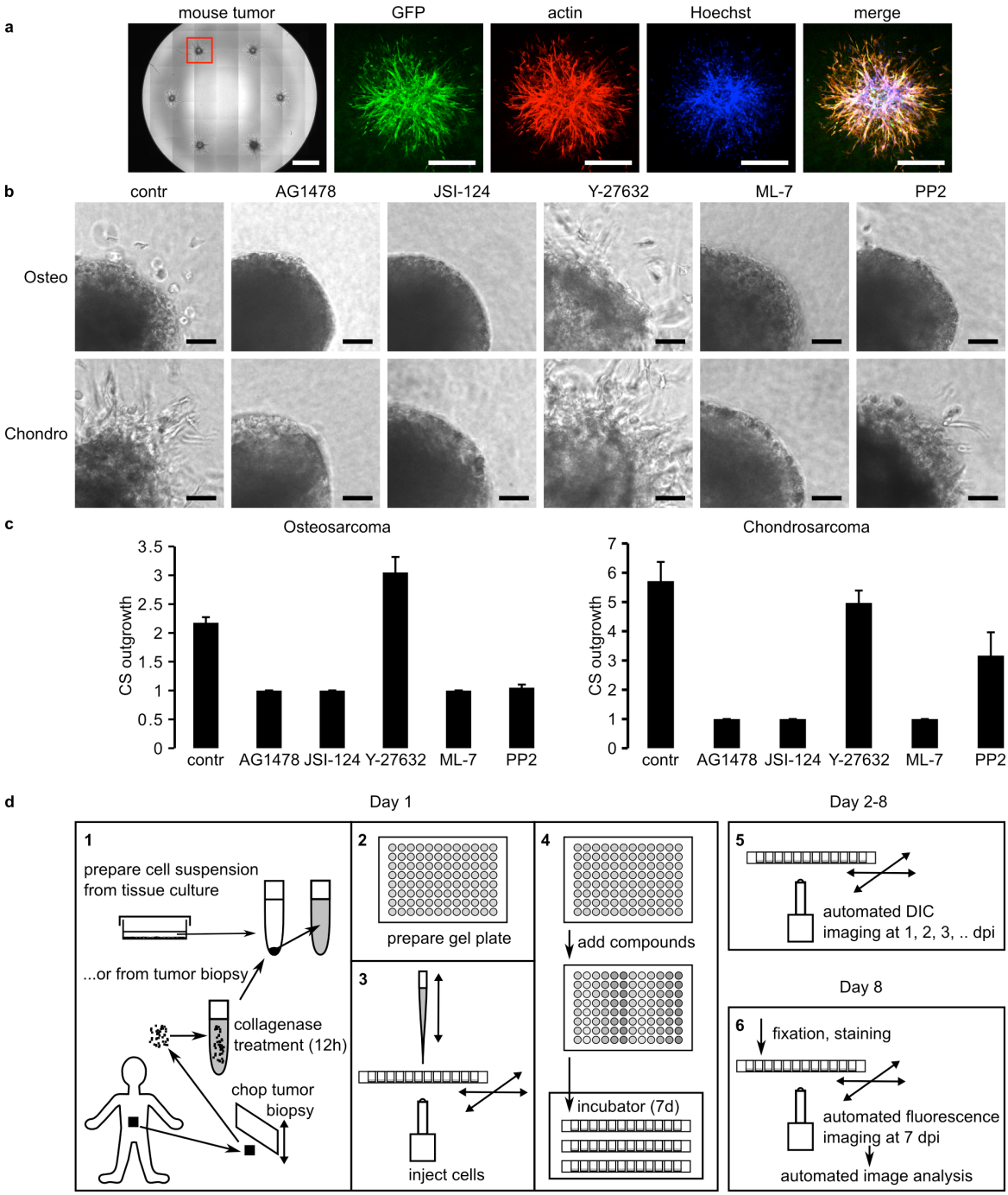

FIGURE 4. *Application to tumor biopsies*. A, Overview DIC image (left) and zoom in on individual spheroid obtained from 4T1-GFP orthotopic mouse breast tumor. Scales, 1 mm (left DIC); 500µm (fluorescent images). B, DIC images showing spheroids derived from osteosarcoma (top) and chondrosarcoma biopsy (bottom) treated with indicated inhibitors. Scale, 100µm. C, effect of indicated inhibitors on CS migration over ~4 days determined from outline of migration strands derived for DIC images in A (mean and SD 12 spheroids derived from 2 wells is shown). D, Schematic overview of high-throughput spheroid screening indicating procedure at day 1 (steps 1-3) and imaging in absence or presence of compounds at days 2-8 (steps 4-6).

DISCUSSION

Here, we describe a method for generation of 3D CS cultures based on microinjection of cell suspensions into premade gels, that has a number of features making it highly useful for drug screening applications: compared to previous methods it is easy (one step procedure) and fast (minutes instead of days); CS are generated with high accuracy at predetermined x-y-z positions in multiwell plates; it is applicable to many different cell types irrespective of the ability of cells to form spontaneous cell-cell contacts; it shows good intra- and inter-well reproducibility with respect to CS size and migration; because of the predefined coordinates of each individual CS the method can easily be combined with fully automated imaging and image analysis protocols (Fig. 5.4d). 2D culture conditions are a very poor representation of the environment cells encounter in vivo. Besides implications for cell biology studies, this has important consequences for the interpretation of genetic - and drug screens (22). So far, these have mostly been performed on 2D cultures. For the study of tumor cell invasion the Boyden chamber assay (trans-well migration assay) is also commonly used. Here, a monolayer of cells migrates through a thin layer of gel to reach the bottom of a filter. This particular assay does not resemble cells disassociating from a solid tumor. For this purpose, CS cultures have been developed that provide a pathophysiological context that mimics solid cancer microenvironments. However, these have not been used for large-scale drug screens due to the complicated procedures, which negatively affect reproducibility of results and lead to higher costs. Reproducibility of CS size is critical for a reliable 3D culture platform. Size and compactness of CS will inevitably affect drug penetration and previous studies have indicated that CS with diameters between 200 and 500µm are required to develop chemical gradients (e.g. of oxygen, nutrients, and catabolites) that may represent conditions found in tumors (3,4,23 - 26). Our automated approach yields spheroids with a diameter of ~300µm, a size that may thus represents solid tumor traits.We have used collagen-based gels but the same method could be easily adapted to studies using alternative 3D matrices. The type and concentration of matrix proteins will have considerable influence on scaffold structure, rigidity, and porosity, which will impact on cell morphology, survival, proliferation, and migration efficiency (8,27,28). We find that changing collagen concentrations has a major impact on CS cell migration and that optimal conditions differ for distinct cell types, in agreement with findings from others (8,27-30). Hence, it is essential that gel formation is standardized and optimized for each cell type. The use of ECM proteins such as collagen has some limitation in terms of controlling batch-to batch variation. Therefore, stabilization by chemical cross-linking may be applied to better control mechanical properties as porosity and mechanical strength. A number of different cross-linking agents that react with specific amino acid residues on the collagen molecule, synthetic biopolymer scaffolds, and self-assembling synthetic oligopeptide gels are available to address this (27,28,31,32). We demonstrate that we can automate each step of the procedure, from injection of cell suspensions to imaging and image analysis, while maintaining reproducibility. Our method not only accelerates and simplifies CS formation but by generating up to 7 CS per well at predefined x-y-z coordinates it is compatible with fully automated imaging procedures, enhanced data collection, and robust statistical analysis. We present a small drug screen to demonstrate such properties. Finally, we show that the method presented here can be used for CS formation directly from freshly isolated tumor biopsy material without the need of any intermediate culture steps. This eliminates artificial traits induced by 2D culture. A fully analyzed CS cancer migration screen in 96 well plates can be derived from a biopsy within 1 week. This opens the door to screening on a patient-by-patient basis for drug sensitivity of tumor cells under conditions that may closely mimic the in-vivo pathophysiological situation. Clinical tests to validate inhibi-

tor effects in CS screens by comparing with therapeutic efficacy can be performed without further modifications of the presented system. Moreover, expansions of this method can be envisioned in which multiple cell types are combined (e.g. cancer cells and cancer-associated fibroblasts and/or endothelial cells) to further improve representation of the complex tumor microenvironment.

MATERIALS AND METHODS

Cell culture

The following cell lines were obtained from ATCC: MDA-MB-231, MTLn3, PC-3, HT1080, 4T1, and MAE. GEβ1 was described earlier(33). All cell lines were cultured under standard cell culture conditions indicated by ATCC or as described (33) at 37.C, 5% CO2 in a humidified incubator. Primary mouse tumor cell suspensions were derived from surplus mouse breast tumor material by mincing using scalpel and tissue chopper followed by 2-hour collagenase treatment at 37 degree celsius. Human biopsy material was obtained from surplus material from patients that were surgically treated for chondrosarcoma or osteosarcoma. Tumor cell suspensions were derived from biopsies by 12h collagenase treatment at 37.C. All human specimens were handled in an anonymized coded fashion according to the National ethical guidelines for secondary use of patient-derived material.

Preparation of collagen

Collagen type I solution was obtained from Upstate-Milipore or isolated from rat-tail collagen by acid extraction as described previously (34). Collagen was diluted to indicated working concentrations of ~2.4 mg/mL in PBS containing 1xDMEM (stock 10x, Gibco), 44 mM NaHCO3 (stock 440 mM, Merck), 0.1 M Hepes (stock 1M, BioSolve).

Hanging drop method

~ 5000 cells in 20 µL droplets were dispensed onto a 10 cm dish that was inverted over a dish containing 10 mL DMEM. After 24h, cell aggregates were harvested using a Pasteur pipette and transferred into 10 cm dishes coated with 0.75% agarose submerged in 10mL DMEM. After 48h, spheroids had formed and these were embedded into a 2.4 mg/mL collagen solution using a Pasteur pipette. Collagen gels were allowed to solidify at 37.C for 30 min and overlaid with DMEM. Cell invasion was recorded for 3 days using an inverted phase contrast light microscope (Nikon Eclipse E600).

Cell preparation for injection method

Cell suspensions derived from trypsin-detached adherent cultures or from collagenase - treated biopsies were filtered to remove clumps, centrifuged at 1000 rpm for 5 minutes, and washed twice with PBS. ~$7x10^6$ cells were re-suspended in 30 µL PBS containing 2% polyvinylpyrrolidone (PVP; Sigma-Aldrich). The PVP/cell suspension was loaded into a beveled pulled glass needle (Eppendorf CustomTip Type III, OD [µm] 60, Front surface 40, Flexibility: rigid).

Manual injection

Cell suspensions in 2% PVP were microinjected (~1x10^4 cells/droplet) with a microinjector (20 psi, PV820 Pneumatic PicoPump, World Precision Instruments, Inc) into solidified collagen gels in 8 well μslides (IBIDI).

Automated injections

A glass-bottom 96 well plate (Greiner) containing 60 μL solidified 2.4 mg/ mL collagen gel per well was placed in a motorized stage (MTmot 200x100 MR, Marzhauser) connected to a controller (Tango, Marzhauser). A motorized micro-manipulator (Injectman II, Eppendorf) was positioned above the stage and connected to a pump (Femtojet Express, Eppendorf) featuring an external compressor (lubricated compressor, model 3-4, JUN-AIR). A firewire camera (DFK41BF02.H, The Imaging Source) equipped with an 8x macro lens (MR8/O, The Imaging Source) was placed beneath the stage for calibration and imaging. All components were connected to the controlling computer (Ubuntu AMD64).

A multi-threaded control program was written in Python using PySerial and wxPython. Coriander software (http://damien.douxchamps.net/ieee1394/coriander) was used for imaging.After the program was calibrated for the 96 well plate the camera height was adjusted to focus on the bottom of the 96 well plate. The plate was then removed for needle calibration: the injection needle was fixed in the Injectman and moved, using the Injectman controller, into the center of the image. The injection height was set to 200μm above the bottom of the (virtual) plate. After the needle was moved up, the plate was placed back in position and the upper left well was used for multiple test injections to adjust pump pressure and injection time for optimization of the droplet size (~8nL ~ 300μm diameter) using video inspection. Subsequently, using a pre-defined macro defining x-y coordinates and number of injections per well, all wells were injected with the same pressure and injection time.

Microscopy and image analysis

Manually injected CS were monitored daily using a Nikon Eclipse E600 microscope. CS generated by automated injection were used for montage imaging using a Nikon TE2000 confocal microscope equipped with a Prior stage controlled by NIS Element Software and a temperature and CO2-controlled incubator. Differential interference contrast (DIC) images were captured using a charged coupled device (CCD) camera with NIS software at 10x dry objective. Quantification of CS invasion area was analyzed from DIC images using ImageJ. The CS ellipsoidal area after three days was estimated using the diameter in x and y axis (pi*radius-x*radius-y) occupied by cells in the 10x montage image in the mid-plane of each spheroid and normalizing to the occupied area 1h after injection. One-way ANOVA was performed to test the significance of the data. The data are presented and plotted as average and standard error of the mean. For automated imaging, wells containing gel-embedded spheroids were treated with a fixation and staining cocktail containing 3.7% paraformaldehyde, 0.2% Triton X-100 (Sigma) and 0.1 μM rhodamine Phalloidin (Sigma) for 3 hrs. Wells were washed extensively with PBS and plates were imaged on a Becton Dickinson Pathway 855 using a 4X lens. A montage of 12 frames was made for each Z plane, with a total of 24 Z planes at an interval of 50 μm. Image stacks were converted into 2D maximum fluorescence intensity projections using ImagePro 7.0. CS were then digitally segmented using ImageJ to identify the outline of individual CS and multiple parameters were measured, including Feret's diameter, roundness, and number of CS scored in each well. For immu-

nostaining of E-cadherin, gels were incubated for 30 mins with 5 µg/ mL collagenase (Clostridium histolyticum, Boehringer Mannheim) at room temperature, fixed with 4% paraformaldehyde, permeabilized in 0.2% Triton X-100, and blocked with 10% FBS. Gels were incubated with E-cadherin antibody (BD Transduction Laboratories) overnight at 4 degree celsius followed by Alexa 488-conjugated secondary antibody (Molecular Probes/Invitrogen) for 2 hrs at room temperature and Hoechst 33258 nuclear staining (Molecular Probes/Invitrogen) for 30 min at room temperature. Preparations were mounted in Aqua-Poly/Mount solution (Polysciences, Inc) and analyzed using a Nikon TE2000 confocal microscope. Z-stacks (~100 stacks, step of 1 µm) were obtained using a 20x dry objective, imported into ImageJ, and collapsed using extended depth of field plugin (Z projection) into a focused composite image.

Drug Treatment

LY-294002 (phosphatidylinositol 3-kinase), JSI-124-cucurbitacin (STAT3/Jak2), NSC23766 (Rac1), and AG-82 (general protein tyrosine kinases) were purchased from Merck/CalBiochem. PP2 (Src) and ML-7 (MLC kinase) were purchased from ENZO. Y-27632 (Rock), SB-431542 (TGFβ) and AG1478 (EGFR) were purchased from BioMol Tocris. Cell migration was analyzed in the absence and presence of inhibitors for 4 days.

ACKNOWLEDGMENTS

We thank ZF-screens B.V. (Leiden, NL) for permitted use of the microinjectorsystem, which was modified for this project, with the technical help of Fred Schenkel and Ewie de Kuyper (Department of Fine Mechanics). We thank Wies van Roosmalen and Sylvia le D.v.dec for mouse tumor biopsy material. We acknowledge financial support from the Netherlands Organization for Science (NWO; Cyttron project), the Dutch Cancer Society (project UL-2006- 3521), and EU FP7 (HEALTH-F2-2008-201439).

REFERENCES

1. Kenny PA, et al. The morphologies of breast cancer cell lines in three-dimensional assays correlate with their profiles of gene expression. Mol Oncol. 1: 84 - 96, (2007).

2. Fischbach C, et al. Engineering tumors with 3D scaffolds. Nat Methods 4: 855 - 860 (2007).

3. Mueller-Klieser W. Multicellular spheroids. J Cancer Res Clin Oncol 113: 101 - 122 (1987).

4. Sutherland RM. Cell and environment interactions in tumor microregions: the multicell spheroid model. Science, 240: 177 - 184 (1988).

5. Keller GM. In vitro differentiation of embryonic stem cells. Curr Opin Cell Biol, 7: 862 - 869 (1995).

6. Kelm JM, Timmins NE, Brown CJ, Fussenegger M & Nielsen LK. Method for generation of homogeneous multicellular tumor spheroids applicable to a wide variety of cell types. Biotechnol Bioeng, 83: 173 - 180 (2003).

7. Lee GY, Kenny PA, Lee EH & Bissell MJ. Three-dimensional culture models of normal and malignant breast epithelial cells. Nat Methods, 4: 359 - 365 (2007).

8. Loessner D, et al. Bioengineered 3D platform to explore cell-ECM interactions and drug resistance of epithelial ovarian cancer cells. Biomaterials 31: 8494 - 8506 (2010).

9. Buxboim A & Discher DE. Stem cells feel the difference. Nat Methods, 7: 695 - 697 (2010).

10. Friedl P & Wolf K. Plasticity of cell migration: a multiscale tuning model. J Cell Biol, 188: 11 - 19 (2010)

11. Levental KR, et al. Matrix crosslinking forces tumor progression by enhancing integrin signaling. Cell, 39: 891 - 906 (2009).

12. Lammermann T & Sixt M. Mechanical modes of ‘amoeboid’ cell migration. Curr Opin Cell Biol, 21: 636 - 644 (2009).

13. Haaf F, Sanner A & Straub F. Polymers of N-Vinylpyrrolidone: Synthesis, Characterization and Uses. Polymer J, 17: 143 - 152 (1985).

14. Ivascu A & Kubbies M. Rapid generation of single-tumor spheroids for high-throughput cell function and toxicity analysis. J Biomol Screen, 11: 922 - 932 (2006).

15. Ivascu A & Kubbies M. Diversity of cell-mediated adhesion in breast cancer spheroids. Int J Oncol, 31: 1403 - 1413 (2007).

16. Bjerkvig R, Tonnesen A, Laerum OD & Backlund EO. Multicellular tumor spheroids from human gliomas maintained in organ culture. J Neurosurg, 72: 463 - 75 (1990).

17. Bissell, M.J. The differentiated state of normal and malignant cells or how to define a “normal” cell in culture. Int Rev Cytol, 70: 27 - 100 (1981).

18. Walpita D & Hay E. Studying actin-dependent processes in tissue culture. Nat Rev Mol Cell Biol, 3: 137 - 141 (2002).

19. Corcoran A, et al. Evolution of the brain tumor spheroid model: transcending current model limitations. Acta Neurochir, 145: 819 - 824 (2003).

20. Beliveau A, et al. Raf-induced MMP9 disrupts tissue architecture of human breast cells in three dimensional culture and is necessary for tumor growth in vivo. Genes Dev, 15: 2800 - 2811 (2010).

21. Sahai E & Marshall CJ. Differing modes of tumor cell invasion have distinct requirements for Rho/ROCK signalling and extracellular proteolysis. Nat Cell Biol, 5: 711 - 719 (2003).

22. Pampaloni F, Reynaud EG & Stelzer EH. The third dimension bridges the gap between cell culture and live tissue. Nat Rev Mol Cell Biol, 10: 839 - 45 (2007).

23. Friedrich J, Ebner R & Kunz-Schughart LA. Experimental anti-tumor therapy in 3-D: spheroids--old hat or new challenge? Int J Radiat Biol, 83: 849 - 871 (2007).

24. Kunz-Schughart LA, Freyer JP, Hofstaedter F & Ebner R. The use of 3-D cultures for high-throughput screening: the multicellular spheroid model. J Biomol Screen, 9: 273 - 285 (2004).

25. Mueller-Klieser,W. Three-dimensional cell cultures: from molecular mechanisms to clinical applications. Am J Physiol, 273: C1109 - 1123 (1997).

26. Mueller-Klieser,W. Tumor biology and experimental therapeutics. Crit Rev Oncol Hematol, 36: 123 - 139 (2000).

27. Bott K, et al. The effect of matrix characteristics on fibroblast proliferation in 3D gels. Biomaterials, 32: 8454 - 8464 (2010).

28. Sung KE, et al. Control of 3-dimensional collagen matrix polymerization for reproducible human mammary fibroblast cell culture in microfluidic devices. Biomaterials, 27: 4833 - 4841 (2009).

29. Cross VL, et al. Dense type I collagen matrices that support cellular remodeling and microfabrication for studies of tumor angiogenesis and vasculogenesis in vitro. Biomaterials, 31: 8596 - 8607 (2010).

30. Zaman MH, et al. Migration of tumor cells in 3D matrices is governed by matrix stiffness along with cell-matrix adhesion and proteolysis. Proc Natl Acad Sci, 103: 10889 - 1089(2006).

31. Rosso F, et al. Smart materials as scaffolds for tissue engineering. J Cell Physiol, 203: 465 - 470 (2005).

32. Peppas, NA, Hilt JZ, Khademhosseini A & Langer R. Hydrogel in Biology and Medicine: From Molecular Principles to Bionanotechnology. Adv. Mater, 18: 1345 - 1360 (2006).

33. Danen EH, Sonneveld P, Brakebusch C, Fassler R & Sonnenberg A. The fibronectin- binding integrins alpha5beta1 and alphavbeta3 differentially modulate RhoA-GTP loading, organization of cell matrix adhesions, and fibronectin fibrillogenesis. J Cell Biol, 159: 1071 - 1086(2002).

34. Rajan N, Habermehl J, Cote M, Doillon CJ, & Mantovani D. Preparation of ready-touse, storable and reconstituted type I collagen from rat-tail tendon for tissue engineering applications. Nat Protocols, 1: 2753 - 2758 (2007).

CHAPTER 3

AUTOMATED WHOLE ANIMAL BIO-IMAGING ASSAY FOR HUMAN CANCER DISSEMINATION

Veerander PS Ghotra[1], Shuning He[2], Hans de Bont[1], Wietske van der Ent[2], Herman P. Spaink[2], Bob van de Water[1], B Ewa Snaar-Jagalska[2], Erik HJ Danen[1]

Published in PloS one. 2012;7:e31281

[1]Division of Toxicology, Leiden Academic Center for Drug Research, Leiden University, Einsteinweg 55, 2333 CC, Leiden,The Netherlands;[2]Institute of Biology, Leiden University, Einsteinweg 55, 2333 CC, Leiden, the Netherlands.

ABSTRACT

A quantitative bio-imaging platform is developed for analysis of human cancer dissemination in a short-term vertebrate xenotransplantation assay. Six days after implantation of cancer cells in zebrafish embryos, automated imaging in 96 well plates coupled to image analysis algorithms quantifies spreading throughout the host. Findings in this model correlate with behavior in long-term rodent xenograft models for panels of poorly- versus highly malignant cell lines derived from breast, colorectal, and prostate cancer. In addition, cancer cells with scattered mesenchymal characteristics show higher dissemination capacity than cell types with epithelial appearance. Moreover, RNA interference establishes the metastasis-suppressor role for E-cadherin in this model. This automated quantitative whole animal bio-imaging assay can serve as a first-line in vivo screening step in the anti-cancer drug target discovery pipeline.

INTRODUCTION

Traditional anti-cancer drug screens are performed using cell lines grown in 2D culture or using in vitro protein binding assays. Cancer progression, however, is a complex process of dynamic interactions between cancer cells and the organism that involves genetic alterations leading to deregulated survival and proliferation, angiogenesis, invasion, and metastasis (1). Ideally, genes that play a role in this process are identified by in vivo ablation or silencing. Although genetic mouse models for cancer and human tumor cell xenotransplantation models in rodents remain essential, such systems are costly, slow, and less amenable to high-throughput assays for cancer drug target discovery. There is a clear need to develop fast, semi-automated in vivo systems for medium to high-throughput screening applications in preclinical target discovery and lead compound identification.

In this respect, zebrafish (ZF) offer a number of unique advantages for investigating the mechanisms that drive cancer formation and progression. ZF are vertebrates that can be raised in large numbers in a cost-effective manner. An almost complete genome sequence reveals that most cancer genes and tumor suppressor genes are highly conserved between ZF and humans, and ZF form spontaneous tumors with similar histopathological and gene expression profiles as human tumors (2-4). Importantly, xenotransplantation with human cancer cells is possible (5,6). ZF embryos that are used for this purpose lack an adaptive immune system, which increases the success of xenotransplantation while they provide a microenvironment where human tumor cells proliferate, migrate, form tumor masses, and stimulate angiogenesis (5-8). ZF embryos are particularly useful for semi high-throughput microscopic analysis platforms as they are translucent, and can be maintained in 96 well plates. The optical transparency of ZF offers exciting research opportunities allowing visualization of the metastatic process at high resolution (8,9). Recent findings indicate that a wide range of pharmaceutically active compounds illicit physiological responses in ZF embryos and inhibit disease development similar to effects in mammalian systems (10-12). These findings underscore the potential for a ZF embryo xenotransplantation model to be used in the anti-cancer drug discovery process. However, at this time, using ZF to screen for cancer relevant drug - and gene targets is limited by the lack of comprehensive automated bioassays. Here, we applied automated imaging and image analysis procedures to a ZF xenotransplantation model to develop the first semi-automated whole-organism quantitative bio-imaging assay for analyzing cancer dissemination in a vertebrate.

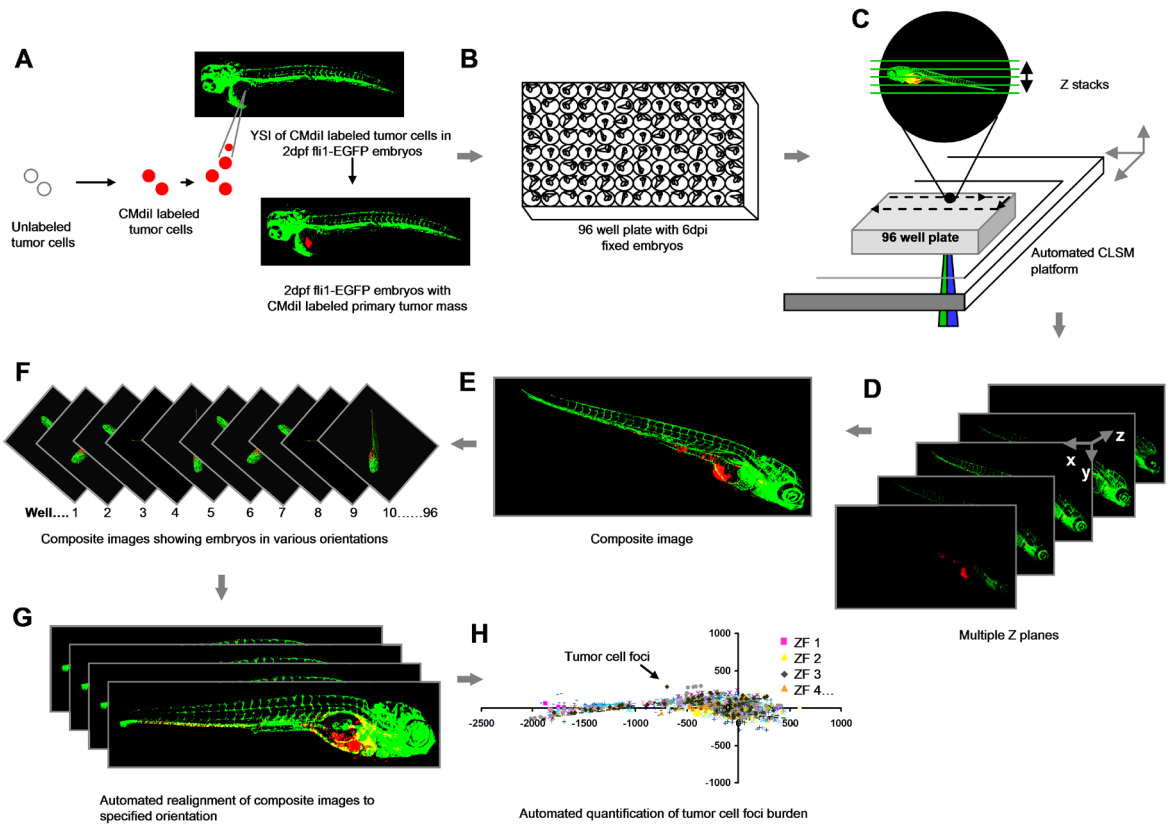

FIGURE 1. *Schematic overview of the procedure*. (A) Yolk sac implantation of CM-DiI labeled tumor cells into Tg (Fli:EGFP) ZF embryos 2 days post-fertilization. (B) Formaldehyde fixed 6dpi embryos arrayed in 96 well plates. (C) Automated image acquisition using CLSM platform equipped with movable stage captures multiple Z stacks per embryo using 488 and 561 nm laser lines. (D and E) Automated creation of extended depth composite images. (F) Multiple extended depth images depicting embryos lying in different lateral orientations. (G) Automated uniform reorientation of images. (H) Scatter plot representing tumor foci burden in multiple embryos belonging to one experimental condition.

RESULTS

We developed a noninvasive, quantitative whole animal bio-imaging method for dissemination of xenotransplanted human cancer cells in ZF embryos in 96-well format. All the steps are briefly outlined in Figure 1.

Automated image capturing and pre-processing

CMDiI-labeled tumor cells were injected in the yolk sac of 2-day-old fli-EGFP embryos (13) and fixed 6 days post-implantation (dpi) (Figure 1A). Fixed embryos were arrayed in 96 well glass bottom plates for automated imaging (<5 minutes per plate) (Figure 1B). Epi-fluorescence microscopy failed to detect disseminated tumor cells due to excessive background from the primary tumor mass. Therefore, using a confocal laser-scanning microscope (CLSM) combined with an automated stage; multiple z stacks per embryo were captured for each well in a fully automated procedure (Figure 1C, 1D and Video S1). Confocal images were

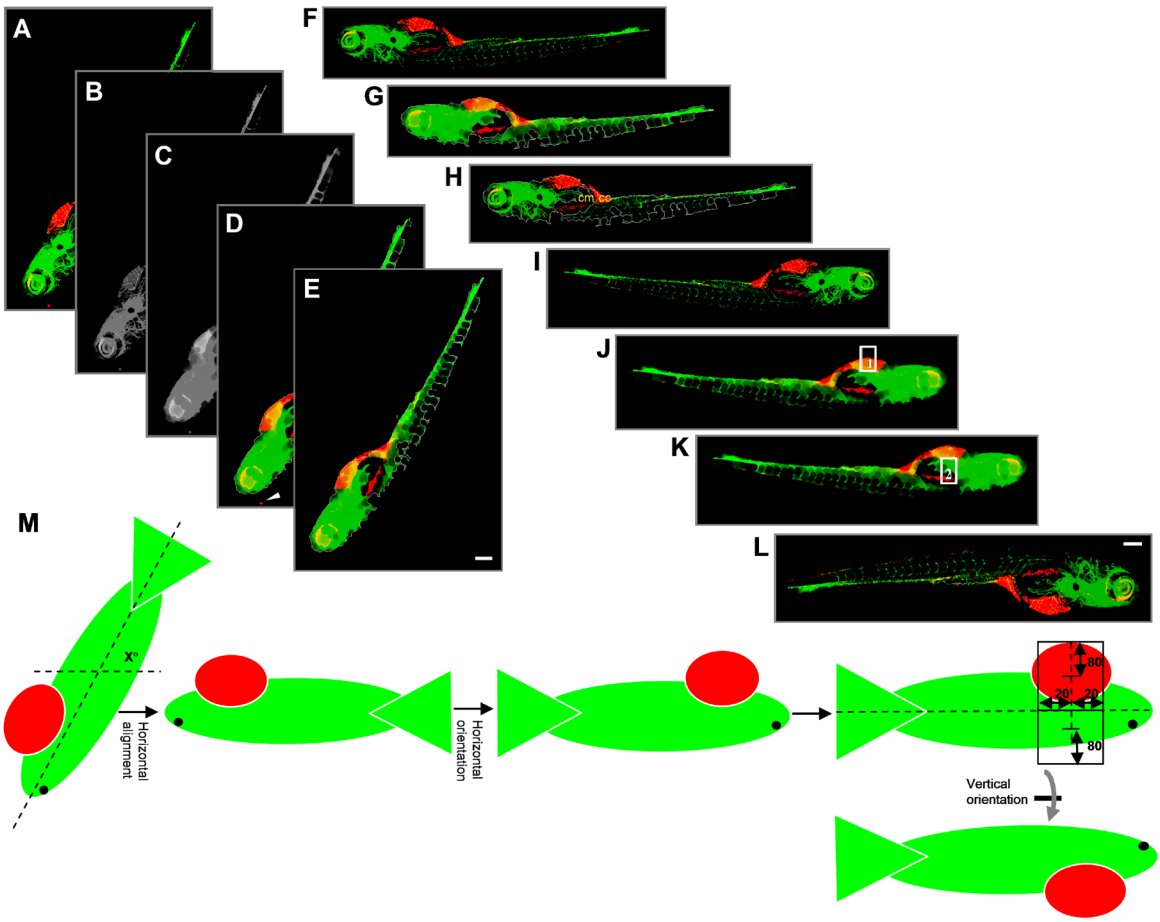

FIGURE 2. *Outline of steps involved in embryo orientation*. (A) Extended depth image of 6dpi ZF embryo. (B) Grey value image from combination of green and red channels. (C) Blurred grey image after applying closing filter to optimize determination of outline. (D) Embryo segmented after applying intensity threshold and area filter. Arrowhead indicates a red object outside the outline that is excluded from segmentation. (E) Cropped image with only selected object. (F) Embryo rotated by x° for horizontal reorientation. (G and H) Determination of the x position value of the center of mass (cm) and center of centroid (cc). (I) Horizontal flip of the image only if cm is on the left side of cc, resulting in images with the head of the embryo always to the right side. (J) Image after applying closed filter to the combined green and red channel to get the outline of the embryo. Point lying at 75% distance from the extreme left of the embryo outline is calculated. Y-axis is drawn at this X-position from upper to lower outline. Upper rectangle 1 is drawn. (K) Lower rectangle 2 is drawn. (L) Vertical flip of the image only if red intensity in rectangle 1 is higher than in rectangle 2. (M) Schematic representation of calculations for steps E-I. Altogether, this procedure results in images where the head is on the right and the yolk sac is on the bottom of the image. Scale bar = 200µm in E and I.

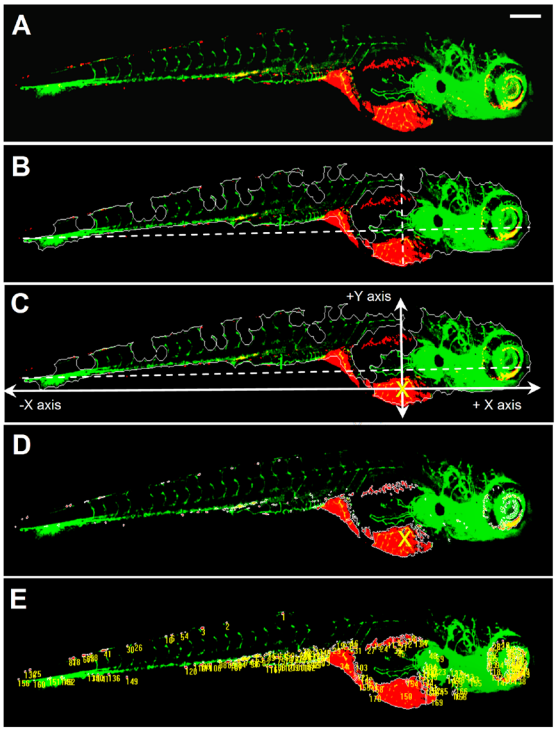

F

Total tumor cell foci	170					
Mean Distance	761					
Mean Intensity	85					
Mean Area	222					
Cumulative distance	129463					
Number	**1**	**2**	**3**	**4**	**5.....170**	
X position	-769	-1116	-1266	-1371	-1395	
Y position	404	359	331	310	306	
Migrated distance (µm)	869	1173	1309	1406	1428	
Intensity	113	74	126	38	92	
Area	68	34	106	18	31	

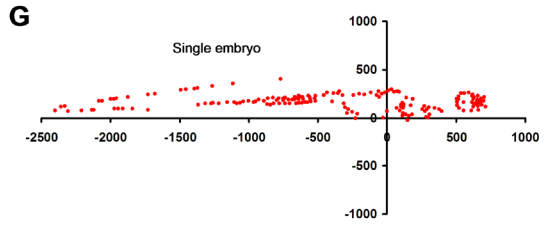

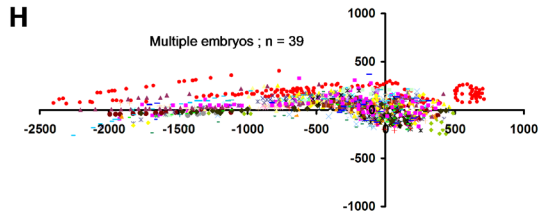

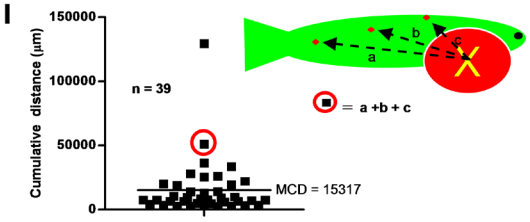

FIGURE 3. *Automated multiparametric quantification of PC3 tumor foci*. (A) Extended depth image of 6dpi fixed embryo after realignment. (B) Embryo outline from segmented GFP channel and Y-axis intersecting X-axis at 75% from extreme left. (C) Calculated injection point at 75% distance from the extreme left and 75% from the top Y position. (D) Segmented red channel showing tumor foci burden in the embryo. (E) Identified tumor foci. (F) Multiple parameters of tumor foci burden calculated per embryo. Each number in the image corresponds to one tumor focus. (G) Tumor foci dissemination in a single embryo represented as scatter plot (coordinates 0,0 represents calculated injection site). (H) Combined scatter plot showing tumor foci dissemination from 39 injected embryos. (I) Quantification of cumulative distance (CD). Each filled square represents cumulative distance from injection point of all identified tumor foci in a single embryo. Mean cumulative distance (MCD) in the 39 injected embryos in this experiment is 15024 m. Scale bar = 200µm in A.

automatically converted into extended depth composite images (Figure 1E) that were rearranged to a uniform orientation (Figure 1F and G) to allow for automated quantitative image analysis (Figure 1H).

Automated multiparametric analysis of cancer cell dissemination

Having established conditions for automated imaging and image pre-processing of tumor cell implanted ZF embryos; we subsequently developed an algorithm for automated analysis of tumor foci burden in the post-processed ZF images. For this, Image-Pro based software was developed, which performed essentially three major functions (see materials and methods section for detailed information on the macro's). 1) Reorientation of the images (Figure 2): all embryos were automatically reoriented to a horizontal orientation, with the head towards the right and the yolk sac towards the bottom. 2) Determination of the injection position of labeled tumor cells (Figure 3A-C): the injection position was calculated from the images based on the segmented GFP channel (and confirmed by visual inspection using the red channel). 3) Detection of tumor foci (Figure 3D and E): The red channel was segmented using an intensity threshold and minimum and maximum area filters. Data were exported to excel and multiple numerical parameters were calculated to describe the tumor cell burden per embryo. These included total number of tumor foci, average distance of tumor foci from the injection site, and cumulative distance travelled from the injection site (Figure 3F). As only the cumulative distance parameter combined number of disseminated cells with their distance from the injection site, we reasoned that this parameter best reflected the tumor dissemination capacity (Figure S1). Data were represented as graphs displaying positions of tumor foci relative to the injection point (at coordinates x,y = 0,0) for each embryo (Figure 3G) or all embryos of a single experimental condition (Figure 3H). From these data, cumulative distance of all detected tumor foci was calculated per embryo (CD) and subsequently averaged for all injected embryos in one experimental group as a final quantitation of tumor cell dissemination (mean cumulative distance (MCD) (Figure 3I and S1). We performed experiments to determine the earliest time point that allowed robust discrimination between poorly aggressive and highly aggressive cell lines. Using LNCaP and PC3 as such an example for prostate cancer (14-19) we observed no difference at 2 dpi; MCD of PC3 could be distinguished from MCD of LNCaP at 4 dpi; and at 6 dpi MCD was markedly higher in PC3 compared to LNCaP with strong significance (Figure 4). Therefore, 6 dpi was chosen for analysis in all further experiments.

To characterize tumor foci identified by this method, we calculated the mean diameter of segmented red objects in the tail region of PC3 implanted embryos. The average mean diameter was ~15µm with some larger objects up to ~45µm but no objects with average diameter <8µm being selected for the analysis, fitting with the identification of individual tumor cells or small clusters (Figure 5A). We further analyzed identified tumor foci by high-resolution imaging, 3D reconstruction, and surface rendering (Figure 5B and Video S2). This confirmed and extended the finding that single tumor cells or small clusters were identified by the automated image analysis and showed tumor cells interacting with the host vasculature (Figure 5B). To rule out artifacts due to CMDiI labeling, we injected mCherry labeled PC3 cells. In complete agreement with the properties of red objects identified after injection of CMDiI-labeled PC3, individual PC3-mCherry cells were observed in close association with host blood vessels (Figure 5C and Video S3). Finally, experiments using unimplanted embryos (Figure 6A) and comparison of CM-DiI-labeled PC3 cells injected into standard fli-

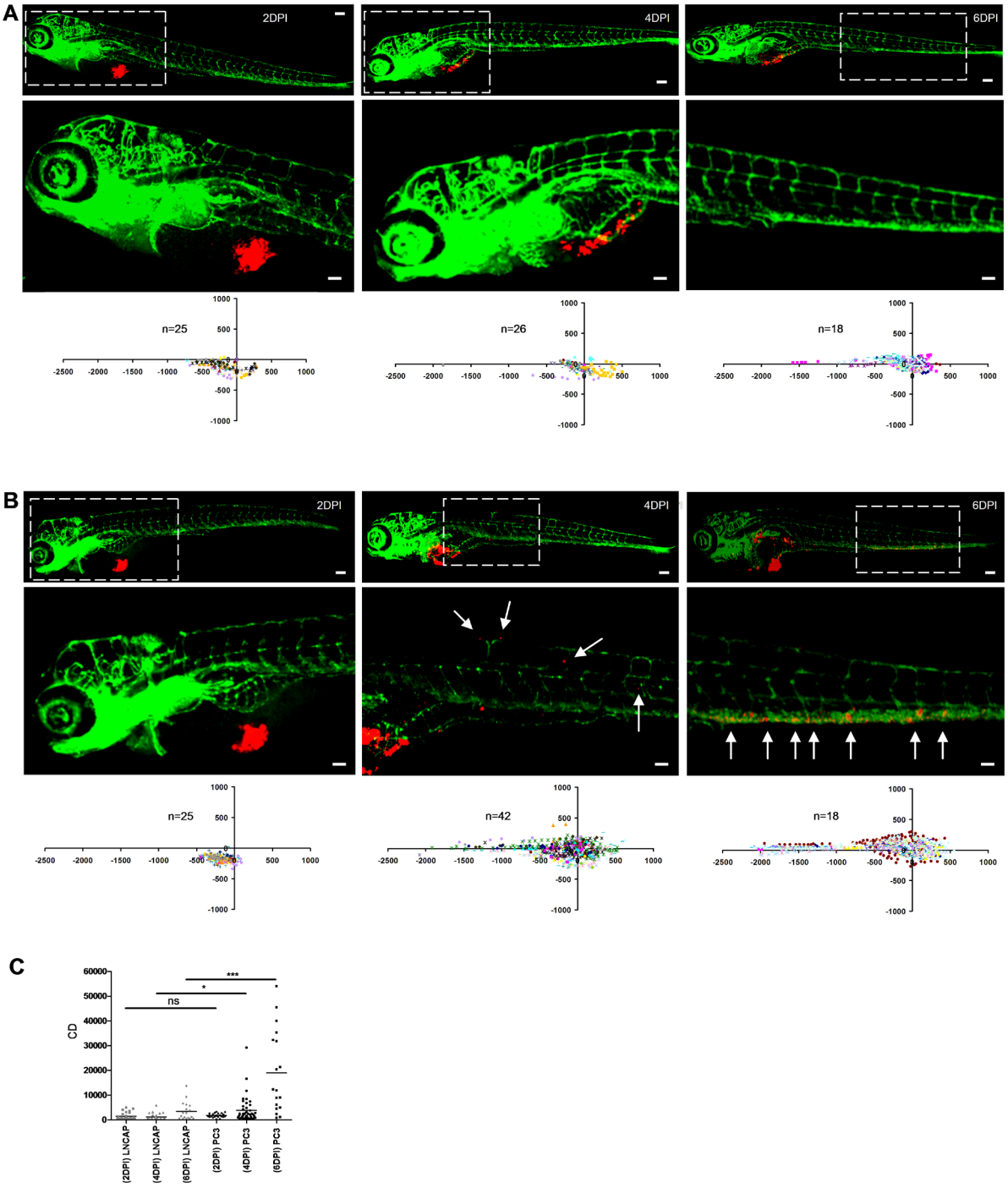

FIGURE 4. *Determination of cancer cell dissemination kinetics*. (A and B) LNCaP (A) or PC3 cells (B) were implanted and embryos were fixed at 2, 4, or 6 dpi for imaging (immunofluorescence images and automated image analysis (scatter plots). Bottom row images (scale bar = 50 µm) show zoom-in of area marked by dotted line in top row images (scale bar = 100 µm). (C) CD at 2, 4 and 6 dpi for LNCaP (grey) and PC3-injected embryos (black) calculated from scatterplots in A and B, respectively. Statistical testing for difference between LNCaP and PC3 at different dpi is indicated. *p<0.05, ***p<0.001.

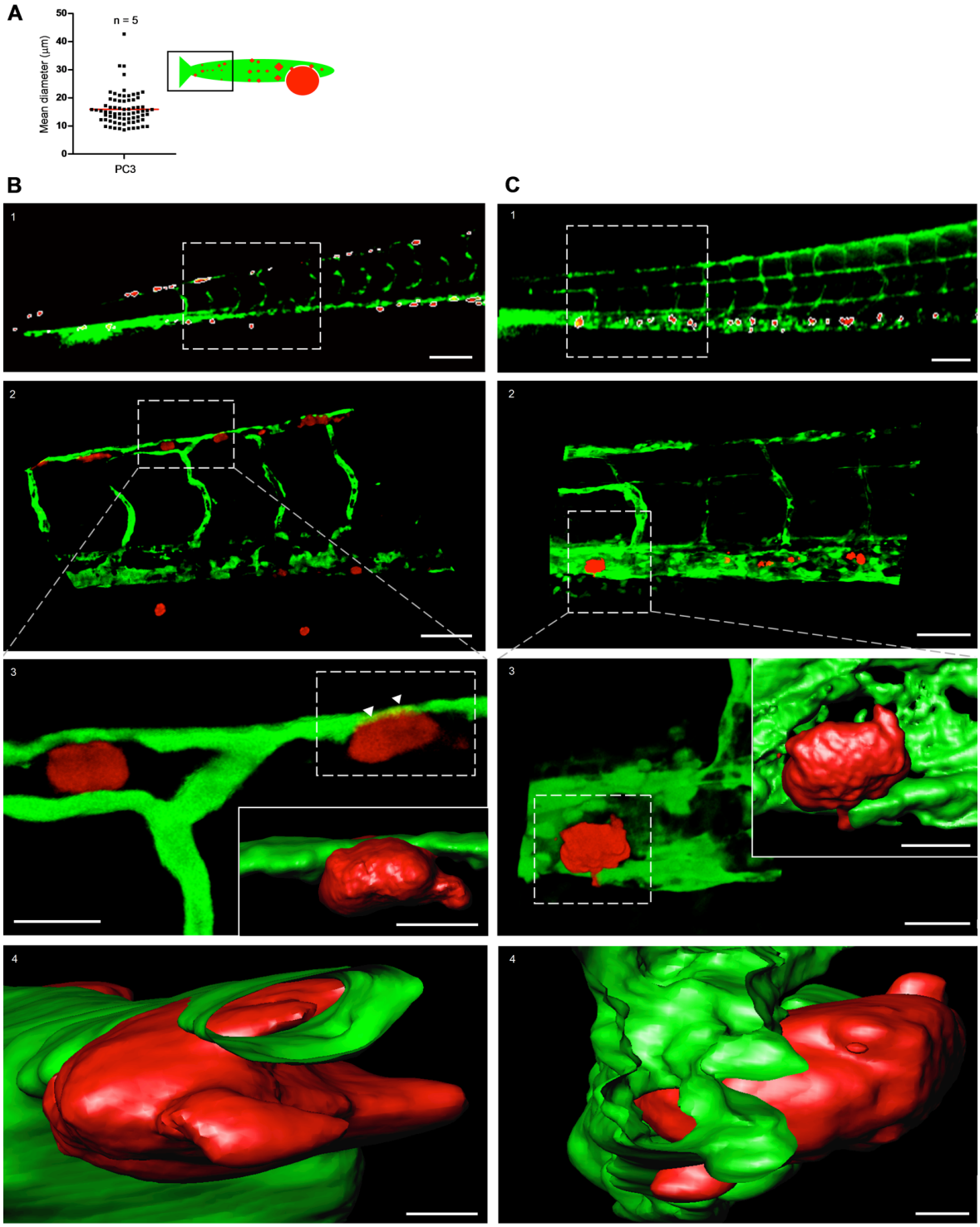

FIGURE 5. *Characterization of tumor cell foci identified by macro using high-resolution imaging*. (A) Quantification of the mean diameter of macro-identified tumor cell foci from the tail region of PC3-injected embryos. Data obtained from 5 embryos. (B) High resolution imaging of CM-DiI-labeled PC3 tumor cell foci. (B1) Macro-identified PC3 tumor cell foci. (B2) Zoom-in on area indicated in B1 shows tumor cells in association with host vasculature. (B3 and B4) Three dimensional reconstruction and surface rendering of area in insert of B2; arrowheads point to tumor cell partly inside distal longitudinal anastomotic vessel (Video S2 and S3). (C) High resolution imaging of PC3-mCherry tumor cell foci. C1-4, as B1-4 for PC3-mCherry. Scale bar is 100 µm in B1 and C1; 50 µm in B2 and C2; 15 µm in B3 and C3; 10 µm in insets in B3 and C3; 5 µm in B4 and C4.

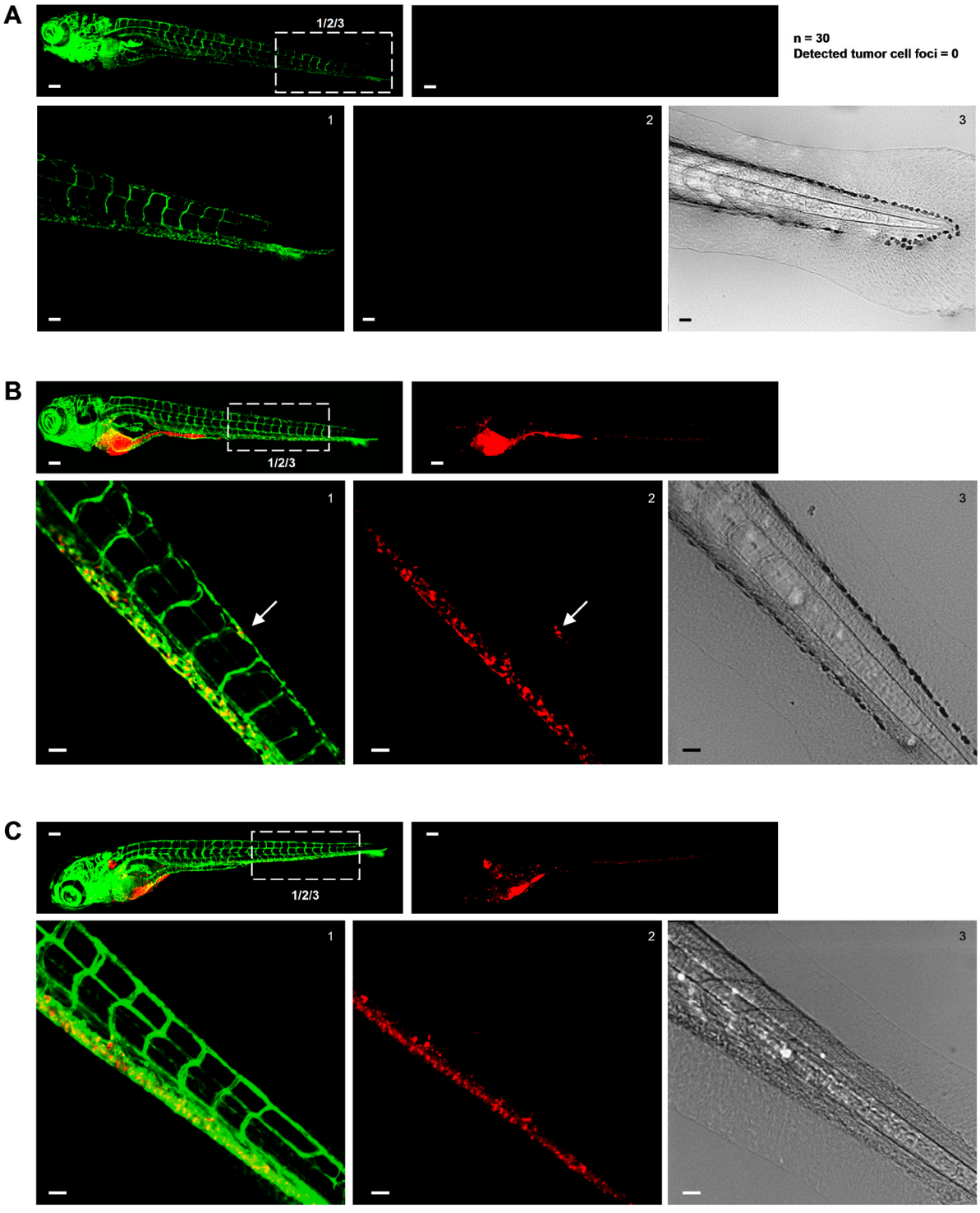

FIGURE 6. *Excluding disturbance of the image analysis by autofluorescence signal from pigment cells.* (A-C) In each case top left image shows green signal (Fli-EGFP) and top right image shows red signal for tumor cells. Bottom images show zooms of boxed area in top left image providing green (left) and red signal (middle) and transmitted light (right). Scale bar is 100 µm in images showing whole embryo and 50 µm in zoomed images. (A) Non-implanted fli-EGFP embryo imaged at 8 days post fertilization. Number of non-implanted embryos and number of tumor cells (falsely) detected by automated imaging and image analysis method is indicated at the right. (B) Fli-EGFP embryo implanted with CM-DiI-labeled PC3 imaged at 6 dpi. (C) Fli-EGFP Casper embryo implanted with CM-DiI-labeled PC3 imaged at 6 dpi.

EGFP or Casper fli-EGFP embryos lacking all pigments (Figure 6B and C), ruled out any false positives due to autofluorescence of pigment cells. Taken together, this method eliminates the need for visual scoring and enables automated generation and archiving of images and numerical data describing dissemination of tumor cells in a vertebrate organism. Moreover, for tumor cells identified by this automated bio-imaging assay, tumor-host interactions can be further studied in detail by high-resolution microscopy.

Assay validation: correlation with behavior in mouse models and epithelial versus scattered phenotype

To demonstrate the applicability of our automated platform to differentiate between poorly aggressive and highly aggressive cancer cells, three different panels of cell lines were analyzed: 1) For prostate cancer, PC3 (highly metastatic in mouse models; prostate carcinoma / bone metastasis; androgen independent; scattered growth in 2D culture; mesenchymal markers) and LNCaP (very poorly metastatic in mouse models; prostate carcinoma / lymph node; expression of prostate differentiation markers; epithelial islands in 2D culture; epithelial markers) were analyzed (14-19). 2) For breast cancer, BT474 (metastatic in mouse models; breast invasive ductal carcinoma / duct; ER+/PR+/p53mutated; high Her2 expression; “weakly luminal epithelial like” phenotype in culture; reduced expression of epithelial markers) and MCF7 (very weak metastatic potential in the absence of ectopically expressed oncogenes; breast adenocarcinoma / pleural effusion; ER+/PR+/p53 normal; low Her2; epithelial islands in 2D culture; epithelial markers) were analyzed (20-23). 3) For colorectal cancer, SW620 (colorectal adenocarcinoma Dukes’ type C / lymph node metastasis; scattered growth in 2D culture; mesenchymal markers) and HT29 (colorectal adenocarcinoma / colon; epithelial islands in 2D culture; epithelial markers) were analyzed (24). Strikingly, for each cancer type tested, dissemination in this ZF xenograft assay significantly correlated with metastatic capacity reported in mouse models and/or characteristics known to be associated with cancer progression including differentiation markers or epithelial versus scattered phenotype (Figure 7A and B; Figure S2). These data validate this short-term automated bio-imaging method and show that it represents a powerful tool to predict aggressiveness of cancer cells in more complex, long-term in vivo systems.

Extensive ZF cellular movement takes place in the region of the yolk sac, where intestinal development occurs within the time frame of our analysis (25). We wanted to exclude any influence of passive migration of implanted tumor cells due to this developmental process near the primary implantation area. For this reason, we expanded the macro with an additional step in which all tumor foci within a square encompassing this region were excluded from the analysis in an unbiased automated fashion (Figure 7C and D). Although this may lead to underestimation of the cumulative distance parameter, we found that this exclusion step even further widened the window between the non-aggressive versus highly aggressive cell types (Figure 7E). Moreover, analysis of several independent experiments using PC3, BT474, and MCF7, demonstrated that this methodology is highly reproducible (Figure 7F). We expanded the analysis to a broader panel of human cancer cell lines from different origins including prostate, breast, lung, colorectal, skin, and connective tissue. Interestingly, when these lines were grouped according to their morphology in 2D culture and expression of epithelial or mesenchymal markers, there was a clear correlation of high dissemination with a scattered phenotype (one notable exception was HT1299, which did not disseminate effectively); all cell lines growing as epithelial islands had very low dissemination capacity (Figure 8A; Table S1). We function-

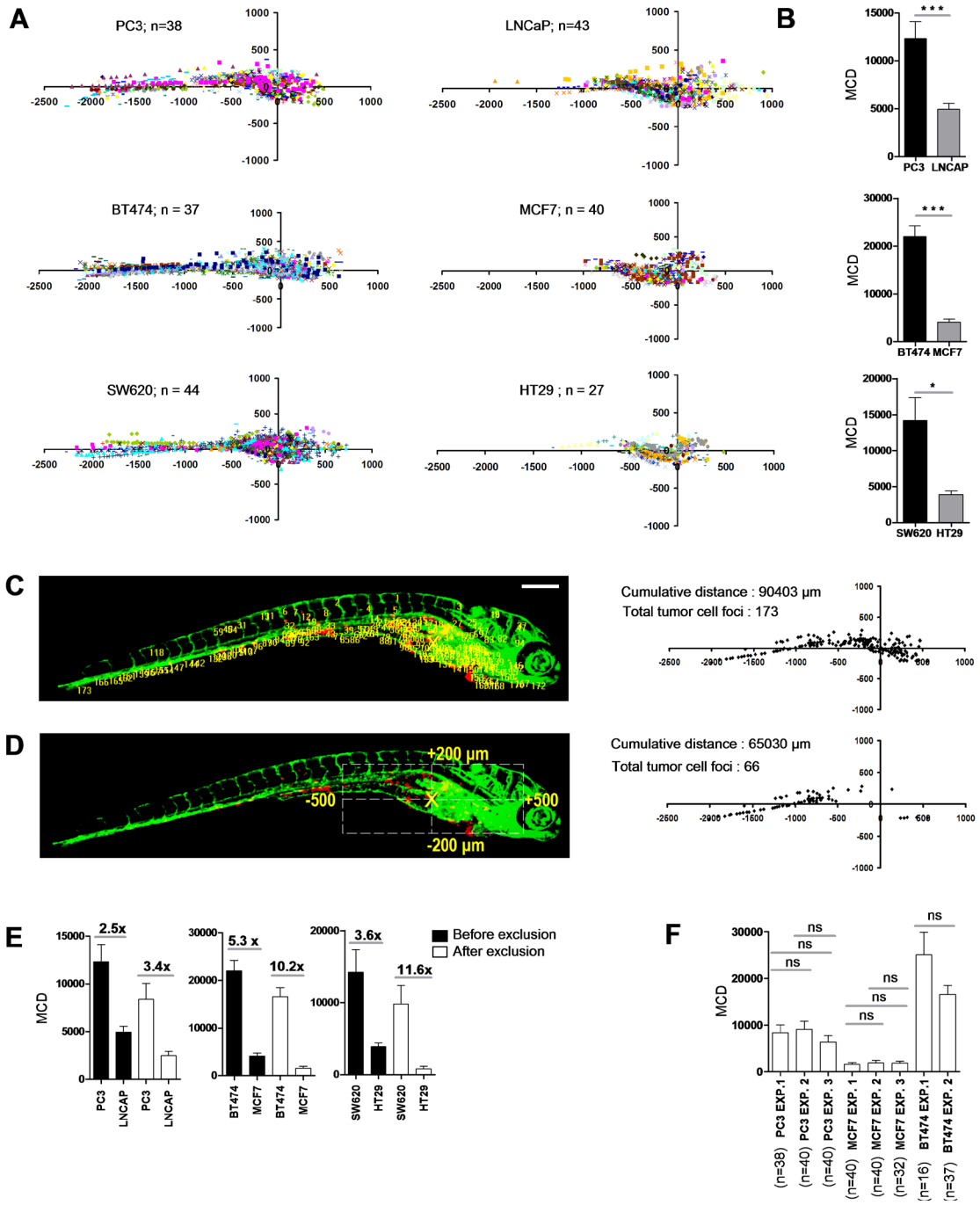

FIGURE 7. *Differentiation between poorly and highly aggressive human cancer cell lines using automated bioimaging assay.* (A) Scatter plot representation of tumor cell dissemination for indicated prostate (upper graphs), breast (middle), and colorectal cancer cell lines (lower graphs). Number of injected embryos from 2 biological replicates is indicated. (B) MCD determined from data represented in A. Data are presented as mean ± s.e.m. *p<0.05, ***p<0.001. (C) 6dpi embryo injected with PC3 showing tumor foci burden determined from segmented red channel (left), and represented as scatter plot (right). (D) Automated determination of region for exclusion of tumor foci around implantation site and in area of intestinal development (left), and remaining tumor foci represented as scatter plot (right). (E) MCD before (black) and after exclusion (white bars) for the indicated prostate (left), breast (middle), and colorectal cancer lines (right graph). Fold difference between poorly and highly aggressive cell lines is indicated. Data are presented as mean ± s.e.m. *p<0.05, ***p<0.001. (F) MCD after exclusion for PC3 and MCF7 in multiple independent experiments demonstrates reproducibility. Data are presented as mean ± s.e.m.

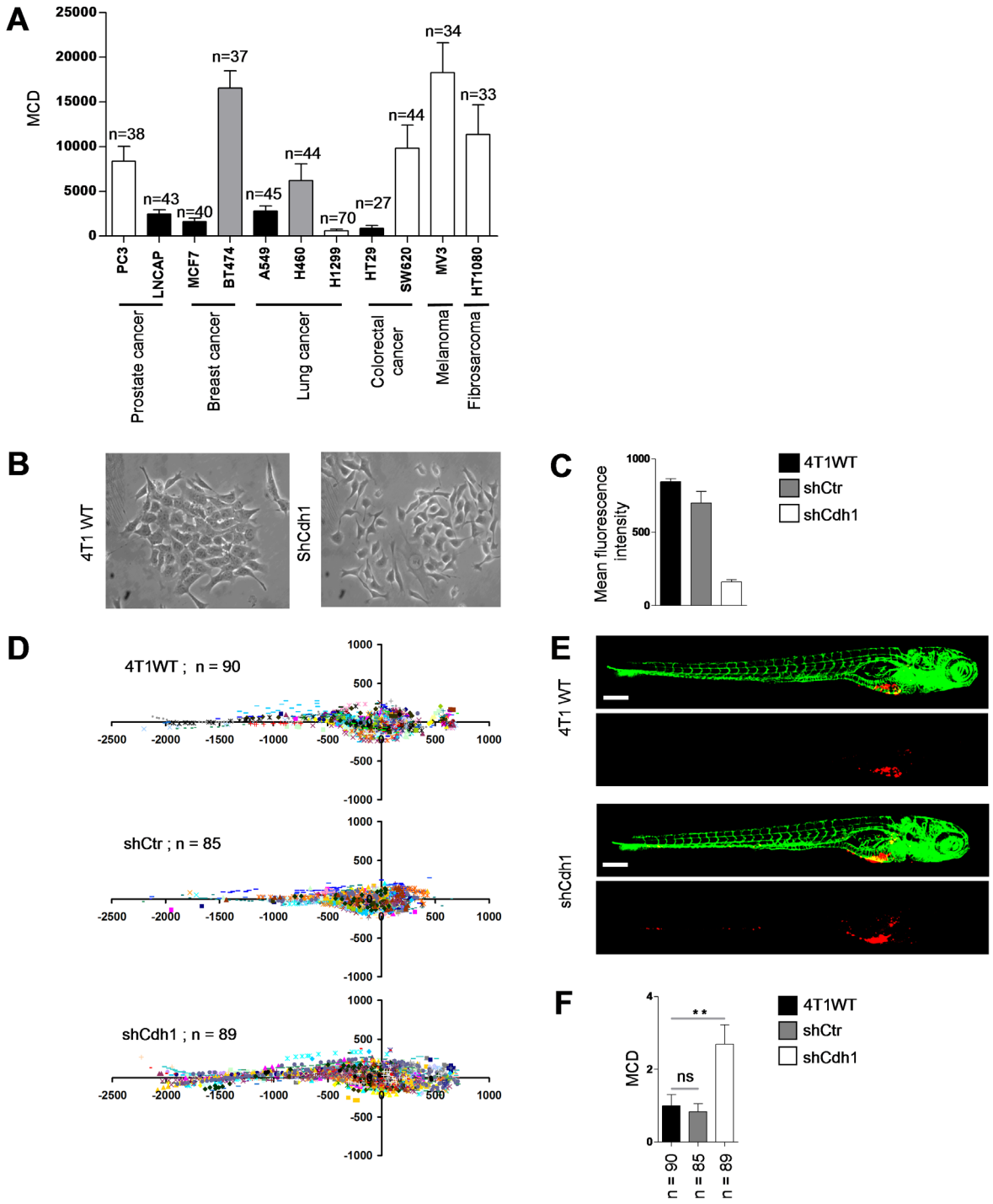

FIGURE 8. *Differentiation between epithelial and mesenchymal cell types using the automated bioimaging assay.* (A) MCD in a panel of human cancer cell lines from different origins. Number of injected embryos is indicated. White bars indicate cell lines showing a scattered phenotype in 2D cell culture. Black bars indicate cell lines growing as epithelial islands in 2D culture. Grey bars indicate cell lines with intermediate/mixed epithelial/mesenchymal characteristics. (B) 4T1 breast cancer cells growing as islands of loosely attached spindle-shaped cells (left) and completely scattered growth of 4T1 cells following E-cadherin silencing (right). (C) E-cadherin surface expression by FACS. (D) Scatter plot representation of indicated 4T1 variants. Number of injected embryos from 2 independent experiments is shown. (E) Representative images of embryos injected with indicated 4T1 variants. (F) MCD determined from data represented in D. Data are presented relative to wild type 4T1 as mean ± s.e.m. **p<0.01. Scale bar is 200 µm in E.

- ally tested the role of one typical marker of the epithelial phenotype, the cell-cell adhesion receptor E-cadherin. For this, we used 4T1 mouse breast carcinoma cells that possess an intermediate phenotype, growing as clusters of loosely attached cells in 2D and expressing E-cadherin as well as some mesenchymal markers such as vimentin (Figure 8B). E-cadherin was silenced resulting in a fully scattered phenotype in 2D (Figure 8B and C) and these cells were injected in ZF to determine dissemination capacity. Indeed, shRNA targeting E-cadherin but not control shRNA strongly increased dissemination of 4T1 cells and the automated bio-imaging method allowed significant separation between 4T1shCdh1 on the one hand and 4T1Wt and 4T1shCtr on the other (Figure 8D-F).

Altogether, a short–term medium throughput fully automated whole-organism bio-imaging model has been developed that distinguishes with good reproducibility cancer cell types that grow as islands or have epithelial markers or have been shown to be poorly aggressive in mouse models from cell lines that are scattered or have more mesenchymal characteristics or are known to metastasize in mice. It is compatible with RNAi for identification of regulators of cancer cell dissemination and allows switching from low-resolution fast imaging to high-resolution detailed analysis to study effects on tumor cell properties or tumor cell-host interactions.

DISCUSSION

Here, we developed a short term in vivo ZF xenograft assay that is compatible with automated imaging in 96 well plates and coupled to fully automated analysis of tumor cell dissemination. This assay represents the first automated whole organism bioimaging assay in a vertebrate that allows for studying aspects of cancer progression. Our findings show that this assay closely reflects the results obtained in more expensive and much lower throughput assays such as rodent xenografts. The ZF xenograft model has been previously applied to cancer migration studies (5-9). There are limitations to this model, including potential differences in the host microenvironment and the need to work at temperatures that are compatible with survival and migration of mammalian cells while at the same time being favorable for normal ZF physiology. Nevertheless, we have modified experimental conditions such that behavior of a large panel of human cancer cell lines from various origins closely resembles known behavior in rodent models. Moreover, our work provides this model with the automation in imaging and image analysis as well as with the statistical power required for application in screening procedures. We provide proof-of-principle for such applicability by testing a known regulator of cancer cell migration. Using a panel of cell lines we show that this imaging platform can discriminate between cell types with more epithelial characteristics or growing in islands versus those with more mesenchymal characteristics or displaying a scattered phenotype. We then combine the assay with RNAi to silence the cell-cell adhesion molecule, E-cadherin. We rapidly obtain data from ~90 animals per experimental group in two biological replicates supporting the inhibitory role of E-cadherin in cancer dissemination.

Taken together, this relatively fast medium throughput assay may be used as a first in vivo analysis platform in the target discovery pipeline. It provides the automation and statistical power to identify those hits from large-scale in vitro RNAi screening efforts that warrant more time- and money-consuming studies in mouse models. Future directions will include incorporation of similarly automated analysis of induction of tumor angi-

ogenesis and tumor cell proliferation to capture multiple aspects of cancer progression within this bio-imaging assay.

MATERIALS AND METHODS

Cell lines and ZF handling

All human cancer cell lines were obtained from ATCC and cultured according to the provided protocol. ZF and embryos were raised, staged and maintained according to standard procedures in compliance with the local animal welfare regulations. The transgenic ZF line Tg (fli1:EGFP) expressing EGFP in endothelial cells in wild type or “Casper” background, was maintained according to standard protocols (http://ZFIN.org). PC3-mCherry cells were generated using a pCMV-mCherry-bc-puro-KI201 lentiviral vector (provided by Dr. R.C. Hoeben, Leiden University Medical Center, Leiden NL). 4T1-shCdh1 and 4T1-shCtr cells were generated by lentiviral transduction using TRC shRNA constructs (Sigma).

Implantation procedure

Mammalian cells were labeled with lipophilic fluorescent cell tracker (CM-DiI; excitation maximum 553 nm, lot no. C7000; Invitrogen) according to the manufacturers instructions. The labeled cell suspension was loaded into borosilicate glass capillary needles (1mm O.D. x 0.78mm I.D.; Harvard Apparatus) and the intray-olk injections were performed using a Pneumatic Pico pump and a manipulator (WPI). Dechorionated 2 days post-fertilization ZF embryos were anesthetized with 0.003% tricaine (Sigma) and positioned on a 10cm petridish coated with 1% agarose. By controlling injection pressure and duration the number of injected cells was set at ~100 per embryo as determined by standard cell counting of injection droplets. Injected embryos were maintained in egg water at 34°C and fixed 6 dpi with 4% paraformaldehyde.

Automated microscopy and high-resolution imaging

Fixed embryos were manually arrayed into 96 well glass bottom plates (material no.655892; Greiner) with each well containing a single embryo. This was easily done in <5 min per plate. Image acquisition was performed by using a Nikon Eclipse Ti CLSM, which integrates advanced optics, fluorescence detection and scanning hardware in a single platform controlled by EZ C1 software. 488 and 561 nm laser lights were used to excite Tg (fli1: EGFP) embryos and DiI- positive tumor cells. Serial sagittal (lateral) sections were captured 6 dpi in an automated fashion (14 x 30 μm) using a Plan Apo 4X Nikon dry objective with 0.2 NA and 20 WD. For three dimensional images 0.5 μm step Z stacks (1024x1024 focal planes, 50-74 μm in depth) were acquired by using 40x Nikon dry plan fluor objective with 0.75 N.A and 0.66 WD.

Image analysis software

Automated image pre-processing, automated analysis, and 3D reconstruction and surface rendering were performed by Image-Pro Plus-based software from Media Cybernetics.

Extended depth of field

The software used Z-stack color images from the confocal microscope. The obtained gray images were pseudo colored with green for GFP and red for CM-DiI labeled tumor cells. A macro was built that uses both

channels for batch processing of all images in a folder. First from the Z-stack a single, in-focus, composite image was made. Pixels in the Z-stack were analyzed. For every position, the pixel from the plane with the largest variance or local contrast was selected. This pixel was then used for the final composite image.

Automated orientation of the embryos (Figure 2)

For the image analysis, all embryos should have the same orientation. For this, a macro was developed in which the images were modified so that all embryos were horizontally oriented, with the head towards the right and the yolk sac towards the bottom of the image.

- Automated horizontal alignment: The color image was converted to a grey value image to give a combination of the GFP and red channels. The embryo was then segmented using mean intensity histogram value and minimum and maximum area filter. Then, a direction value of the segmented object was determined, which was used to give the embryo a horizontal position.

- Automated horizontal orientation: The X position value of the center of mass was determined from the grey combined GFP and red channels. If this value was located left from the center of centroid, the image was flipped horizontally. In all cases, this provided images in which the head of the embryo was oriented to the right.

- Automated vertical orientation: From the outer horizontal positions, the point lying on the X-axis at 75% distance from the extreme left of the embryo outline was determined. At this X-position the Y-axis was drawn from top to bottom outlines. A rectangle was drawn from -20 to +20 pixels horizontally from the calculated 75% point and vertically 80 pixels above the middle of the upper Y-axis. Another rectangle was drawn with identical horizontal parameters and vertically 80 pixels below the middle of the lower Y-axis. The average fluorescence intensity in the red channel was determined for both rectangles. If intensity was higher in the upper rectangle compared to the lower rectangle, the image was flipped vertically. The same procedure could be performed using the GFP channel in which case images were flipped if intensity was higher in the bottom rectangle. Visual inspection showed that this procedure, in all cases resulted in images where the yolk sac was oriented to the bottom of the image.

- Automated calculation of the injection position of the Cy3 labeled cells:
First the leftmost and the rightmost X positions of the embryo outline were determined. From these X positions, a point lying at 75% from the extreme left was determined. Then, from this X position the uppermost and lowermost Y positions were determined. Subsequently, from these Y positions a point lying at 75% from the uppermost Y position was determined, which was designated as the arbitrary injection point. Visual inspection showed that the arbitrary injection point by this procedure, always resided within the primary tumor mass.

Automated detection of CMDil labeled tumor cells

The pseudo colored red objects were segmented using a threshold value, and by applying a minimum and maximum area filter. After the segmentation, a mild watershed separation was applied. For all detected red

objects the distance (in µm) from the injection point was calculated. A positive X value indicates tumor foci towards the head; a positive Y value indicates tumor foci towards the dorsal region of the embryo. Various other parameters, including number of objects, mean distance, cumulative distance, mean area, and mean intensity were calculated for segmented red objects.

Processing of the results in excel

All data, together with the image were exported into excel. In excel 2 macro's were used:
a) Exclusion of tumor foci where [X absolute] is within 500 µm and [Y absolute] is within 200 µm from the calculated injection point; b) Calculation of the average of all analyzed embryos. The major calculation chosen for representation of the data was "mean cumulative distance" (MCD) of tumor foci from injection position.

Statistical analysis

Statistical analysis was performed with Prism 4 software (GraphPad) using two tailed, unpaired t-test. ns, not significant; *, $P<0.05$; **, $P<0.01$; ***, $P<0.0001$.

ACKNOWLEDGEMENTS

We thank Dr. Rob Hoeben for generously providing the mCherry expression construct.

REFERENCES

1. Hanahan D ,Weinberg RA . Hallmarks of Cancer (2011) The Next Generation. Cell 144:646-74 .

2. Amatruda JF, Shepard JL, Stern HM, Zon LI (2002) Zebrafish as a cancer model system. Cancer Cell 1:229– 231.

3. Berghmans S, Jette C, Langenau D, Hsu K, Stewart R, et al.(2005) Making waves in cancer research: new models in the zebrafish. Biotechnology 39:27–237.

4. Lam SH, Gong Z (2006) Modeling liver cancer using zebrafish: a comparative oncogenomics approach. Cell Cycle 5:573–577.

5. Haldi MC, Ton C, Seng WL, McGrath P (2006) Human melanoma cells transplanted into ZF proliferate, migrate, produce melanin, form masses and stimulate angiogenesis in zebrafish. Angiogenesis 9:139–151 .

6. Lee LM, Seftor EA, Bonde G, Cornell RA, Hendrix MJ (2005) The fate of human malignant melanoma cells transplanted into zebrafish embryos: Assessment of migration and cell division in the absence of tumor formation. Dev Dyn 233: 1560-70.

7. Nicoli S, Ribatti D, Cotelli F, Presta M (2007) Mammalian tumor xenografts induce neovascularization in zebrafish embryos. Cancer Res 67:2927–2931.

8. Stoletov K, Montel V, Lester RD, Gonias SL, Klemke R (2007) High-resolution imaging of the dynamic tumor cell vascular interface in transparent ZF. Proc Natl Acad Sci 104: 17406–17411 .

9. Stoletov K, Kato H, Zardouzian E, Kelber J, Yang J, et al. (2010) Visualizing extravasation dynamics of metastatic tumor cells. Journal of Cell Science 123:2332-2341.

10. Stern HM, Zon LI (2003) Cancer genetics and drug discovery in the zebrafish. Nat Rev Cancer 3: 533–539.

11. Zon LI, Peterson RT (2005) In vivo drug discovery in the zebrafish. Nat Rev Drug Dis 4:35-44.

12. Amatruda, JF, Patton EE (2008) Genetic models of cancer in zebrafish. Int Rev Cell Mol Biol 271:1-34.

13. Lawson ND, Weinstein BM (2002) In vivo imaging of embryonic vascular development using transgenic ze brafish. Dev Biol 248: 307-18.

14. Ware JJ, Paulson DF, Mickey GH, Webb KS (1982) Spontaneous metastasis of cells of the human prostate carcinoma cell line PC-3 in athymic nude mice. J Urol 128:1064–7.

15. Giroldi LA, Schalken JA (1993) Decreased expression of the intercellular adhesion molecule E-cadherin in prostate cancer: Biological significance and clinical implications. Cancer and Met Reviews 12: 29-37.

16. Kukreja SD, Ghosh S, Lad LT (1998) Development of skeletal metastasis by human prostate cancer in athymic nude mice. Clin Exp Metastasis 6 : 401–9.

17. Wu TT, Sikes RA, Cui Q, Thalmann GN, Kao C, et al. (1998) Establishing human prostate cancer cell xenografts in bone: Induction of osteoblastic reaction by prostate specific antigen-producing tumors in athymic and SCID/bg mice using LNCaP and lineage-derived metastatic sublines. Int J Cancer 77:887–94.

18. Lim DJ, Liu XL, Sutkowski DM, Braun EJ, Lee C, et al. (1993) Growth of an androgen-sensitive human prostate cancer cell line, LNCaP, in nude mice. Prostate 22:109–1.

19. Rembrink K, Romijn JC, Kwast TH, Rubben H, Schroder FH (1997) Orthotopic implantation of human prostate cancer cell lines: A clinically relevant animal model for metastatic prostate cancer. Prostate 31: 168–74.

20. Ross DT, Perou CM (2001) A comparison of gene expression signatures from breast tumors and breast tissue derived cell lines. Dis Markers 17: 99–109.

21. Lacroix M, Leclercq G (2004) Relevance of breast cancer cell lines as models for breast tumors: an update. Breast Cancer Res and Treatment 83: 249-289.

22.Van Sloooten HJ, Bonsing BA, Hiller AJ, Colbern GT, van Dierendonck JH, et al. (1995) Outgrowth of BT-474 human breast cancer cells in immune-deficient mice: a new in vivo model for hormone-dependent breast cancer. Br J Cancer 72: 22-30.

23. Zhang L, Kharbanda S, Chen D, Bullocks J, Miller DL, et al. (1997) MCF-7 breast carcinoma cells over-expressing FGF-1 form vascularized, metastatic tumors in ovariectomized or tamoxifen-treated nude mice. Oncogene 15:2093-2108.

24. Buck E, Eyzaguirre A, Barr S, Thompson S, Sennello R, et al. (2007) Loss of homotypic cell adhesion by epithelial-mesenchymal transition or mutation limits sensitivity to epidermal growth factor receptor inhibition. Mol Cancer Ther 6:532-541.

25. Kimmel CB, Ballard WW, Kimmel SR, Ullmann B, Schilling TF (1995) Stages of embryonic development of the zebrafish. Dev Dyn 203:253-310.

CHAPTER 4

TARGETED RADIOSENSITIZATION IN PROSTATE CANCER

Veerander P.S. Ghotra*[1], Albert A. Geldof*[2] and Erik H.J.Danen[1]

*corresponding authors

Published in Current pharmaceutical design 2013;19(15):2819-28.

[1]Division of Toxicology, Leiden Academic Center for Drug Research, Leiden University, Einsteinweg 55, 2333 CC, the Netherlands; [2]Department of Urology and dept. Nuclear Medicine & PET Research, VU University Medical Center, PO Box 7057, 1007, MB Amsterdam, the Netherlands

ABSTRACT

Radiotherapy is one of the treatment options for locally or regionally advanced prostate cancer, but radioresistance of prostate cancer cells is a practical limitation of radiotherapy. The identification of molecular targets of radioresistance in prostate cancer is important to improve therapeutic intervention. The aim of this review is to give more biological insight into some well known processes involved in radioresistance of prostate cancer especially Apoptotic pathway; DNA damage response; and NF-kB signaling pathway. This review integrates salient, published, research findings with underlying molecular mechanisms, preclinical efficacy, and potential clinical applications of combining radiotherapy with these molecular targeted agents for the treatment of prostate cancer.

INTRODUCTION

The standard treatment regimen for clinically localized disease in prostate cancer is either radical prostatectomy or radiation therapy through external beam irradiation or local radioactive seed implants (brachytherapy) (1). A major reason for failure to eradicate local disease in prostate cancer and other solid tumors by radiotherapy (RT) is the radioresistance (2). Generally, there are two types of radioresistance in solid tumors: External mediated by interactions with microenvironment (Cell-cell and cell-matrix interactions (3) and local paracrine signaling), and internal (mediated by the general survival pathways like mutated p53) (4), amplification of DNA repair genes, overexpression of anti-apoptotic genes, increased levels of reactive oxygen species scavengers, activation of prosurvival/poor prognosis oncogenes such as Epidermal growth factor receptor (EGFR) (5,6) or c-MET(also known as hepatocyte growth factor receptor) (7,8). Molecular targeting of these survival mechanisms is now becoming a reality with new treatments designed to target processes that are thought to be tumor specific, or where there are quantitative differences in target expression between cancer and normal cells. The relative tumor-specificity of most molecular targeted agents may offer a theoretical advantage over chemotherapy, as overlapping toxicity with RT on normal tissue is potentially minimized. Furthermore, the intrinsic radiosensitivity of certain tumors may be modified by agents that target specific gene and protein expression. An illustrative example of this advantage is the targeting of EGFR expression to reduce proliferation of head and neck cancer cells without affecting the repopulation of normal mucosal epithelial cells required for healing during radiotherapy (9-11). This fundamental information has, in turn, suggested that targeting such radio response regulatory molecules can serve as a strategy for developing radiation sensitizers.

OVERCOMING RADIORESISTANCE IN PROSTATE CANCER BY TARGETING APOPTOSIS

Irradiation-induced tumor apoptosis can be enhanced by targeting of apoptotic machinery that involves a system of messengers.The challenge of apoptosis-targeting, as in all therapies, is to selectively target pathways operational in tumor cells over those operational in normal cells.

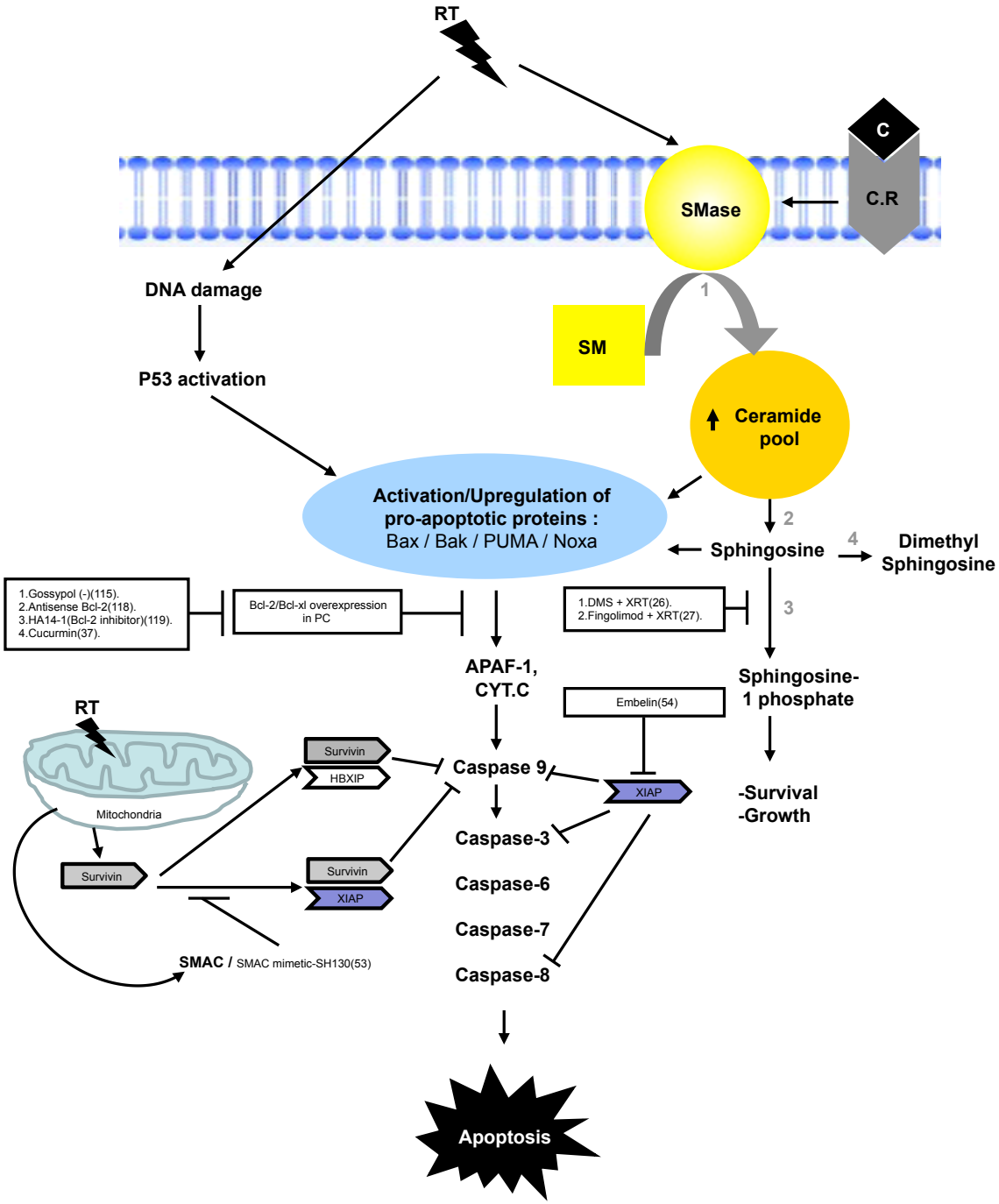

FIGURE 1.*Schematic model showing the activation of different pathways leading to apoptosis in the prostate cancer cell lines* (LNCaP/PC3). Pro-apoptotic signaling is activated via upregulation of p53, release of ceramide (e.g., by sphingomyelinase (SMase) due to XRT or by various cytokines like TNF- alpha. Ceramide is metabolized by a ceramidase to generate sphingosine. Sphingosine is phosphorylated by sphingosine kinase to form Sphingosine-1-Phosphate (S-1P). S-1P antagonizes ceramide-mediated apoptosis. All signals are integrated at the level of mitochondria by activation or upregulation of pro-apoptotic molecules belonging to the pro-apoptotic Bcl-2 family (Bax, Bak, Puma, Noxa). The relative level of pro and anti-apoptotic Bcl-2 molecules is the key decision point regarding cell death induction. In case of relative overweight of pro-apoptotic Bcl-2 members, cytochrome c is released from mitochondria and triggers execution of apoptosis by activation of caspase-9 and secondary caspases that cleave intracellular substrates, thereby inducing the apoptotic phenotype, including nuclear chromatin condensation and fragmentation. XIAP and survivin which belongs to the class of IAP (Inhibitor of apoptosis) proteins, inhibit the activation of the caspase cascade leading to the radioresistance.

Abbreviations: Smase: sphingomyelinase; SM: sphingomyelin; CS: ceramide synthase; C: Cytokine; CR: Cytokine Receptor; DMS: N,N-Dimethyl sphingosine 1. Smase 2. Ceramidase 3. sphingosine kinase; 4.Sphingosine N-methyl transferase

By Targeting Sphingomyelin-Ceramide Pathways

Radiation targets either the cell membrane or the nucleus to activate different apoptotic pathways (12-14). Sphingomyelin-Ceramide apoptotic pathway (Fig. 1) is initiated by hydrolysis of sphingomyelin through activated sphingomyelin-specific forms of phospholipase C, termed sphingomyelinases (SMases) that leads to generation of ceramide (12-14). Ceramide, in turn, can activate several pathways important for the induction of apoptosis (14). Also, Ceramide is further metabolized by ceramidase to generate sphingosine (Fig. 1), which in turn, can be phosphorylated by sphingosine kinase (Sphk) to form Sphingosine-1-phosphate (S-1P) (15,16). Conversely, S-1P has been implicated as a signaling molecule that antagonizes ceramide-mediated apoptosis (17). The modulation of ceramidase, sphingosine kinase, and S-1P phosphatase activities play a pivotal role in the regulation of apoptosis by regulating the intracellular ratio between ceramide, sphingosine, and S- 1P (17). Furthermore, Sphk1/S1P pathway has been linked to oncogenic transformation and cancer progression via increased rate of cell proliferation, and apoptotic resistance (18-20). Sphk1 is highly expressed in various human tumor tissues (21,22) and has been shown to be associated with poor prognosis in gastric cancer (23), glioma (24) and breast cancer (25). Radioresistance of Prostate cancer has been reported to be linked to sustained sphingokinase- 1(Sphk-1) activity (26). Recently, a new sphingosine analogue FTY720 (Finglimod) has been shown to induce radiosensitization and inhibition of tumor growth in in vitro and in vivo models (27).

Various in vitro studies (outlined in Table 1) have shown that the Sphingomyelin-Ceramide pathway is a very attractive target for radio-sensitization in prostate cancer. After critically analyzing all these in vitro studies it can be hypothesized that ceramide generation is a critical component of radiation-induced apoptosis in human prostate cancer cells and blockage of ceramide generation may provide a selective advantage in the development of radioresistance of prostate tumors. Because of the central role of Sphingomyelin-Ceramide pathway in radiation induced apoptosis, pharmacologic manipulation of the intracellular ceramide levels in conjunction with radiation could offer significant improvement to the clinical treatment of prostate cancer.

By Targeting Anti-apoptotic Bcl-2 Family of Proteins

Antiapoptotic Bcl-2 (B-cell lymphoma 2) protein is overexpressed in a variety of human cancers, including prostate cancer (28,29). Bcl-2 overexpression is frequently found in both primary and metastatic human prostate cancers (30,31). It is observed to be overexpressed in 30% to 60% of prostate cancer at diagnosis and in nearly 100% of hormone-refractory prostate cancers (31). Also, Bcl-xL (B-cell lymphoma-extra large) is found to be overexpressed in 80% to 100% of hormone-refractory prostate cancers, where it is associated with bad prognosis, shortened survival and advanced disease (32). Bcl-2/Bcl-xL overexpression decreases the pro-apoptotic response to such cellular insults as irradiation, chemotherapy, and androgen withdrawal, leading to resistance to treatment (33). Primary prostate tumors overexpressing Bcl-2 exhibit a high Gleason score and a high rate of cancer recurrence after radical prostatectomy (30,31). The most definitive evidence supporting a positive correlation between Bcl-2 and prostate cancer progression is that Bcl-2 overexpression leads to metastatic and chemo- or radioresistant phenotypes (34,35). Reversal of prostate cancer cell radioresistance in vitro has been achieved by downregulating Bcl-2 (36,37). Bcl-2 and Bcl-xL represent an attractive target for the development of new anti-prostate cancer agents that have either direct cytotoxic effects on prostate cancer cells or improve the efficacy of conventional radio- or chemotherapy by sensitizing

TARGET	APPROACH	CELL LINE	MECHANISM	REF.
SPHINGOSINE CERAMIDE PATHWAY	TNF- alpha + irradiation	LNCaP	↑Intracellular ceramide levels → Enhanced activation of the intrinsic mitochondrial apoptosis pathway. ↑Sphingosine and ↓SPP levels.	115
	Exogenous C2 ceramide+ irradiation	LNCaP	↑Intracellular ceramide levels → enhanced activation of the intrinsic mitochondrial apoptosis pathway	116
	Exogenous sphingosine + irradiation	LNCaP	↑Sphingosine levels → enhanced apoptosis of the radiation resistant prostate cancer cells.	26
	Sphingosine kinase inhibitor (N,N-DMS) + Irradiation.	LNCaP	↑Sphingosine levels → enhanced apoptosis of the radiation resistant prostate cancer cells.	26
	TPA +irrradiation	LNCaP	↑Ceramide synthase activity →ceramide levels (in- Vivo pathway) → enhanced apoptosis	115
TARGETING ANTIAPOPTOTIC BcL-2 FAMILY	(-)Gossypol+ irrradiation	- PC-3 - PC-3 xenograft	Blocks heterodimerization of Bcl-xL with Bax, Bad and Bim → enhanced response to radiation therapy.	115
	Antisense BcL-2+ irrradiation	-PC-3 -LNcaP	Reduction in Bcl-2 protein levels and a significant reduction in clonogenic survival.	117
	HA14 -1+ irrradiation	-PC-3 -LNcaP	HA14 –1 is an organic Bcl-2 inhibitor → enhanced response to radiation.	118
	Curcumin+ irrradiation	PC-3	Downregulation of endogenous and radiation Induced Bcl-2 protein expression → enhanced radiation induced apoptosis.	37
TARGETING IAP MEMBER OF PROTEINS	Smac mimetic SH-130	DU-145	Functional blocking of IAPs → enhanced radiation induced apoptosis.	53
	Embelin	PC-3	Inhibits XIAP → enhanced radiation induced apoptosis	54

TABLE 1. Shows preclinical studies, which demonstrate the potential of targeting Sphingomyelin-Ceramide pathway, Bcl-2 antiapoptotic and IAP family of proteins for prostate cancer radio-sensitization.

prostate cancer cells (Fig. 1). Various in vitro studies as shown in (Table 1) provide firm evidence, that targeting antiapoptotic Bcl-2 family of proteins represents an attractive target for prostate cancer radiosensitization.

Targeting the IAP (Inhibitor of Apoptosis) Member of Proteins

IAPs represent a class of apoptosis regulatory proteins consisting of eight family members: Neuronal apoptosis inhibitory protein (NAIP; also known as BIRC1), cellular IAP1 (c-IAP1; also known as BIRC2), cellular IAP2 (c-IAP2; also known as BIRC3), X chromosome-linked IAP (XIAP; also known as BIRC4), survivin (BIRC5), ubiquitin-conjugating BIR domain enzyme apollon (also known as BIRC6), melanoma IAP (ML-IAP; also known as BIRC7), and IAP-like protein 2 (ILP2; also known as BIRC8) (38,39). Among all human IAP proteins, XIAP and survivin have been reported to have the most prominent and strongest antiapoptotic function (40,41). IAPs function as potent endogenous apoptosis inhibitor (Fig. 1) due to their ability to bind and effectively inhibit two effector caspases (-3 and -7) and one initiator caspase-9 (42). A notable exception is-survivin which only inhibits active caspase 9 after binding to its cofactor hepatitis B-X-interacting protein (HBXIP) (43). Additionally, it has been shown that anti-apoptotic action of survivin could be mediated by its interaction with XIAP leading to increased stability of XIAP (44). IAPs suppress apoptosis against a variety of

apoptotic stimuli, which include radiation, chemotherapy and immunotherapy in cancer cells (38). Specifically, radiation triggers release of mitochondrial proteins (Smac, cytochrome-c and survivin) into the cytoplasm (41,45). Consequently the released Smac binds to XIAP and other IAP proteins, thus abolishing their anti-apoptotic function (45). It has been shown that IAPs are highly expressed in many types of cancer including prostate cancer (39,42,46,47). Expression of cIAP1, cIAP2, XIAP, survivin, and NAIP has been examined in the NCI -60 human tumor cell line panel, which revealed widespread expression of cIAP1, XIAP, and survivin in tumor lines of diverse tissue origins (48). Genome wide analysis has confirmed the differential expression of survivin in tumors versus normal tissues (49). Survivin has been shown to be overexpressed in prostate cancer cell lines, aggressive prostate cancers with higher gleason grades, lymph node and distant metastasis (50-52). Because IAPs suppress apoptosis against a variety of apoptotic stimuli, including radiation, strategies targeting IAPs may prove to be highly effective in overcoming radiation resistance (Fig. 1). Against this background a number of different strategies have been developed to antagonize aberrant IAP protein function and/or expression in human prostate cancers as to overcome radioresistance (53,54). Some of these strategies are briefly outlined in the (Table 1).

TARGETING DNA DAMAGE RESPONSE PATHWAYS

Ionizing radiation (IR) leads to the formation of DNA single or double-strand breaks, altered or lost DNA bases and DNA-DNA or DNA protein cross-links (55). The DNA-damage response pathway begins with 'sensor' proteins that sense the DNA damage and/or chromatin alterations that occur after induction of DNA damage (56). These 'sensor' proteins convey the damage signal to transducers which in turn transmit it to numerous downstream effectors(56). The DNA-double strand breaks (dsbs) are first recognized by the (Telomere binding protein) TRF2 and Mre11– Rad50– Nbs1 (MRN) sensor complex. The MRN sensor complex is the most important sensor complex (Fig. 2) comprising the nuclease Mre11, the structural maintenance of chromosomes protein Rad50 and the protein Nbs1 (57,58). The transducers consist of a group of conserved nuclear protein kinases (59) and the 'phosphatidylinositol-3-OH kinase (PI (3) K)-related protein kinases' (PIKKs), which consists further of the DNA-dependent protein kinase (DNA-PK), ataxia-telangiectasia-mutated (ATM), the ATM and Rad3-related (ATR) protein and hSMG-1 (60,61). Current evidence suggest that the MRE11–RAD50–NBS1 complex (MRN complex) is the primary DSB sensor that recruits ATM to the DNA-dsbs (62). Another early step in the response to a DSB involves phosphorylation of the H2A histone family, member X, H2AX, which is redundantly carried out by ATM or DNA-dependent protein kinase (DNA-PK)(63). Phosphorylation of H2AFX produces discrete, microscopically detectable foci (64). The MRE-11 and H2AFX proteins further recruit DNA repair complexes and cell cycle checkpoint proteins (e.g. tumor protein 53 binding protein 1 (TP53BP1), mediator of DNA damage checkpoint 1 (MDC1), breast cancer 1, early onset (BRCA1), and check point kinase 2 (CHK2) (65). After initial sensing and activation of downstream pathways, parallel activation of human DNA-double strand break repair pathways homologous recombination (HR) and non-homologous recombination takes place, which can both interact or compete with each other during cell cycle transitions (66).

Cell cycle checkpoints or DNA repair pathways are commonly altered during the process of prostate cancer (66). Tumors having these genetic alterations are hypothetically sensitive to radiation upon further disruption of remaining checkpoint functions or remaining DNA repair pathways. The most important DNA-dsb damage

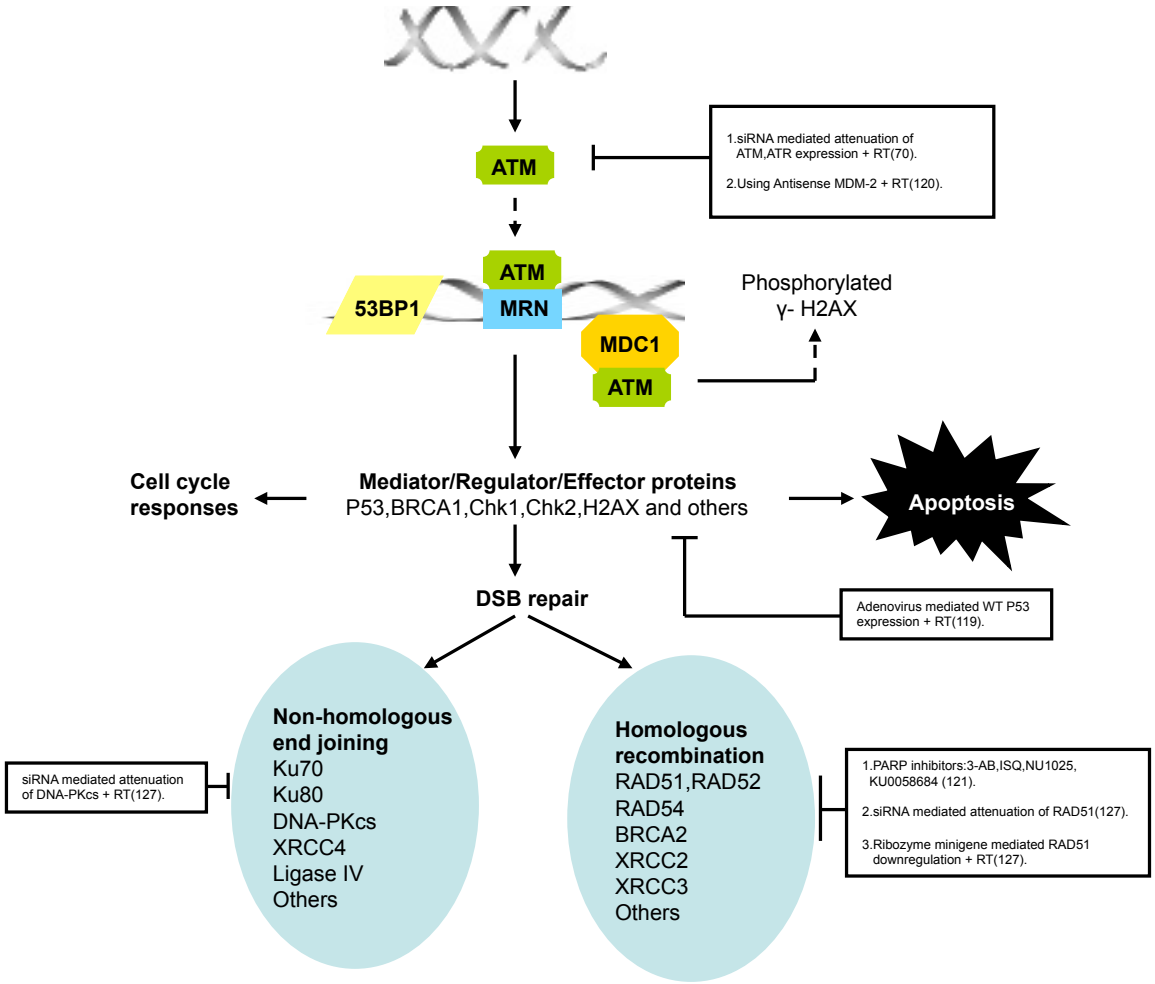

FIGURE 2. *Showing schematic outline of DNA damage response pathway and possible therapeutic strategies for radiosensitization in the prostate cancer.* For more information refer to the (Table 2).

TARGET	AGENT USED	MODEL USED	MECHANISM	REF.
ATM – P53 – MDM2 PATHWAY	Adenoviral mediated P53gene expression + XRT	-P53 defficient PC3 line -P53 wild type LNCAP cell line	Restoration/enhancement of normal p53 function ➔Enhancement of apoptosis.	119
	Antisense MDM2+AD+XRT	P53 wild type LNCAP cell line	- ↓MDM2 expression and ↑P53 and p21 expression. - ↑Apoptosis and ↓clonogenic survival.	120
	siRNA mediated attenuation of the ATM, ATR expression + XRT	- DU 145 - PC-3	↓Post-transfection levels of the ATM, ATR proteins ➔ decreased clonogenic survival	114
HR REPAIR PATHWAY	Genetically engineered PARP mutant, expressing dominant negative mutant of PARP in tumor cells+ XRT	Tumor xenograft	- PARP is required for the efficient repair of DNA singlestrand breaks (SSBs) during base excision repair and PARP inhibition leads to persistent singlestrand gaps in DNA➔these gaps are encountered by a replication fork, leading to arrest, and the single-strand gaps may degenerate into DSBs. - In the absence of BRCA1 or BRCA2, the replication fork cannot be restarted and collapse , causing persistent chromatid breaks Repair of these breaks by alternative error prone DSB repair mechanisms would cause large numbers of chromatid breaks and aberrations, leading to loss of viability.	121-126
	siRNA /antisense /Ribozyme minigene mediate attenuation of RAD51	LNCaP	Downregulation of RAD 51	127

TABLE 2. Showing various pre-clinical studies which have showed the potential of targeting DNA damage response pathway for prostate cancer radiosensitization.

-response genes associated with prostate cancer risk includes the ATM-p53 signalling axis, such as ATM, p53, and CHK2 (67). It has been shown that ATM expression is higher in the high gleason score prostate tumors, when compared to the normal tissues (68). Prostate cancer specimens have been shown to harbor p53 mutations that have been documented to be associated with androgen independence, metastasis, decreased disease free survival and radioresistance (59,69). Keeping this background in mind, ATM has been targeted in prostate cancer using specific antisense or siRNA approaches resulting in radiosensitization (70).Small molecular inhibitors or peptides have been generated to bind to mutant forms of p53 and reverting them to wild type conformation and leading to cell cycle arrest and apoptosis (69). Malignant prostate cancer cell lines express higher levels of RAD51, XRCC3, RAD52 and RAD54 genes involved in homologous recombination in comparison to normal prostate epithelial cells (71). Strategies that target DNA repair increase radiosensitization in vitro and in vivo after treating prostate, glioma and lung cancer cells with siRNA to RAD51 (72,73). Prostate cancer arising in BRCA2 mutation carriers display an aggressive tumor phenotype and present more poorly differentiated tumors when compared with non-carrier prostate cancer controls (74-76). It has been shown that cells defective in BRCA1 and BRCA-2 proteins exhibit reduced RAD51 activity and foci formation and show increased sensitivity to ionizing radiation (77,78). Furthermore, It has been observed that BRCA1 and BRCA2 deficiency sensitizes cells to the inhibition of Poly (ADP-

Ribose) Polymerase (PARP) enzymatic activity, which consequently leads to chromosomal instability, cell cycle arrest and apoptosis (79). PARP-1 (accounting for 80% of total PARP cellular activity) binds to both single and double strand DNA breaks and is involved in DNA single strand break (ssb) repair and break excision repair (80,81). It has been documented that inhibition of PARP increases the level of unrepaired DNA double strand breaks by a variety of mechanisms.Based on these principles, Ashworth and colleagues adopted an siRNA approach and observed an increased sensitivity to PARP inhibition in a variety of cells which were made deficient in proteins in HR or Fanconi's anemia pathway (like RAD51, RAD54, DSS1, RPA1, NBS1, ATR, ATM, CHK1, CHK2, FANCD2, FANCA or FANCC) (83). Targeting cancer cells harboring a specific DNA repair defect by inhibiting a second repair pathway is a representation of synergistic lethality (84), and this approach is rapidly being translated into effective treatments for hereditary BRCA1 or BRCA2 deficient cancers or with tumors harboring defects in HR repair pathways (85). Utilizing this principle, specific and potent inhibitors of PARP inhibitors (Fig. 2) have been developed that are very effective tumor radiosensitizers in in-vitro and in-vivo (84).

The various preclinical studies which have demonstrated the potential of targeting these pathways for prostate cancer radiosensitization are outlined in (Table 2). These studies support the concept that the predetermination of the repair capacity of tumor cells may help to select appropriate agents for use in combination with radiotherapy in prostate cancer.

BY TARGETING RADIATION INDUCED RADIOADAPTIVE NF- kB PATHWAY

Radio-adaptive response is assumed to be induced by activation of the specific prosurvival signaling network in irradiated mammalian cells leading to reduced cell sensitivity to a subsequent higher challenging dose when a smaller inducing radiation dose had been already applied (86). The earliest response of mammalian cells to ionizing irradiation consists of activation of transcription factors, like AP-1, p53 (also known as TP53), and NF-kB (87,88). Out of all these, NF-kB has served as a model system for inducible transcription in a broad range of physiological and medical effects. The mammalian NF-kB family of proteins consists of five members: RelA, RelB, c-Rel, p50 (NF-kB1) and p52 (NF-kB2) (89). All members of the NF-kB family posses a Rel-homology domain (RHD) containing a NLS (nuclear localization sequence), which is important for dimerization, DNA binding and its interaction with IkB proteins (most important inhibitors of NF-kB activation). In the majority of circumstances NF-kB is found in the cytoplasm where it is negatively regulated by its interaction with the IkB family of proteins. These IkB family of proteins possesses multiple ankyrin repeats which bind to the RHD and masks NLS of NF-kB (90). There are various stimuli that activate NF-kB, which results in the regulation of a myriad NF-kB target genes. The majority of proteins encoded by NF-kB target genes participate in the host immune response (91,92), cell adhesion and stress response (91), apoptosis regulators (93), growth factors (94), cell cycle regulators (95) and inflammatory cytokines (96).In cancer cells, it regulates the expression of many anti-apoptotic proteins (IAP1, IAP2, XIAP,cFLIP and BclxL). It also regulates the progression of the cell cycle by positively regulating the expresson of various cyclins (D1,D2, D3, and E) and c-myc (97). NF-kB is also known to stimulate invasion and angiogenesis by regulating the

expression of different matrix metalloproteinases (MMP-2, MMP-9) (98) and various angiogenic factors (IL-8 and VEGF) (94,96).

Moreover, the activation of NF-kB is considered to be the most important factor, involved in the inflammatory response generated by irradiation (99,100). It has been shown that increased basal NF- kB activity in certain cancers has been associated with tumor resistance to radiation and chemotherapy (101). NF-kB is activated after phosphorylation of IkB at two serine residues (Ser-32 and Ser-36) by IkB kinases, which is later polyubiquitinated, and then degraded by 26S proteasome (Fig. 3). The free NF-kB translocates to the nucleus and activates its target genetic programs (102) including manganese superoxide dismutase (MnSOD), an enzyme that catalyses the conversions of toxic superoxide radicals to hydrogen peroxide and molecular oxygen (103-105). The radioadaptive response mediated by the NF-kB members increases the expression of MnSOD leading to protection of tumor cells (106,107). NF-kB also modulates the apoptotic signals at various levels. The best example is found in the TNF receptor I signaling pathway (108). (Fig. 3) provides the schematic representation of NF-kB signaling network in radiation induced adaptive radioresistance in prostate cancer.

Numerous studies have demonstrated the importance of the NF- kB pathway and its role as a cause of radioresistance in prostate cancer cell lines:

a). Josson and colleagues demonstrated that, constitutive nuclear level of RelB are significantly higher in PC-3 compared to LNCaP cells. They also showed that PC3 cells have a higher basal levels of MnSOD as compared to the LNCaP cells. These results suggest that comparatively higher levels of nuclear RelB and MnSOD protein may be responsible for the intrinsic radiation resistance of PC-3 cells (109). Selective inhibition of RelB decreased the levels of MnSOD leading to increase in the sensitivity of prostate cancer cells to radiation treatment (109). Xu and colleagues showed that interaction of 1-alpha, 25-dihydroxyvitamin D3 (1alpha, 25-(OH) 2D3) with the Vitamin D receptor (VDR) enhanced the radiosensitivity of prostate cancer cell lines at clinically relevant radiation doses. The radiosensitization effect of 1-alpha, 25-(OH)2D3 is partly mediated by selectively suppressing IR-mediated RelB activation, leading to decreased expression of manganese superoxide dismutase (MnSOD), suggesting that suppression of MnSOD is a mechanism by which 1-alpha, 25-(OH) 2D3 exerts its radiosensitization effect. Therefore, 1-alpha, 25-(OH) 2D3 is a high potential effective pharmacologic agent for selectively sensitizing prostate carcinoma cells to irradiation via suppression of antioxidant responses in mitochondria (110). Yulan Sun and colleagues showed that inhibition of NF-kB pathway is also a common mechanism for the radiosensitization effect of parthenolide in prostate cancer cells LNCaP, DU145, and PC3 (111). Radiation-induced NF-kappaB DNA-binding activity is inhibited by parthenolide leading to the decreased transcription of the sod2 gene, the gene coding for an important antiapoptotic and antioxidant enzyme (manganese superoxide dismutase) in the three prostate cancer cell lines (111). Using immunohistochemical studies, Lessard and colleagues demonstrated that all the members of the NF-kB family were expressed in normal prostate tissues, prostatic intraepithelial neoplasia and prostate cancer. However, only the nuclear localization of RelB correlated with the prostate cancer patient's Gleason scores (112), suggesting that the level of RelB is associated with prostate cancer progression. These studies provide us convincing evidence that RelB plays an important role in redox regulation of the cell and protects

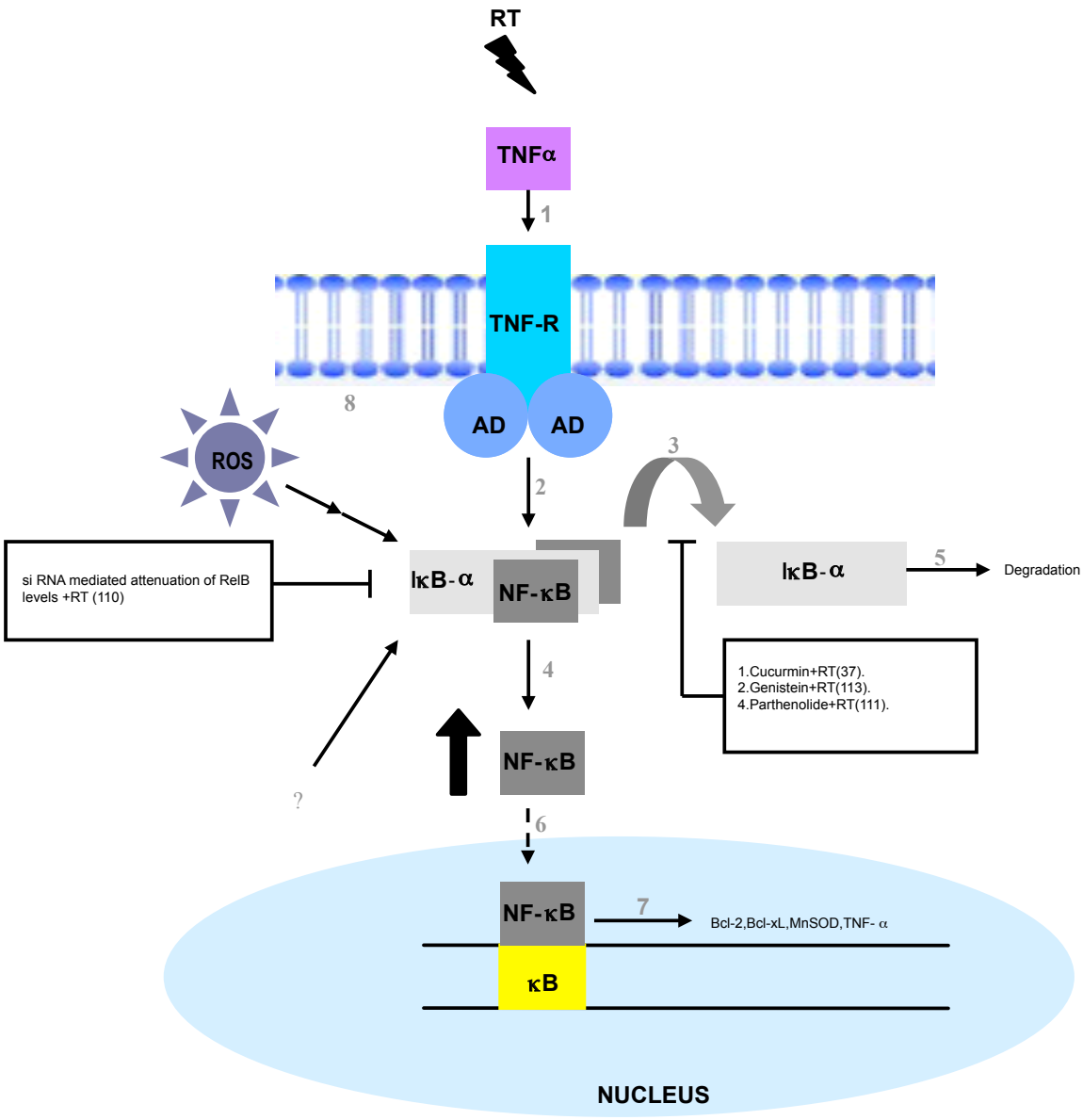

FIGURE 3. *Schematic presentation of the NF-kB signaling network in radiation-induced adaptive radioresistance in prostate cancer.* 1. Radiation induces TNF-alpha ligand expression. Binding of TNF-alpha to its receptor, leading to recruitment of adaptor proteins (AD). 2/3. Activation of NF-kB by phosphorylation of IkB by IkB kinases; 5. Polyubiquitination, and degradation of IkB by 26S proteasome. 4.increased free NF-kB levels in the cytoplasm. 6. Translocation of NF-kB to the nucleus. 7. Activation of NFkB target genetic programs. 8. ROS also stimulates the formation of free NF-kB.

Abbreviations: RT = Radiotherapy; ROS=Reactive Oxygen Species

aggressive prostate cancer cells against radiation-induced cell death. Thus, inhibition of RelB could be a novel mechanism to radiosensitize prostate cancer.

b). Damodaran and colleagues demonstrated using p53 deficient PC-3 cell line, that radiation also causes an induction of TNF- alpha protein expression, NF-kB activity and Bcl-2 upregulation (37). They also showed that radiation-induced NF-kB activity depends on radiation induced expression of TNF-alpha. Curcumin in combination with radiation caused inhibition of TNF- alpha - mediated NF-kB activity resulting in downregulation of bcl-2 protein leading to the enhanced radiation-induced clonogenic inhibition and radiation-induced apoptosis in p53 deficient PC-3 cells (113). Curcumin inhibits NF-kB activation by inhibiting phosphorylation of IkB-alpha, which is required to export NF-kB from cytosol to nucleus as to activate its target genes (113). Together, these mechanisms strongly suggest that the natural compound Curcumin is a potent radiosensitizer, and that it acts by overcoming the effects of radiation-induced prosurvival gene expression in prostate cancer.

c). Julian and colleagues showed that Genistein (4', 5,7 trihydroxyisoflavone) combined with radiation causes greater inhibition in PC-3 colony formation compared to genistein or radiation alone due to the strong inhibition of the NF-kB activity (113). Their findings support the novel strategy of combining genistein with radiation for the treatment of prostate cancer. All these studies demonstrate the role of NF-kB as a stress factor in prostate cancer cells. NF-kB is a crucial element of the cell's protective response to radiation and represents therefore an attractive target in new therapeutic approaches to fight prostate cancer. Inhibition of NF-kB is expected to increase the therapeutic efficiency of radiation.

CONCLUSIONS AND REMAINING QUESTIONS

The identification of molecular targets of radioresistance in prostate cancer cells is very important to improve therapeutic intervention in prostate cancer. Anyhow, an ideal molecular targeting agent should improve the therapeutic efficacy of radiotherapy by targeting specific pathway(s), in practice, but this may be difficult to achieve with predictability because of the complex molecular cross-talk between signaling pathways (113). The most challenging part for a clinical investigator is to interpret this large amount of preclinical data and, then to select the most promising molecular targeting agent suitable for human clinical trials. Moreover, there are other challenges that are faced during the designing of the early clinical trials for molecular targeted agents. It is unknown whether expression of the molecular target can adequately predict clinical response to molecular agents (55). There are also several issues in studying radiosensitizers at the molecular level using prostate cancer cell lines, including their heterogeneity, different growth properties, hormone responsiveness, originated from metastatic tissue,etc. Nevertheless, these cellular models have provided considerable understanding of the biology of prostate cancer and are important for the initial investigation process. Moreover, our current knowledge of radiation-induced pathways is incomplete, and it does not provide direct proof for improving the efficacy of radiation therapy. In this context, the advent of RNA interference technology (114) can provide us a better insight into the radiation induced biomolecular pathways by virtue of its high selectivity for molecular targets. Functional genomic studies utilizing siRNA high throughput libraries can produce unbiased information regarding the molecules involved in the prostate cancer radioresistance. This ge-

nome wide approach will reveal new molecules involved in prostate cancer radioresistance, and it will lead to the development of new molecular targeted radiosensitizing strategies in prostate cancer.

CONFLICT OF INTEREST

The authors confirm that this article content has no conflicts of interest

ACKNOWLEDGEMENTS

The work of V.P.S. Ghotra is funded by the EU FP7 ZF Cancer project(HEALTH-F2-2008-201439).

REFERENCES

1. Walsh PC, DeWeese TL, Eisenberger MA. Clinical practice.Localized prostate cancer. N Engl J Med 2007; 357: 2696-705.

2. Rosser CJ, Gaar M, Porvasnik S. Molecular fingerprinting of radiation resistant tumors: can we apprehend and rehabilitate the suspects? BMC Cancer 2009; 9: 225.

3. Sandfort V, Koch U, Cordes N. Cell adhesion-mediated radioresistance revisited. Int J Radiat Biol 2007; 83: 727-32.

4. Dey S, Spring PM, Arnold S, et al. Low-dose fractionated radiation potentiates the effects of Paclitaxel in wild-type and mutant p53 head and neck tumor cell lines. Clin Cancer Res 2003; 9: 1557-65.

5. Nix PA, Greenman J, Cawkwell L, Stafford N. Radioresistant laryngeal cancer: beyond the TNM stage. Clin Otolaryngol Allied Sci 2004; 29: 105-14.

6. Smith BD, Haffty BG. Molecular markers as prognostic factors for local recurrence and radioresistance in head and neck squamous cell carcinoma. Radiat Oncol Investig 1999; 7: 125-44.

7. Aebersold DM, Kollar A, Beer KT, Laissue J, Greiner RH, Djonov V. Involvement of the hepatocyte growth factor/scatter factor receptor c-met and of Bcl-xL in the resistance of oropharyngeal cancer to ionizing radiation. Int J Cancer 2001; 96: 41-54.

8. Uchida D, Kawamata H, Omotehara F, et al. Role of HGF/c-met system in invasion and metastasis of oral squamous cell carcinoma cells in vitro and its clinical significance. Int J Cancer 2001; 93: 489-96.

9. Rubin Grandis J, Chakraborty A, Melhem MF, Zeng Q, Tweardy DJ. Inhibition of epidermal growth factor receptor gene expression and function decreases proliferation of head and neck squamous carcinoma but not normal mucosal epithelial cells. Oncogene 1997; 15: 409-16.

10. Pigott K, Dische S, Saunders MI. Where exactly does failure occur after radiation in head and neck cancer ? Radiother Oncol 1995; 37: 17-9.

11. Shukovsky LJ. Dose, time, volume relationships in squamous cell carcinoma of the supraglottic larynx. Am J Roentgenol Radium Ther Nucl Med 1970; 108: 27-9.

12. Santana P, Pena LA, Haimovitz-Friedman A, et al. Acid sphingomyelinase-deficient human lymphoblasts and mice are defective in radiation-induced apoptosis. Cell 1996; 86: 189-99.

13. Liao WC, Haimovitz-Friedman A, Persaud RS, et al. Ataxia telangiectasia-mutated gene product inhibits DNA damage-induced apoptosis via ceramide synthase. J Biol Chem 1999; 274: 17908- 17.

14. Haimovitz-Friedman A, Kan CC, Ehleiter D, et al. Ionizing radiation acts on cellular membranes to generate ceramide and initiate apoptosis. J Exp Med 1994; 180: 525-35.

15. Hannun YA. Functions of ceramide in coordinating cellular responses to stress. Science 1996; 274: 1855-9.

16. Kolesnick RN, Kronke M. Regulation of ceramide production and apoptosis. Annu Rev Physiol 1998; 60: 643-65.

17. Cuvillier O, Pirianov G, Kleuser B, et al. Suppression of ceramide mediated programmed cell death by sphingosine-1-phosphate. Nature 1996; 381: 800-3.

18. Olivera A, Kohama T, Edsall L, et al. Sphingosine kinase expression increases intracellular sphingosine-1-phosphate and promotes cell growth and survival. J Cell Biol 1999; 147: 545-58.

19. Xia P, Wang L, Gamble JR, Vadas MA. Activation of sphingosine kinase by tumor necrosis factor-alpha inhibits apoptosis in human endothelial cells. J Biol Chem 1999; 274: 34499-505.

20. Xia P, Gamble JR, Wang L, et al. An oncogenic role of sphingosine kinase. Curr Biol 2000; 10: 1527-30.

21. Bayerl MG, Bruggeman RD, Conroy EJ, et al. Sphingosine kinase 1 protein and mRNA are overexpressed in non-Hodgkin lymphomas and are attractive targets for novel pharmacological interventions. Leuk Lymphoma 2008; 49: 948-54.

22. French KJ, Schrecengost RS, Lee BD, et al. Discovery and evaluation of inhibitors of human sphingosine kinase. Cancer Res 2003; 63: 5962-9.

23. Li W, Yu CP, Xia JT, et al. Sphingosine kinase 1 is associated with gastric cancer progression and poor survival of patients. Clin Cancer Res 2009; 15: 1393-9.

24. Van Brocklyn JR, Jackson CA, Pearl DK, Kotur MS, Snyder PJ, Prior TW. Sphingosine kinase-1 expression correlates with poor survival of patients with glioblastoma multiforme: roles of sphingosine kinase isoforms in growth of glioblastoma cell lines. J Neuropathol Exp Neurol 2005; 64: 695-705.

25. Ruckhaberle E, Rody A, Engels K, et al. Microarray analysis of altered sphingolipid metabolism reveals prognostic significance of sphingosine kinase 1 in breast cancer. Breast Cancer Res Treat 2008; 112: 41-52.

26. Nava VE, Cuvillier O, Edsall LC, et al. Sphingosine enhances apoptosis of radiation-resistant prostate cancer cells. Cancer Res2000; 60: 4468-74.

27. Pchejetski D, Bohler T, Brizuela L, et al. FTY720 (fingolimod) sensitizes prostate cancer cells to radiotherapy by inhibition of sphingosine kinase-1. Cancer Res; 70: 8651-61.

28. McDonnell TJ, Troncoso P, Brisbay SM, et al. Expression of the protooncogene bcl-2 in the prostate and its association with emergence of androgen-independent prostate cancer. Cancer Res 1992; 52: 6940-4.

29. Apakama I, Robinson MC, Walter NM, et al. bcl-2 overexpression combined with p53 protein accumulation correlates with hormonerefractory prostate cancer. Br J Cancer 1996; 74: 1258-62.

30. Bauer JJ, Sesterhenn IA, Mostofi FK, McLeod DG, Srivastava S, Moul JW. Elevated levels of apoptosis regulator proteins p53 and bcl-2 are independent prognostic biomarkers in surgically treated clinically localized prostate cancer. J Urol 1996; 156: 1511-6.

31. Krajewska M, Krajewski S, Epstein JI, et al. Immunohistochemical analysis of bcl-2, bax, bcl-X, and mcl-1 expression in prostate cancers. Am J Pathol 1996; 148: 1567-76.

32. Furuya Y, Krajewski S, Epstein JI, Reed JC, Isaacs JT. Expression of bcl-2 and the progression of human and rodent prostatic cancers. Clin Cancer Res 1996; 2: 389-98.

33. Deveraux QL, Takahashi R, Salvesen GS, Reed JC. X-linked IAP is a direct inhibitor of cell-death proteases. Nature 1997; 388: 300- 4.

34. McConkey DJ, Greene G, Pettaway CA. Apoptosis resistance increases with metastatic potential in cells of the human LNCaP prostate carcinoma line. Cancer Res 1996; 56: 5594-9.

35. Chaudhary KS, Abel PD, Stamp GW, Lalani E. Differential expression of cell death regulators in response to thapsigargin and adriamycin in Bcl-2 transfected DU145 prostatic cancer cells. J Pathol 2001; 193: 522-9.

36. Scott SL, Higdon R, Beckett L, et al. BCL2 antisense reduces prostate cancer cell survival following irradiation. Cancer Biother Radiopharm 2002; 17: 647-56.

37. Chendil D, Ranga RS, Meigooni D, Sathishkumar S, Ahmed MM. Curcumin confers radiosensitizing effect in prostate cancer cell line PC-3. Oncogene 2004; 23: 1599-607.

38. Salvesen GS, Duckett CS. IAP proteins: blocking the road to death's door. Nature reviews Molecular cell biology 2002; 3: 401- 10.

39. Vucic D. Targeting IAP (inhibitor of apoptosis) proteins for therapeutic intervention in tumors. Current cancer drug targets 2008; 8: 110-7

40. Deveraux QL, Takahashi R, Salvesen GS, Reed JC. X-linked IAP is a direct inhibitor of cell-death proteases. Nature 1997; 388: 300-4.

41. Mita AC, Mita MM, Nawrocki ST, Giles FJ. Survivin: Key regulator of mitosis and apoptosis and novel target for cancer therapeutics. Clinical Cancer Research 2008; 14: 5000-5.

42. Schimmer AD. Inhibitor of apoptosis proteins: Translating basic knowledge into clinical practice. Cancer Research 2004; 64: 7183-90.

43. Marusawa H, Matsuzawa S, Welsh K, et al. HBXIP functions as a cofactor of survivin in apoptosis suppression. The EMBO journal 2003; 22: 2729-40.

44. Dohi T, Okada K, Xia F, et al. An IAP-IAP complex inhibits apoptosis. J Biol Chem 2004; 279: 34087-90.

45. Du CY, Fang M, Li YC, Li L, Wang XD. Smac, a mitochondrial protein that promotes cytochrome c-dependent caspase activation by eliminating IAP inhibition. Cell 2000; 102: 33-42.

46. Velculescu VE, Madden SL, Zhang L, et al. Analysis of human transcriptomes. Nature genetics 1999; 23: 387-8.

47. Krajewska M, Krajewski S, Banares S, et al. Elevated expression of inhibitor of apoptosis proteins in prostate cancer. Clin Cancer Res 2003; 9: 4914-25.

48. Tamm I, Kornblau SM, Segall H, et al. Expression and prognostic significance of IAP-family genes in human cancers and myeloid leukemias. Clin Cancer Res 2000; 6: 1796-803.

49. Islam A, Kageyama H, Takada N, et al. High expression of Survivin, mapped to 17q25, is significantly associated with poor prognostic factors and promotes cell survival in human neuroblastoma. Oncogene 2000; 19: 617-23.

50. McEleny KR, Watson RW, Coffey RN, O'Neill AJ, Fitzpatrick JM. Inhibitors of apoptosis proteins in prostate cancer cell lines. Prostate 2002; 51: 133-40.

51. Kishi H, Igawa M, Kikuno N, Yoshino T, Urakami S, Shiina H. Expression of the survivin gene in prostate cancer: correlation with clinicopathological characteristics, proliferative activity and apoptosis. J Urol 2004; 171: 1855-60.

52. Shariat SF, Lotan Y, Saboorian H, et al. Survivin expression is associated with features of biologically aggressive prostate carcinoma. Cancer 2004; 100: 751-7.

53. Dai Y, Liu M, Tang W, et al. Molecularly targeted radiosensitization of human prostate cancer by modulating inhibitor of apoptosis. Clin Cancer Res 2008; 14: 7701-10.

54. Dai Y, Desano J, Qu Y, et al. Natural IAP inhibitor Embelin enhances therapeutic efficacy of ionizing radiation in prostate cancer. American journal of cancer research 2011; 1: 128-43.

55. Ma BBY, Bristow RG, Kim J, Siu LL. Combined-modality treatment of solid tumors using radiotherapy and molecular targeted agents. Journal of Clinical Oncology 2003; 21: 2760-76.

56. Zhou BBS, Elledge SJ. The DNA damage response: putting checkpoints in perspective. Nature 2000; 408: 433-9.

57. Stracker TH, Theunissen JWF, Morales M, Petrini JHJ. The Mre11 complex and the metabolism of chromosome breaks: the importance of communicating and holding things together. DNA Repair 2004; 3: 845-54.

58. Moreno-Herrero F, de Jager M, Dekker NH, Kanaar R, Wyman C, Dekker C. Mesoscale conformational changes in the DNA-repair complex Rad50/Mre11/Nbs1 upon binding DNA. Nature 2005; 437: 440-3.

59. Dong JT. Prevalent mutations in prostate cancer. J Cell Biochem 2006; 97: 433-47.

60. Shiloh Y. ATM: Sounding the double-strand break alarm. Cold Spring Harb Sym 2000; 65: 527-33.

61. Shiloh Y. ATM and related protein kinases: Safeguarding genome integrity. Nat Rev Cancer 2003; 3: 155-68.

62. Falck J, Coates J, Jackson SP. Conserved modes of recruitment of ATM, ATR and DNA-PKcs to sites of DNA damage. Nature 2005; 434: 605-11.

63. Stiff T, O'Driscoll M, Rief N, Iwabuchi K, Lobrich M, Jeggo PA. ATM and DNA-PK function redundantly to phosphorylate H2AX after exposure to ionizing radiation. Cancer Research 2004; 64: 2390-6.

64. Fernandez-Capetillo O, Lee A, Nussenzweig M, Nussenzweig A. H2AX: the histone guardian of the genome. DNA Repair (Amst) 2004; 3: 959-67.

65. Stucki M, Jackson SP. gammaH2AX and MDC1: anchoring the DNA-damage-response machinery to broken chromosomes. DNA Repair (Amst) 2006; 5: 534-43.

66. Choudhury A, Cuddihy A, Bristow RG. Radiation and new molecular agents part I: targeting ATM-ATR checkpoints, DNA repair, and the proteasome. Semin Radiat Oncol 2006; 16: 51-8.

67. Al Rashid ST, Dellaire G, Cuddihy A, et al. Evidence for the direct binding of phosphorylated p53 to sites of DNA breaks in vivo. Cancer Res 2005; 65: 10810-21.

68. Angele S, Falconer A, Foster CS, Taniere P, Eeles RA, Hall J. ATM protein overexpression in prostate tumors: possible role in telomere maintenance. American journal of clinical pathology 2004; 121: 231-6.

69. Cuddihy AR, Bristow RG. The p53 protein family and radiation sensitivity: Yes or no? Cancer metastasis reviews 2004; 23: 237-57.

70. Collis SJ, Swartz MJ, Nelson WG, DeWeese TL. Enhanced radiation and chemotherapy-mediated cell killing of human cancer cells by small inhibitory RNA silencing of DNA repair factors. Cancer Res 2003; 63: 1550-4.

71. Fan R, Kumaravel TS, Jalali F, Marrano P, Squire JA, Bristow RG. Defective DNA strand break repair after DNA damage in prostate cancer cells: implications for genetic instability and prostate cancer progression. Cancer Res 2004; 64: 8526-33.

72. Fan R, Kumaravel TS, Jalali F, Marrano P, Squire JA, Bristow RG. Defective DNA strand break repair after DNA damage in prostate cancer cells: Implications for genetic instability and prostate cancer progression. Cancer Research 2004; 64: 8526-33.

73. Collis SJ, Tighe A, Scott SD, Roberts SA, Hendry JH, Margison GP. Ribozyme minigene-mediated RAD51 down-regulation increases radiosensitivity of human prostate cancer cells. Nucleic Acids Res 2001; 29: 1534-8.

74. Willems AJ, Dawson SJ, Samaratunga H, et al. Loss of heterozygosity at the BRCA2 locus detected by multiplex ligation dependent probe amplification is common in prostate cancers from men with a germline BRCA2 mutation. Clinical Cancer Research 2008; 14: 2953-61.

75. Mitra A, Fisher C, Foster CS, et al. Prostate cancer in male BRCA1 and BRCA2 mutation carriers has a more aggressive phenotype. Br J Cancer 2008; 98: 502-7.

76. Gallagher DJ, Gaudet MM, Pal P, et al. Germline BRCA mutations denote a clinicopathologic subset of prostate cancer. Clin Cancer Res 2010; 16: 2115-21.

77. Farmer H, McCabe N, Lord CJ, et al. Targeting the DNA repair defect in BRCA mutant cells as a therapeutic strategy. Nature 2005; 434: 917-21.

78. Wyman C, Ristic D, Kanaar R. Homologous recombination mediated double-strand break repair. DNA Repair 2004; 3: 827-33.

79. Bryant HE, Schultz N, Thomas HD, et al. Specific killing of BRCA2-deficient tumors with inhibitors of poly(ADP-ribose) polymerase. Nature 2005; 434: 913-7.

80. D'Amours D, Desnoyers S, D'Silva I, Poirier GG. Poly(ADPribosyl)ation reactions in the regulation of nuclear functions. Biochem J 1999; 342 (Pt 2): 249-68.

81. Petermann E, Keil C, Oei SL. Importance of poly(ADP-ribose) polymerases in the regulation of DNA-dependent processes. Cell Mol Life Sci 2005; 62: 731-8.

82. Godon C, Cordelieres FP, Biard D, et al. PARP inhibition versus PARP-1 silencing: different outcomes in terms of single-strand break repair and radiation susceptibility. Nucleic Acids Res 2008; 36: 4454-64.

83. McCabe N, Turner NC, Lord CJ, et al. Deficiency in the repair of DNA damage by homologous recombination and sensitivity to poly(ADP-ribose) polymerase inhibition. Cancer Res 2006; 66: 8109-15.

84. Chalmers AJ, Lakshman M, Chan N, Bristow RG. Poly(ADPRibose) Polymerase Inhibition as a Model for Synthetic Lethality in Developing Radiation Oncology Targets. Seminars in Radiation Oncology 2010; 20: 274-81.

85. Fong PC, Boss DS, Yap TA, et al. Inhibition of Poly(ADP-Ribose) Polymerase in Tumors from BRCA Mutation Carriers. New Engl J Med 2009; 361: 123-34.

86. Stecca C, Gerber GB. Adaptive response to DNA-damaging agents - A review of potential mechanisms. Biochem Pharmacol 1998; 55: 941-51.

87. Prasad AV, Mohan N, Chandrasekar B, Meltz ML. Induction of Transcription of Immediate-Early Genes by Low-Dose Ionizing- Radiation. Radiat Res 1995; 143: 263-72.

88. Weichselbaum RR, Hallahan D, Fuks Z, Kufe D. Radiation Induction of Immediate-Early Genes - Effectors of the Radiation- Stress Response. Int J Radiat Oncol 1994; 30: 229-34.

89. Hayden MS, Ghosh S. Signaling to NF-kappaB. Genes Dev 2004; 18: 2195-224.

90. Karin M, Ben-Neriah Y. Phosphorylation meets ubiquitination: the control of NF-[kappa]B activity. Annu Rev Immunol 2000; 18: 621-63.

91. Pahl HL. Activators and target genes of Rel/NF-kappaB transcription factors. Oncogene 1999; 18: 6853-66.

92. Alcamo E, Mizgerd JP, Horwitz BH, et al. Targeted mutation of TNF receptor I rescues the RelA-deficient mouse and reveals a critical role for NF-kappa B in leukocyte recruitment. J Immunol 2001; 167: 1592-600.

93. Chen C, Edelstein LC, Gelinas C. The Rel/NF-kappaB family directly activates expression of the apoptosis inhibitor Bcl-x(L). Mol Cell Biol 2000; 20: 2687-95.

94. Chilov D, Kukk E, Taira S, et al. Genomic organization of human and mouse genes for vascular endothelial growth factor C. J Biol Chem 1997; 272: 25176-83.

95. Guttridge DC, Albanese C, Reuther JY, Pestell RG, Baldwin AS. NF-kappa B controls cell growth and differentiation through transcriptional regulation of cyclin D1. Mol Cell Biol 1999; 19: 5785-99.

96. Kunsch C, Rosen CA. NF-kappa B subunit-specific regulation of the interleukin-8 promoter. Mol Cell Biol 1993; 13: 6137-46.

97. Lee CH, Jeon YT, Kim SH, Song YS. NF-kappaB as a potential molecular target for cancer therapy. Biofactors 2007; 29: 19-35.

98. Felx M, Guyot MC, Isler M, et al. Endothelin-1 (ET-1) promotes MMP-2 and MMP-9 induction involving the transcription factor NF-kappaB in human osteosarcoma. Clin Sci (Lond) 2006; 110: 645-54.

99. May MJ, Ghosh S. Signal transduction through NF-kappa B. Immunol Today 1998; 19: 80-8.

100. Hong JH, Chiang CS, Campbell IL, Sun JR, Withers HR, Mcbride WH. Induction of Acute-Phase Gene-Expression by Brain Irradiation. Int J Radiat Oncol 1995; 33: 619-26.

101. Orlowski RZ, Baldwin AS. NF-kappa B as a therapeutic target in cancer. Trends Mol Med 2002; 8: 385-9.

102. Baeuerle PA, Baltimore D. NF-kappa B: Ten years after. Cell 1996; 87: 13-20.

103. Xu Y, Kiningham KK, Devalaraja MN, et al. An intronic NF kappa Belement is essential for induction of the human manganese superoxide dismutase gene by tumor necrosis factor-alpha and interleukin-1beta. DNA Cell Biol 1999; 18: 709-22.

104. Kiningham KK, Xu Y, Daosukho C, Popova B, St Clair DK. Nuclear factor kappaB-dependent mechanisms coordinate the synergistic effect of PMA and cytokines on the induction of superoxide dismutase 2. Biochem J 2001; 353: 147-56.

105. Dhar SK, Lynn BC, Daosukho C, St Clair DK. Identification of nucleophosmin as an NF-kappaB coactivator for the induction of the human SOD2 gene. J Biol Chem 2004; 279: 28209-19.

106. Guo GZ, Yan-Sanders Y, Lyn-Cook BD, et al. Manganese superoxide dismutase-mediated gene expression in radiationinduced adaptive responses. Mol Cell Biol 2003; 23: 2362-78.

107. Murley JS, Kataoka Y, Cao D, Li JJ, Oberley LW, Grdina DJ. Delayed radioprotection by NFkappaB-mediated induction of Sod2 (MnSOD) in SA-NH tumor cells after exposure to clinically used thiol-containing drugs. Radiat Res 2004; 162: 536-46.

108. Chen GQ, Goeddel DV. TNF-R1 signaling: A beautiful pathway. Science 2002; 296: 1634-5.

109. Josson S, Xu Y, Fang F, Dhar SK, St Clair DK, St Clair WH. RelB regulates manganese superoxide dismutase gene and resistance to ionizing radiation of prostate cancer cells. Oncogene 2006; 25: 1554-9.

110. Xu Y, Fang F, St Clair DK, et al. Suppression of RelB-mediated manganese superoxide dismutase expression reveals a primary mechanism for radiosensitization effect of 1alpha,25-dihydroxyvitamin D(3) in prostate cancer cells. Mol Cancer Ther 2007; 6: 2048-56.

111. Sun Y, St Clair DK, Fang F, et al. The radiosensitization effect of parthenolide in prostate cancer cells is mediated by nuclear factor kappa B inhibition and enhanced by the presence of PTEN. Mol Cancer Ther 2007; 6: 2477-86.

112. Lessard L, Begin LR, Gleave ME, Mes-Masson AM, Saad F.Nuclear localisation of nuclear factor-kappaB transcription factors in prostate cancer: an immunohistochemical study. Brit J Cancer 2005; 93: 1019-23.

113. Raffoul JJ, Wang Y, Kucuk O, Forman JD, Sarkar FH, Hillman GG. Genistein inhibits radiation-induced activation of NF-kappaB in prostate cancer cells promoting apoptosis and G2/M cell cycle arrest. BMC Cancer 2006; 6: 107.

114. Collis SJ, Swartz MJ, Nelson WG, DeWeese TL. Enhanced radiation and chemotherapy-mediated cell killing of human cancer cells by small inhibitory RNA silencing of DNA repair factors. Cancer Research 2003; 63: 1550-4.

115. Xu L, Yang DJ, Wang SM, et al. (-)-gossypol enhances response to radiation therapy and results in tumor regression of human prostate cancer. Mol Cancer Ther 2005; 4: 197-205.

116. Kimura K, Bowen C, Spiegel S, Gelmann EP. Tumor necrosis factor-alpha sensitizes prostate cancer cells to gamma-irradiation induced apoptosis. Cancer Res 1999; 59: 1606-14.

117. Mu ZM, Hachem P, Pollack A. Antisense Bcl-2 sensitizes prostate cancer cells to radiation. Prostate 2005; 65: 331-40.

118. An J, Chervin AS, Nie A, Ducoff HS, Huang Z. Overcoming the radioresistance of prostate cancer cells with a novel Bcl-2 inhibitor. Oncogene 2007; 26: 652-61.

119. Colletier PJ, Ashoori F, Cowen D, et al. Adenoviral-mediated p53 transgene expression sensitizes both wild-type and null p53 prostate cancer cells in vitro to radiation. Int J Radiat Oncol 2000; 48: 1507-12.

120. Mu ZM, Hachem P, Agrawal S, Pollack A. Antisense MDM2 sensitizes prostate cancer cells to androgen deprivation, radiation,and the combination. Int J Radiat Oncol 2004; 58: 336-43.

121. Zhang L, Gokhale P, Mewani R, Li BH, Dritschilo A, Soldatenkov V. Prostate cancer radiosensitization by targeting poly(ADP-ribose) polymerase. Mol Ther 2004; 9: S234-S.

122. Hoeijmakers JHJ. Genome maintenance mechanisms for preventing cancer. Nature 2001; 411: 366-74.

123. Audebert M, Salles B, Calsou P. Involvement of poly(ADP-ribose) polymerase-1 and XRCC1/DNA ligase III in an alternative route for DNA double-strand breaks rejoining. J Biol Chem 2004; 279: 55117-26.

124. Boulton S, Kyle S, Durkacz BW. Interactive effects of inhibitors of poly(ADP-ribose) polymerase and DNA-dependent protein kinase on cellular responses to DNA damage. Carcinogenesis 1999; 20: 199-203.

125. Haber JE. DNA recombination: the replication connection. TrendsBiochem Sci 1999; 24: 271-5.

126. Lomonosov M, Anand S, Sangrithi M, Davies R, Venkitaraman AR. Stabilization of stalled DNA replication forks by the BRCA2 breast cancer susceptibility protein. Gene Dev 2003; 17: 3017-22.

127. Collis SJ, Tighe A, Scott SD, Roberts SA, Hendry JH, Margison GP. Ribozyme minigene-mediated RAD51 down-regulation increases radiosensitivity of human prostate cancer cells. Nucleic Acids Res 2001; 29: 1534-8.

CHAPTER 5

IN VIVO RNAI IDENTIFIES SYK AS A CANDIDATE DRUG TARGET FOR PROSTATE CANCER

Veerander PS Ghotra [1], Shuning He [2], Geertje van der Horst [3], Steffen Nijhoff [4], Hans de Bont [1], Annemarie Lekkerkerker [4], Richard Janssen [4], Gabri van der Pluijm[3], Guido Jenster [5], Geert JLH van Leenders [6], A. Marije Hoogland [6], Zuzanna Baranski [1], Bob van de Water [1], B. Ewa Snaar-Jagalska [2] and Erik HJ Danen [1]

Submitted

[1]Division of Toxicology, Leiden Academic Center for Drug Research and [2]Department of Molecular cell Biology, Institute of Biology, Leiden University, Leiden, the Netherlands; [3]Division of Urology, Leiden University Medical Center, Leiden, The Netherlands; [4]Galapagos BV, Leiden, The Netherlands; [5]Department of Urology and [6]Department of Pathology, Erasmus University Medical Center, Rotterdam, The Netherlands

ABSTRACT

In an adenoviral RNAi screen using a zebrafish xenograft automated bioimaging platform (1), we identify SYK as a kinase supporting human prostate cancer dissemination. SYK has not been previously implicated in prostate cancer and we confirm SYK mRNA and protein expression in human prostate cancer specimens. Stable lentiviral silencing confirms a role for SYK in zebrafish xenografts and demonstrates that SYK supports in vitro invasive outgrowth of prostate cancer spheroids. In a mouse experimental prostate cancer metastasis model, SYK RNAi prevents bone colonization and this effect is reversed by wild type but not kinase dead SYK expression. In absence of SYK, cell surface expression of the progression-associated adhesion receptors, integrin alpha-2 and CD44 is diminished and silencing alpha-2 phenocopies SYK depletion in vitro and in vivo. Finally, pharmacological inactivation of SYK similarly interferes with invasive growth and dissemination. As SYK inhibitors are already in Phase I-II clinical trials for rheumatoid arthritis and lymphoid malignancies (2, 3), these preclinical findings can be immediately translated to the clinic to assess efficacy in the treatment of prostate cancer.

INTRODUCTION

Prostate cancer is the most common cancer in males and the second leading cause of cancer deaths among men in the Western world (4). Non-detectable micro-metastatic disease may be present in up to 40% of patients (5) while 8–14% may have visible or symptomatic bone metastases at diagnosis (6). Although the majority of prostate cancers are diagnosed as organ-confined disease, which is curable by prostatectomy or radiation therapy, 20-25% of patients will experience relapse within 5 years of treatment (7). Once the disease has spread beyond the prostate, no curative treatments are currently available (8). In addition to screening programs for early diagnosis and treatment of localized disease, there is an urgent need for novel targeted therapies to improve treatment of metastatic prostate cancer.

RESULTS AND DISCUSSION

A panel of prostate cancer cell lines was xenografted in the yolk of zebrafish and dissemination was analyzed using a whole animal automated bioimaging platform as described (1). Prostate cancer cell lines reported to be androgen-independent and/or metastatic in mice (LNCaP-derived C4-2 and C4-2B; DU145 and PC3) showed enhanced dissemination in comparison with androgen-dependent non-metastatic cells (LNCaP) (9-12) (Fig S1). We therefore devised an adenovirus-based RNAi screen for mediators of prostate cancer dissemination using this platform (Fig 1a). Two independent shRNAs targeting the protein tyrosine kinase, SYK were identified that significantly inhibited PC3 spreading in two independent experiments using ~25 embryos per condition (Fig 1b,c; Fig S2). Additional genes fulfilling these criteria included the cell surface hyaluronan receptor, CD44 and the tyrosine kinase, Src (Fig 1b) that have already been linked to growth and progression of prostate cancer (13-16).

SYK has been extensively implicated in lymphoid malignancies (3) and appears to play opposing roles in different solid tumors (17, 18) but has not been previously associated with prostate cancer. Two independent lentiviral SYK shRNAs confirmed the role of SYK in dissemination in the zebrafish xenograft model (Fig 1d; Fig S3). SYK RNAi also appeared to reduce outgrowth of cells at the primary injection site (Fig S2) and SYK-depleted PC3 cells showed impaired colony formation capacity in vitro (Fig 1e). Moreover, in a model

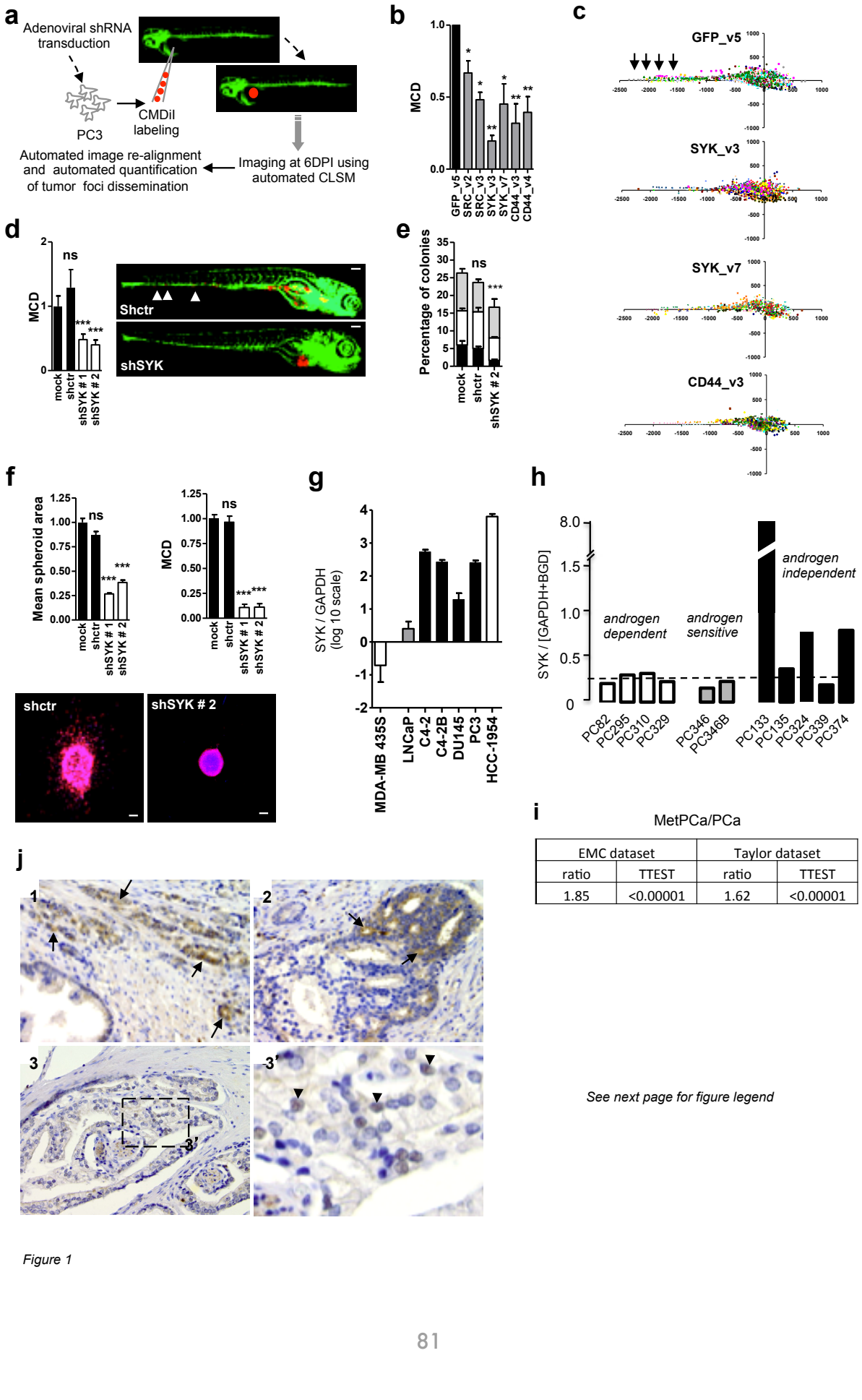

EMC dataset		Taylor dataset	
ratio	TTEST	ratio	TTEST
1.85	<0.00001	1.62	<0.00001

See next page for figure legend

Figure 1

FIGURE 1. *SYK is expressed in human prostate cancer and supports growth, invasion, and dissemination of prostate cancer cells.* (a) Schematic overview of the in-vivo screening procedure. (b) Mean cumulative distance (MCD) of tumor foci relative to site of injection for PC3 cells transiently transduced with indicated adenoviral shRNAs calculated from >40 xenografts obtained from two independent experiments. (c) Representative scatter plots showing tumor foci detected by automated confocal imaging and automated image analysis as described (1) in zebrafish injected with PC3 cells expressing indicated adenoviral shRNAs. Each color shows foci detected in one embryo. Arrows indicate foci in tail region. (d) MCD and representative images for dissemination in zebrafish of PC3 cells stably expressing indicated lentiviral SYK shRNAs (combined data from 2 independent experiments using >32 embryos per condition are shown). (e) Quantification of colony formation assay for PC3 cells expressing indicated lentiviral SYK shRNAs. Grey, small; white, medium; black, large colonies. (f) Representative images and quantification of expansion (mean spheroid area) and ECM invasion (MCD) for control and shSYK PC3 cell spheroids 6 days post-injection in collagen gels (blue, Hoechst; red, Phalloidin). Scale bars, 100 µm. (g) SYK RNA expression determined by qPCR in indicated cell lines. MDA-MB-435S (hypermethylated SYK gene promoter (35, 36)) and HCC-1954 breast cancer cells (high SYK expression (36)) were used as negative and positive controls, respectively. (h) SYK RNA expression in human prostate cancer resection specimens xenografted in mice. (i) Ratio between SYK RNA expression in prostate cancer metastases (MetPCa) and primary prostate cancers (PCa) and significance (TTEST) in two different datasets. (j) Immunohistochemical staining of SYK protein in three different prostate cancer specimens (1-3). Arrows point to cytoplasmic staining in cancer cells. Arrowheads in enlargement 3' point to infrequently observed nuclear staining. ns, not significant; *p<0.05; ** p<0.01; ***p<0.005.

where cell spheroids are embedded in three dimensional (3D) extracellular matrix (ECM) scaffolds (19), silencing SYK attenuated spheroid expansion and effectively blocked ECM invasion (Fig 1f; Fig S4; Video S1). No signs of increased nuclear fragmentation in SYK-depleted spheroids were observed, pointing to decreased proliferation rather than cell death as the underlying mechanism (Fig S4).

We next analyzed SYK expression in human prostate cancer. Compared to LNCaP, mRNA expression was increased in the androgen-independent LNCaP-derived C4-2 and C4-2B sublines and in DU145 and PC3 androgen-independent, metastatic prostate cancer cell lines (Fig 1g). Likewise, in a series of human prostate cancer xenografts (20), SYK mRNA expression was higher in androgen-independent tumors (Fig 1h) and SYK expression in prostate cancer metastasis resection specimens was significantly increased compared to primary prostate cancer in two datasets (Fig 1i). Since the stromal compartment may affect mRNA analysis in clinical samples, SYK protein expression was analyzed in a set of primary prostate cancer specimens. Immunohistochemistry validated SYK expression in prostate cancer cells and expression was increased in prostate cancer versus normal prostate epithelium (Fig 1j).

In acute lymphoid leukemia (AML), inhibition of SYK promotes differentiation (21). We analyzed a set of transcripts previously associated with undifferentiated characteristics of prostate cancer cells (22) but observed no gross changes in the expression of these genes upon depletion of SYK. However, while mRNA levels of the prostate cancer progression-associated markers CD44 and integrin α2β1 (13, 14, 23-25) were unaffected (Fig S5); their cell surface expression was lost following SYK depletion (Fig 2a). SYK has been previously reported to regulate surface expression of transmembrane receptors (26, 27) and two adenoviral CD44 shRNAs were identified as hits in our primary screen (Fig 1b). Moreover, lentiviral silencing of α2 or β1 integrin subunits, each by two independent shRNAs, suppressed 3D ECM invasion as well as dissemination in the zebrafish model (Fig 2b,c; Fig S6). A role for β1 integrins in intravascular locomotion of tumor cells in zebrafish has been previously reported (28). Together, these results identify regulation of surface expression of adhesion receptors as a potential underlying mechanism for the support of prostate cancer dissemination by SYK.

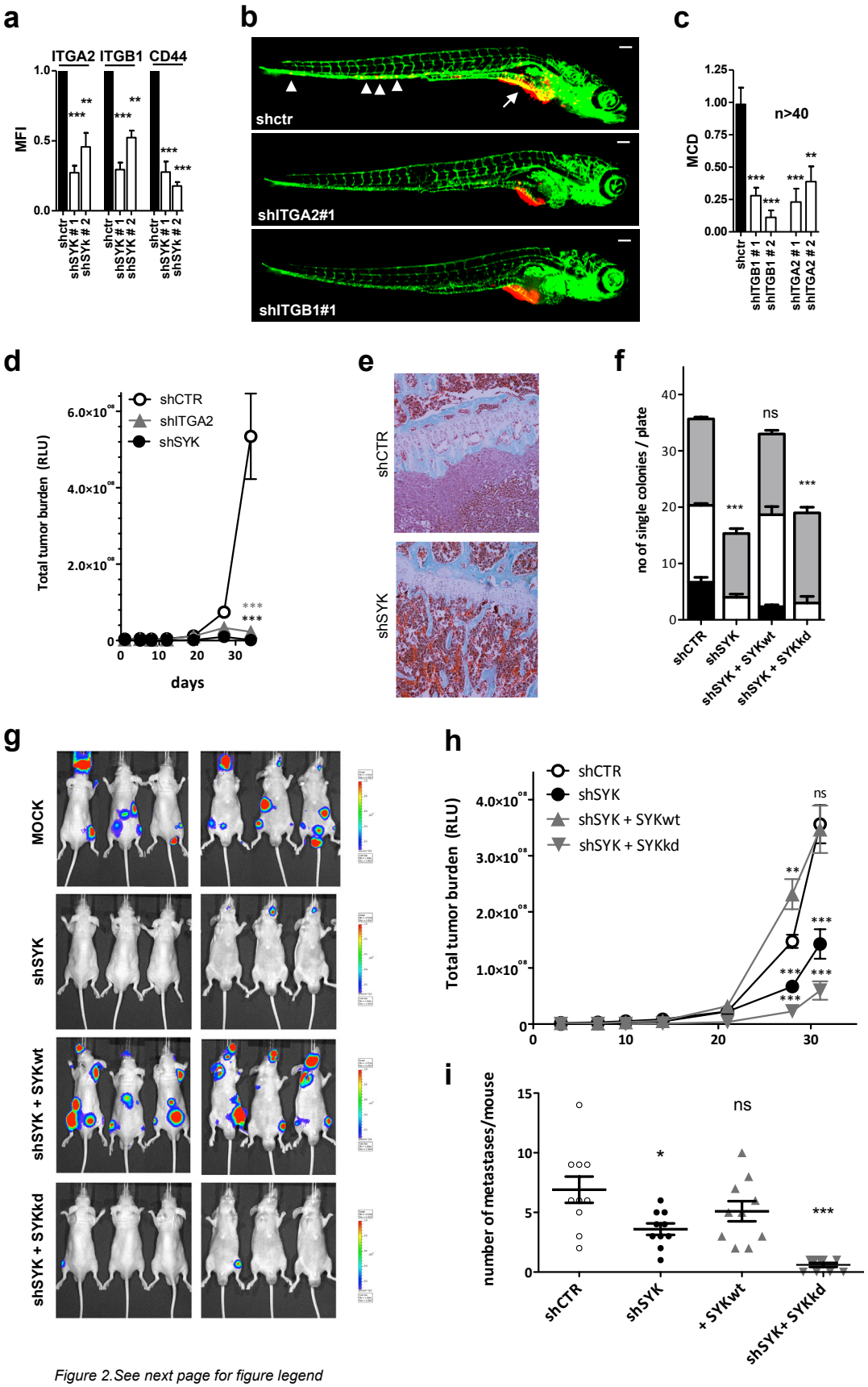

Figure 2.See next page for figure legend

FIGURE 2. *SYK regulation of adhesion receptor surface expression in human prostate cancer cells modulates dissemination in zebrafish and metastatic colonization in mice.* (a) FACS analysis of surface expression of CD44 and integrin subunits α2(ITGA2) and β1(ITGB1) in PC3 cells expressing indicated SYK shRNAs. MFI, mean fluorescence intensity. (b,c) Representative images (b) and quantified MCD (c) for dissemination in zebrafish of PC3 cells expressing indicated lentiviral shRNAs (combined data from 2 independent experiments using > 40 embryo's per condition are shown; Scale bar is 100 μm). Arrow heads indicate tumor foci in tail region. (d) Total metastatic tumor burden determined by BLI monitoring at indicated time points following intra-cardiac inoculation in immune-compromised mice for PC3M-Pro4luc variants expressing indicated lentiviral shRNAs (data obtained from at least 9 mice per experimental group). (e) Bones of mice collected 31 days after intracardiac inoculation with PC3M-Pro4-luc shCTR or shSYK cells and stained with Goldner staining. *, tumor lesion. (f) Quantification of colony formation assay for PC3M-Pro4-luc cells expressing control or SYK shRNAs in combination with wild type (SYKwt) or kinase dead SYK (SYKkd) expression vectors. Grey, small; white, medium; black, large colonies. (g) BLI images of PC3M-Pro4luc variants expressing control or SYK shRNAs in combination with wild type (SYKwt) or kinase dead (SYKkd) expression vectors taken 31 days following intra-cardiac inoculation. (h,i) Quantification of the experiment shown in (g) where total metastatic tumor burden was determined by BLI monitoring at indicated time points (h) and the number of metastatic colonies was determined by counting of BLI foci at 31 days following intra-cardiac inoculation (data obtained from at least 10 mice per experimental group) (i). ns, non significant; *p<0.05; ** p<0.01; ***p<0.005 versus shCTR.

We next addressed the role of SYK in a preclinical mouse xenograft model for prostate cancer bone metastasis (29). Depletion of SYK led to a strong reduction in metastatic tumor burden following intracardiac inoculation of PC3M-Pro4luc cells (Fig 2d,e). Similar to its effect in vitro and in zebrafish xenografts; shRNA targeting integrin 2-subunit mRNA, phenocopied shSYK in this model (Fig 2d). To further interrogate the specific role for SYK kinase activity in prostate cancer bone colonization, wild type or kinase dead SYK was expressed in PC3M-Pro4luc cells expressing an shRNA targeting the SYK 3'UTR. Wild type but not kinase dead SYK rescued the in vitro colony forming ability of these cells (Fig 2f). Moreover, effective bone colonization of shSYK cells was restored by wild type SYK while expression of kinase dead SYK even further suppressed the process with very few detectable metastases (Fig 2g-i).

Based on these findings, we performed initial experiments to evaluate whether pharmacological inhibition of SYK could interfere with in vitro invasive outgrowth and in vivo dissemination using zebrafish xenografts. Small molecule inhibitors of SYK are in clinical development for autoimmune diseases and lymphoid malignancies (2, 3). Two of these compounds, R-406 and BAY-61-3606 show efficacy in preclinical leukemia and retinoblastoma studies (21, 30-33). When used at 1-10μM, the concentration widely used in vitro (21, 30-33) these compounds reduced spheroid outgrowth and ECM invasion of PC3 as well as C4-2B cells (Fig 3a-c). Moreover, R-406 significantly inhibited dissemination of PC3 cells (Fig 3d) without significant signs of toxicity at 10μM (e.g. yolk sac edema, cardiac edema, bending of the tail, hepatic necrosis, and impaired cardiovascular function were compared for R-406 and vehicle control treated animals). Thus, pharmacological inactivation of SYK using R-406 and BAY-61-3606 recapitulated the effect of silencing the SYK gene in vitro and in zebrafish xenografts.

In summary, we demonstrate that a semi-automated whole animal bioimaging assay based on zebrafish xenotransplantation (1) can be productive in RNAi-based preclinical target discovery and lead compound identification. We show that genetic and pharmacological inactivation points to a role for SYK in invasive growth and dissemination of prostate cancer. SYK mRNA and protein is detected in human prostate cancer tissues and SYK inhibitors have already been tested in phase I-II clinical trials for other diseases. Altogether, this establishes SYK as a potential new drug target in prostate cancer for which existing pharmacological inhibitors with known toxicological profiles can be tested for clinical efficacy.

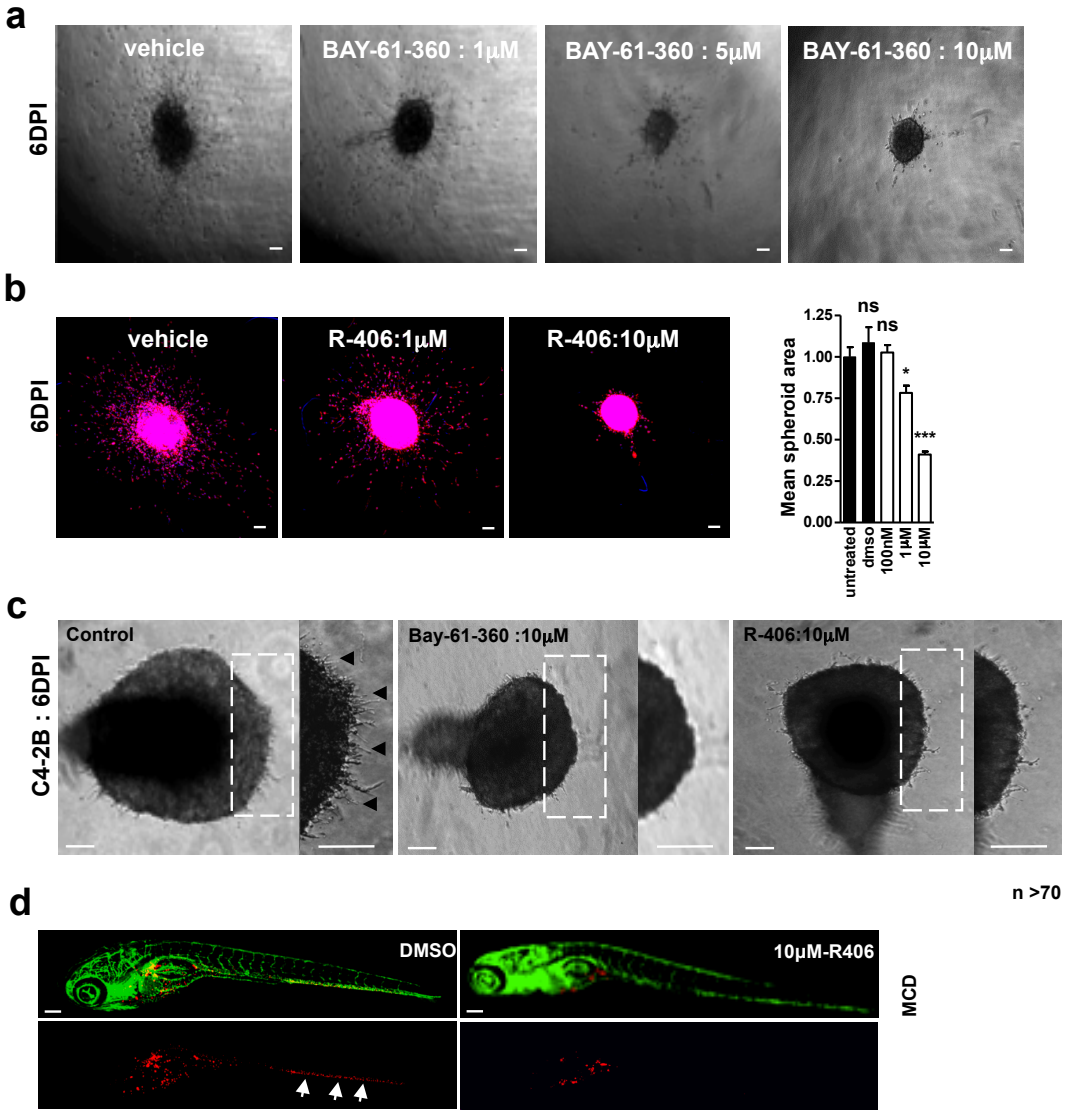

FIGURE 3. *Pharmacological inhibition of SYK prevents growth, invasion, and dissemination of prostate cancer cells*. (a) Bright field images showing PC3 spheroids 6 days post-injection into collagen gels in the absence or presence of the indicated concentrations of BAY-61-360 (one of three experiments is shown). (b) Representative images and quantification of expansion (mean spheroid area) and ECM invasion (MCD) for PC3 cell spheroids measured at 6 days post-injection in collagen gels and treated with indicated concentrations of R-406 (blue, Hoechst; red, Phalloidin; scale bar is 120 µm). (c) Brightfield images showing C4-2B cell spheroids at 6 days post formation in the absence or presence of the indicated concentrations of SYK inhibitors. Arrowheads point to ECM invading strands seen under control conditions, which are not observed in presence of inhibitors. Scale bar is 120 µm. (d) Representative images and quantified MCD for dissemination in zebrafish of PC3 cells in the absence or presence of indicated concentrations of R-406. Combined data from 2 independent experiments using >70 embryos per condition are shown. Arrows point to cells disseminated to tail region. Scale bar is 100µm; ns, not significant; *p<0.05; ** p<0.01; ***p<0.005.

METHODS

See supplemental information for detailed Materials and Methods.

LNCaP, PC3 and DU-145 cells were obtained from ATCC and cultured according to the provided protocol. PC3M-Pro4luc cells have been described previously (29). LNCaP-derived cell lines C4-2 and C4-2 B were grown in T-Medium. Zebrafish embryo xenografting followed by automated confocal imaging and image analysis algorithms were previously described (1). Dissemination is described as cumulative distance from injection site of tumor cells in each embryo averaged over all embryos (mean cumulative distance; MCD). For the shRNA screen, PC3 cells were transduced with adenoviral shRNA constructs 5 days prior to xeno-transplantation. Stable PC3 and PC3M-Pro4-luc cell lines were generated by lentiviral shRNA (TRC; Sigma) transduction followed by bulk puromycin selection. Wild type or kinase dead (K402R) SYK retrovirus (34) (a kind gift from Drs. Wei Zou and Steven Teitelbaum, Washington University, St Louis MO) was transduced in PC3M-Pro4-luc cells stably expressing shRNA targeting the SYK 3'UTR, followed by bulk blasticydin selection. RNA isolation, qPCR, immunohistochemistry on paraffin-embedded tissues, and FACS were done using standard protocols. Growth and ECM invasion was studied for cell spheroids embedded in collagen gels as described (19) and quantified using an automated Image pro 7-based plugin to calculate surface area of spheroid, number of cells migrating out and cumulative distance travelled by these cells. The latter is described as MCD. Experimental bone metastasis in mice was analyzed by weekly whole body bioluminescent imaging (BLI) and Goldner bone staining in nude mice following intracardiac injection with PC3M-Pro4luc cells as described (29). Data for all experiments are presented as mean ± SEM of at least 3 independent biological replicates unless otherwise stated. Student's t test (two-tailed) was used to compare groups.

ACKNOWLEDGEMENTS

We thank Drs Wei Zou and Steven Teitelbaum for kindly providing SYK plasmids. This work was supported by grants from EU FP7 (HEALTH−F2−2008−201439) and Dutch Cancer Society (UL−2010−4670).

AUTHOR CONTRIBUTIONS

V.P.S.G.,S.H,G.v.d.H,S.N,H.d.B.,A.M.H.,A.L.,Z.B.,and E.H.J.D.designed and performed experiments.
R.J.,G.v.d.P.,G.J.,G.J.L.H.v.L,B.v.d.W.,B.E.S-J.,and E.H.J.D.analyzed and interpreted data.
V.P.S.G. and E.H.J.D. wrote the manuscript.

SUPPLEMENTARY INFORMATION : METHODS

Cell lines and antibodies

LNCaP, PC3 and DU-145 cells were obtained from ATCC and cultured according to the provided protocol. PC3-M-Pro4luc cells have been described previously (1). LNCaP−derived cell lines C4-2 and C4-2B were grown in T-Medium. For FACS, primary antibodies included AIIB2 anti-human integrin β1, 4A10 anti human integrin α2, and sc-18849 anti-human CD44 (Santa-Cruz). Goat-anti-mouse APC and donkey-anti-rat PE (Jackson laboratories) were used as secondary antibodies. For immunohistochemistry in patient tumor samples Syk N−19 Ab (sc-1077; Santa Cruz) was used.

Zebrafish xenotransplantation experiments

For quantification of tumor cell spreading, tumor cells were labeled with CM--DiI (Invitrogen), mixed with 2% PVP, and injected into the yolk sac of enzymatically dechorionated, two-day old Casper fli-EGFP transgenic zebrafish embryos using an air driven microinjector (20 psi, PV820 Pneumatic PicoPump; World precision Inc). Embryos were maintained in egg water at 34°C for 6 days and subsequently fixed with 4% paraformaldehyde. Imaging was done in 96 well plates containing a single embryo per well using a Nikon Eclipse Ti confocal laser-scanning microscope. Z stacks (12 x 30 µm) were obtained using a Plan Apo 4X Nikon dry objective with 0.2 NA and 20 WD. Images were converted into a single Z projection in Image-Pro Plus (Version 6.2; Media Cybernetics). Automated quantification of cumulative tumor cell spreading per embryo was carried out using an in-house built Image-Pro Plus plugin as previously described (2).

Transient adenoviral shRNA transduction

PC3 cells were transduced one day after seeding with adenoviral shRNA constructs from Galapagos BV (Leiden, the Netherlands) using an MOI of 15 for 24 h. After 3 days, medium was replaced and after an additional two days, the transduced PC3 cells were detached with trypsin and single cell suspensions were used for zebrafish xenotransplantation.

Stable shRNA and cDNA expression

PC3 or PC3-M-Pro4luc cells were transduced using Sigma's MISSION library lentiviral shRNAs (shSYK#1: TRCN0000003167, shSYK#2:TRCN0000199566; shITGB1#1:TRCN0000029645, shITGB1#2:TRCN0000029646; shITGA2#1: TRCN0000057730, shITGA2#2: TRCN00000057731). For lentivirus production, HEK293T cells were transfected with the short hairpin constructs together with the packaging plasmids REV, GAG and VSV in a 1:1:1:1 ratio using PE (Sigma) as transfection reagent. Lentiviral supernatant was collected 48 h after transfection and used for transduction or target cells in the presence of 8 µg Polybrene (Sigma). Transduced cells were bulk selected in medium containing 2 µg/ml puromycin. Lentiviral shRNA vector targeting TurboGFP was used as a negative control. Retroviral cDNAs for wild type and kinase dead SYK were a gift from Drs. Wei Zou and Steven Teitelbaum, Washington University, St Louis MO (3). Retrovirus was produced in Plat-E packaging cells and used for transduction of PC3-M-Pro4-luc cells stably expressing shRNA targeting SYK 3'UTR, followed by bulk blasticidin selection.

mRNA expression analysis

For qPCR, total RNA was extracted using RNA easy Plus Mini Kit (Qiagen). cDNA was randomly primed from 50 ng total RNA using iScript cDNA synthesis kit (BioRad) and real-time qPCR was subsequently performed in triplicate using SYBR green PCR (Applied Biosystems) on a 7900HT fast real-time PCR system (Applied Biosystems).

The following qPCR primer sets were used:

GAPDH: forward AGCCACATCGCTCAGACACC, reverse ACCCGTTGACTCCGACCTT;
SYK forward GATGCTGGTTATGGAGATG, reverse TCTATGATGTTCTTATCCTTGAC;
CD44 forward TGGCACCCGCTATGTCCAG, reverse GTAGCAGGGATTCTGTCTG;
ITGB1 forward ATTGACCTCTACTACCTT, reverse GTGTTGTGCTAATGTAAG;
ITGA2 forward AACTCTTTGGATTTGCGTGTG, reverse TGGCAGTCTCAGAATAGGCTTC.

Data were collected and analyzed using SDS2.3 software (Applied Biosystems). Relative mRNA levels after correction for GAPDH control mRNA, were expressed using 2^(-ΔΔCt) method. For mRNA expression analysis of human prostate cancer patient material either directly or following xenografting in mice, existing datasets were queried as described (4).

Colony-Forming Assay

Cells were seeded into a 96-well plate containing ~1 cell per well. After 1 to 3 weeks, percentage of wells showing colonies and colony size was determined by microscopy (Zeiss Axiovert 200M).

3D invasion assays

Cell suspensions in PBS containing 2% polyvinylpyrrolidone (PVP; Sigma-Aldrich) were microinjected (~1x104 cells/droplet) using an air driven microinjector (20 psi, PV820 Pneumatic PicoPump; World precision Inc) into solidified 3D collagen gels in 8 well μslides (IBIDI) as previously described (5). Collagen gels were prepared from 2.5 mg/ml acid-extracted rat tail collagen type 1. Collagen was diluted to working concentration of 1 mg/ml in complete medium containing 44 mM NaHCO3 (stock 440 mM, Merck) and 0.1 M Hepes (stock 1M, BioSolve). Tumor cell spheroids were monitored for ~1 week using Nikon eclipse TS100. For immunostaining, gels were incubated for 1 hour with 5 μg/ml collagenase (Clostridium histolyticum, Boehringer Mannheim) at room temperature, fixed with 4% paraformaldehyde, and permeabilized in 0.2% Triton X-100. After fixation, collagen gels were stained using a cocktail containing 4 % paraformaldehyde, 0.2% Triton X-100 (Sigma) and 0.1 μM rhodamine Phalloidin (Sigma) for 3 hrs. Thereafter, wells were washed with PBS. Preparations were then mounted in Aqua-Poly/Mount solution (Polysciences, Inc) and imaged using a Plan Apo 4X Nikon dry objective with 0.2 NA and 20 WD. A total of 15 Z planes at an interval of 30 μm were captured. Image stacks were converted into two dimensional maximum intensity projections using Image Pro 7.0. Cell spheroids were analyzed using an automated Image pro 7-based plugin to calculate surface area of spheroid, number of cells migrating out of the cell spheroid and cumulative distance travelled by these cells.

Immunohistochemistry

Normal prostate (n=3) and primary prostate cancer specimens (n=21) were mounted on aminoacetylsilane-coated glass slides (Starfrost, Berlin, Germany), deparaffinized in xylene and dehydrated in ethanol. Endogenous peroxidase activity was blocked by 1% hydrogen peroxide in methanol for 20 min. Incubation with citrate buffer was used for antigen retrieval. Slides were incubated with 1:500 dilution of Syk antibody (sc-1077; Santa Cruz) overnight at 4°C, followed by chromogenic visualization using the EnVision DAKO kit (Dako, Glostrup, Denmark). After counterstaining with hematoxylin, slides were thoroughly washed, dehydrated, cleared in xylene and mounted in malinol (Chroma-Geselschaft, Körgen, Germany).

Experimental bone metastasis assay

Male nude (BALB/c nu/nu) mice were anesthetized and injected with a single-cell suspension of 10^5 cells/100 µl in PBS into the left cardiac ventricle. Outgrowth of spread PC3-M-Pro4luc cells was monitored weekly by whole body bioluminescent imaging (BLI) using an intensified charge-coupled device (I-CCD) video camera of the in vivo Imaging System (IVIS100; Xenogen, Alameda, CA, USA) as described previously (1). Values are expressed as RLUs in photons/s. Bone metastases were also examined by Goldner staining after mice were sacrificed using decalcified bone.

Flow cytometry

For flowcytometry, surface expression levels were determined using primary antibodies, followed by fluorescence-conjugated secondary antibodies, and analysis on a FACSCanto or sorting on a FACS Calibur (Becton Dickinson).

Statistical analysis

Data are presented as mean ± SEM of at least 3 independent biological replicates unless otherwise stated. Student's t test (two-tailed) was used to compare groups.

References concerning methods

1. van den Hoogen, C., van der Horst, G., Cheung, H., Buijs, J.T., Pelger, R.C., and van der Pluijm, G. 2011. Integrin alphav expression is required for the acquisition of a metastatic stem/progenitor cell phenotype in human prostate cancer. Am J Pathol 179:2559-2568.

2.Ghotra, V.P., He, S., de Bont, H., van der Ent, W., Spaink, H.P., van de Water, B., Snaar-Jagalska, B.E., and Danen, E.H. 2012. Automated whole animal bio-imaging assay for human cancer dissemination. PLoS One 7:e31281.

3.Zou, W., Reeve, J.L., Zhao, H., Ross, F.P., and Teitelbaum, S.L. 2009. Syk tyrosine 317 negatively regulates osteoclast function via the ubiquitin-protein isopeptide ligase activity of Cbl. J Biol Chem 284:18833-18839.

4.Martens-Uzunova, E.S., Jalava, S.E., Dits, N.F., van Leenders, G.J., Moller, S., Trapman, J., Bangma, C.H., Litman, T., Visakorpi, T., and Jenster, G. 2012. Diagnostic and prognostic signatures from the small non-coding RNA transcriptome in prostate cancer. Oncogene 31:978-991.

5.Truong, H.H., de Sonneville, J., Ghotra, V.P., Xiong, J., Price, L., Hogendoorn, P.C., Spaink, H.H., van de Water, B., and Danen, E.H. 2012. Automated microinjection of cell-polymer suspensions in 3D ECM scaffolds for high-throughput quantitative cancer invasion screens. Biomaterials 33:181-188.

SUPPLEMENTARY FIGURES

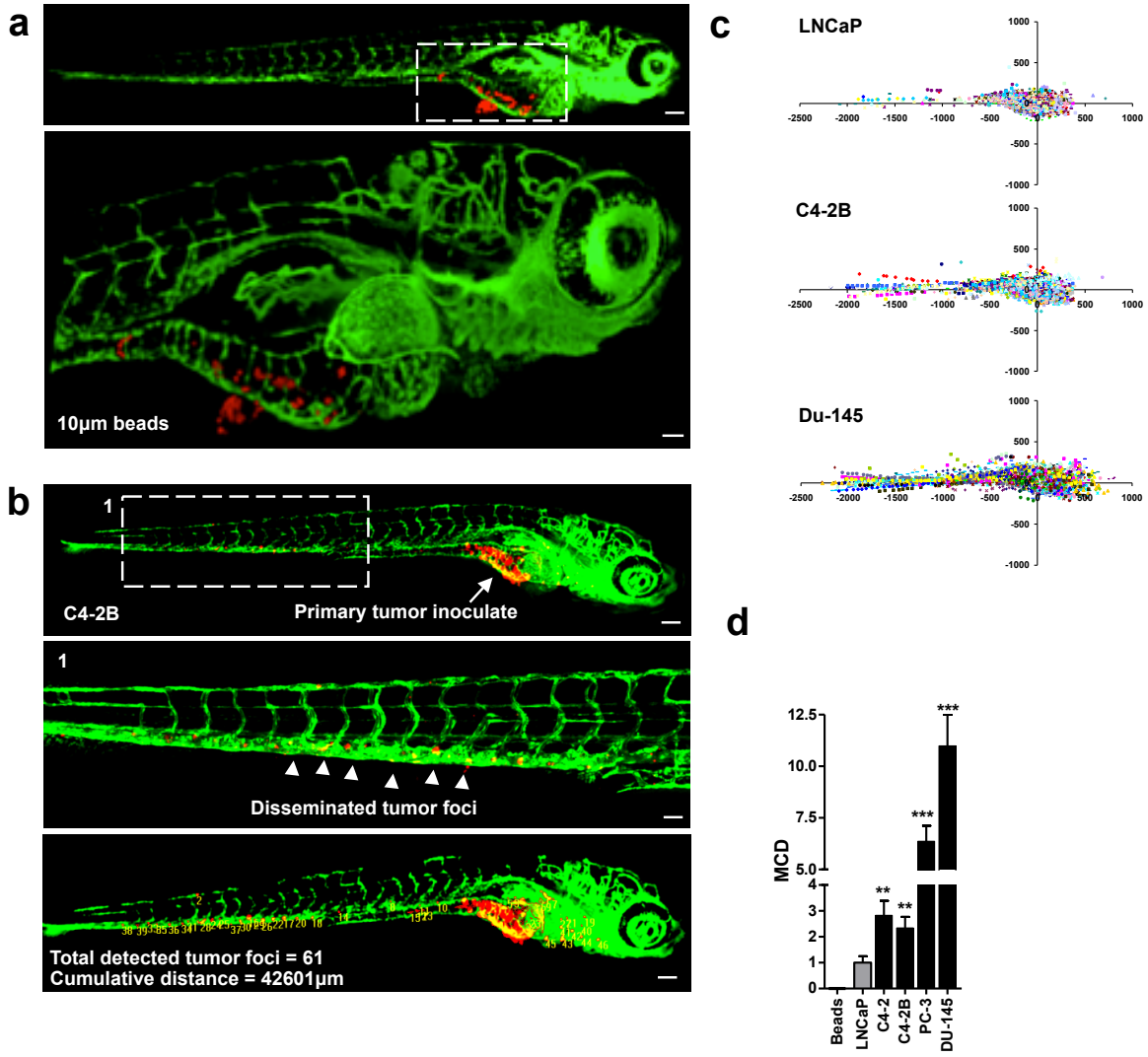

FIGURE S1. *Whole organism automated bioimaging assay differentiates between androgen independent / metastatic and androgen-dependent / non-metastatic prostate cancer cells.* (a) Representative image of Casper fli- EGFP embryo 6 days following yolk sac implantation of 10µm fluorescent beads. Scale bar is 100µm for upper image, and 50µm for lower enlargement of area in inset. Passive spreading of beads was virtually undetectable and used as threshold for cancer cell dissemination. (b) Representative image of C4-2B implanted embryos 6 days following xenotransplantation. Top, scale bar is 100 µm; middle, enlargement of inset, arrowheads point to disseminated tumor cells, scale bar is 50 µm; bottom, automated imaging and image analysis derived tumor foci – scale bar is 100 µm). (c) Scatter plots derived from automated imaging and image analysis of zebrafish xenografts with indicated cell lines 6 days following xenotransplantation in the yolk of Casper fli-EGFP embryos. Colors represent tumor cell foci detected in individual embryos. (d) Mean cumulative distance (MCD) determined from scatter plots represented in c for indicated cell lines using 10µm fluorescent beads as negative control. Data from 2 independent experiments are combined. In total 5 embryos were transplanted with beads, 128 with LNCaP, 147 with C4-2B, 147 with DU145, and 147 with PC3. ns, not significant; *p<0.05; ** p<0.01; ***p<0.005.

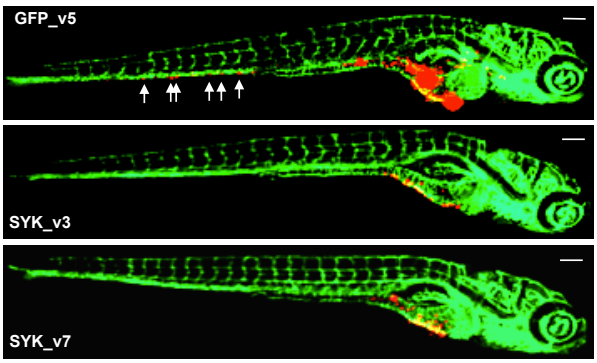

FIGURE S2. *SYK depletion attenuates PC3 dissemination in zebrafish xenografts*. Representative images of embryos implanted with PC3 cells expressing indicated adenoviral shRNAs at 6 days following xenotransplantation. Arrows point to tumor foci in tail region.

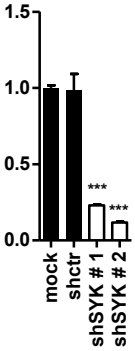

FIGURE S3. *Generation of stable lentiviral bulk-puromycin selected PC3 shSYK lines*. qPCR analysis of SYK expression in PC3 cells stably expressing indicated lentiviral SYK shRNAs.

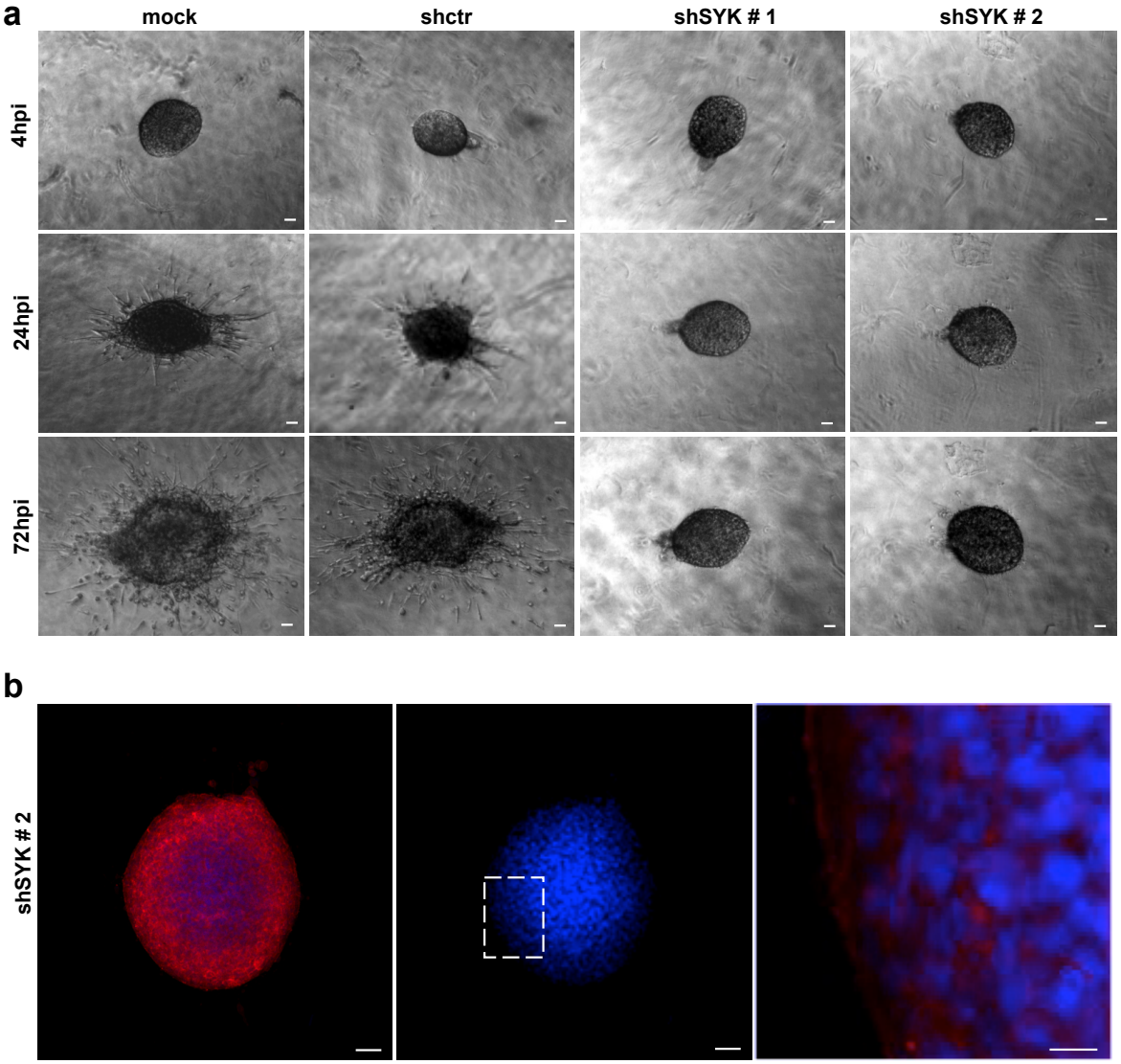

FIGURE S4. *SYK depletion attenuates PC3 3D ECM invasion*. (a) Bright field images showing representative spheroids of PC3 cells expressing indicated lentiviral shRNAs at 6 days post-injection into collagen gels. Scale bar is 120µm. (b) PC3shSYK spheroid 6 days post-formation in collagen gel, (blue, Hoechst; red, Phalloidin). Scale bars are 100µm.

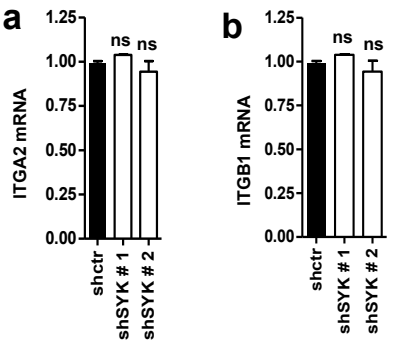

FIGURE S5. *SYK depletion does not downregulate integrin expression at mRNA level.* qPCR analysis of integrin α2 and β1 subunits in two independent lentiviral shSYK expressing PC3 lines

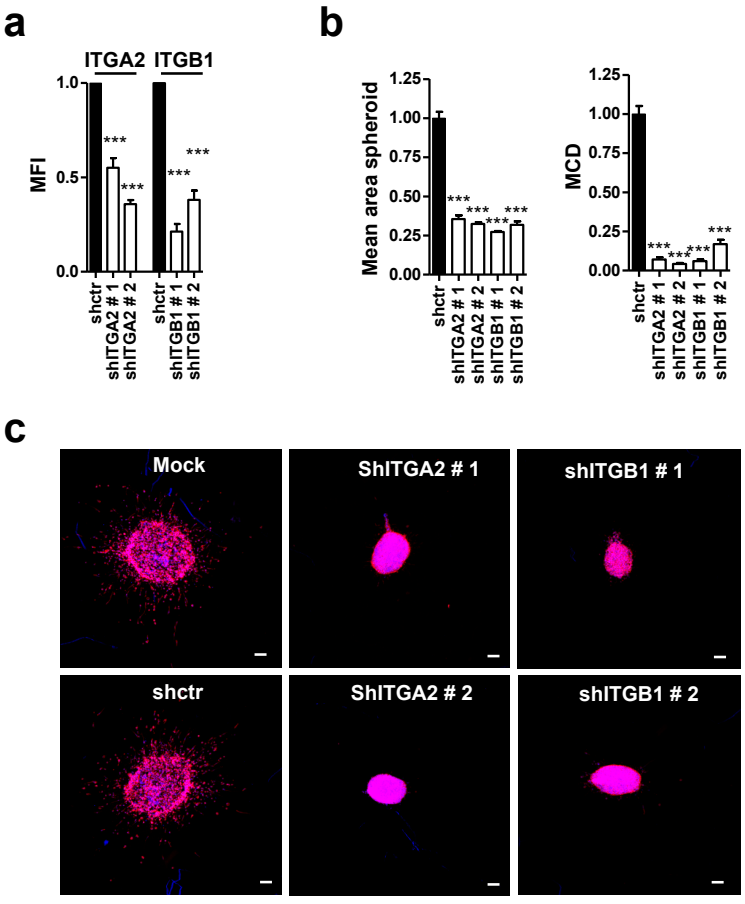

FIGURE S6. *Silencing integrin α2β1 inhibits 3D ECM invasion and outgrowth of PC3 spheroids.* (a) FACS analysis of surface expression of integrin subunits α2 and β1 in PC3 cells expressing lentiviral shRNAs targeting indicated integrin subunits. (b) Quantification of expansion (mean spheroid area) and ECM invasion (MCD) for cell spheroids derived from control PC3 or PC3 expressing lentiviral shRNAs targeting integrin subunits measured at 6 days post-injection in collagen gels. (c) Representative images of cell spheroids analyzed for b (blue, Hoechst; red,Phalloidin). Scale bar is 120 μm.

REFERENCES

1.Ghotra, V.P., He, S., de Bont, H., van der Ent, W., Spaink, H.P., van de Water, B., Snaar-Jagalska, B.E., and Danen, E.H. 2012. Automated whole animal bio-imaging assay for human cancer dissemination. PLoS One 7:e31281.

2.Weinblatt, M.E., Kavanaugh, A., Genovese, M.C., Musser, T.K., Grossbard, E.B., and Magilavy, D.B. 2010. An oral spleen tyrosine kinase (Syk) inhibitor for rheumatoid arthritis. The New England journal of medicine 363:1303-1312.

3.Friedberg, J.W., Sharman, J., Sweetenham, J., Johnston, P.B., Vose, J.M., Lacasce, A., Schaefer-Cutillo, J., De Vos, S., Sinha, R., Leonard, J.P., et al. 2010. Inhibition of Syk with fostamatinib disodium has significant clinical activity in non-Hodgkin lymphoma and chronic lymphocytic leukemia. Blood 115:2578-2585.

4.Nelson, W.G., De Marzo, A.M., and Isaacs, W.B. 2003. Prostate cancer. N Engl J Med 349:366-381.

5.Freedland, S.J., Humphreys, E.B., Mangold, L.A., Eisenberger, M., Dorey, F.J., Walsh, P.C., and Partin, A.W. 2005. Risk of prostate cancer-specific mortality following biochemical recurrence after radical prostatectomy. JAMA 294:433-439.

6.Landis, S.H., Murray, T., Bolden, S., and Wingo, P.A. 1999. Cancer statistics, 1999. CA Cancer J Clin 49:8-31, 31.

7.Wirth, M.P., See, W.A., McLeod, D.G., Iversen, P., Morris, T., and Carroll, K. 2004. Bicalutamide 150 mg in addition to standard care in patients with localized or locally advanced prostate cancer: results from the second analysis of the early prostate cancer program at median followup of 5.4 years. J Urol 172:1865-1870.

8.Mundy, G.R. 2002. Metastasis to bone: causes, consequences and therapeutic opportunities. Nat Rev Cancer 2:584-593.

9.Thalmann, G.N., Anezinis, P.E., Chang, S.M., Zhau, H.E., Kim, E.E., Hopwood, V.L., Pathak, S., von Eschenbach, A.C., and Chung, L.W. 1994. Androgen-independent cancer progression and bone metastasis in the LNCaP model of human prostate cancer. Cancer Res 54:2577-2581.

10.Shevrin, D.H., Kukreja, S.C., Ghosh, L., and Lad, T.E. 1988. Development of skeletal metastasis by human prostate cancer in athymic nude mice. Clin Exp Metastasis 6:401-409.

11.Wu, T.T., Sikes, R.A., Cui, Q., Thalmann, G.N., Kao, C., Murphy, C.F., Yang, H., Zhau, H.E., Balian, G., and Chung, L.W. 1998. Establishing human prostate cancer cell xenografts in bone: induction of osteoblastic reaction by prostate-specific antigen-producing tumors in athymic and SCID/bg mice using LNCaP and lineage-derived metastatic sublines. Int J Cancer 77:887-894.

12.Ware, J.L., Paulson, D.F., Mickey, G.H., and Webb, K.S. 1982. Spontaneous metastasis of cells of the human prostate carcinoma cell line PC-3 in athymic nude mice. J Urol 128:1064-1067.

13.Paradis, V., Eschwege, P., Loric, S., Dumas, F., Ba, N., Benoit, G., Jardin, A., and Bedossa, P. 1998. De novo expression of CD44 in prostate carcinoma is correlated with systemic dissemination of prostate cancer. J Clin Pathol 51:798-802.

14.Desai, B., Rogers, M.J., and Chellaiah, M.A. 2007. Mechanisms of osteopontin and CD44 as metastatic principles in prostate cancer cells. Molecular cancer 6:18.

15.Slack, J.K., Adams, R.B., Rovin, J.D., Bissonette, E.A., Stoker, C.E., and Parsons, J.T. 2001. Alterations in the focal adhesion kinase/Src signal transduction pathway correlate with increased migratory capacity of prostate carcinoma cells. Oncogene 20:1152-1163.

16.Agoulnik, I.U., Vaid, A., Bingman, W.E., 3rd, Erdeme, H., Frolov, A., Smith, C.L., Ayala, G., Ittmann, M.M., and Weigel, N.L. 2005. Role of SRC-1 in the promotion of prostate cancer cell growth and tumor progression. Cancer Res 65:7959-7967.

17.Luangdilok, S., Box, C., Patterson, L., Court, W., Harrington, K., Pitkin, L., Rhys-Evans, P., O-charoenrat, P., and Eccles, S. 2007. Syk tyrosine kinase is linked to cell motility and progression in squamous cell carcinomas of the head and neck. Cancer Research 67:7907-7916.

18.Coopman, P.J., Do, M.T., Barth, M., Bowden, E.T., Hayes, A.J., Basyuk, E., Blancato, J.K., Vezza, P.R., McLeskey, S.W., Mangeat, P.H., et al. 2000. The Syk tyrosine kinase suppresses malignant growth of human breast cancer cells. Nature 406:742-747.

19.Truong, H.H., de Sonneville, J., Ghotra, V.P., Xiong, J., Price, L., Hogendoorn, P.C., Spaink, H.H., van de Water, B., and Danen, E.H. 2012. Automated microinjection of cell-polymer suspensions in 3D ECM scaffolds for high-throughput quantitative cancer invasion screens. Biomaterials 33:181-188.

20.van Weerden, W.M., de Ridder, C.M., Verdaasdonk, C.L., Romijn, J.C., van der Kwast, T.H., Schroder, F.H., and van Steenbrugge, G.J. 1996. Development of seven new human prostate tumor xenograft models and their histopathological characterization. Am J Pathol 149:1055-1062.

21.Hahn, C.K., Berchuck, J.E., Ross, K.N., Kakoza, R.M., Clauser, K., Schinzel, A.C., Ross, L., Galinsky, I., Davis, T.N., Silver, S.J., et al. 2009. Proteomic and genetic approaches identify Syk as an AML target. Cancer cell 16:281-294.

22.Floryk, D., Tollaksen, S.L., Giometti, C.S., and Huberman, E. 2004. Differentiation of human prostate cancer PC-3 cells induced by inhibitors of inosine 5'-monophosphate dehydrogenase. Cancer Res 64:9049-9056.

23.Hall, C.L., Dubyk, C.W., Riesenberger, T.A., Shein, D., Keller, E.T., and van Golen, K.L. 2008. Type I collagen receptor (alpha2beta1) signaling promotes prostate cancer invasion through RhoC GTPase. Neoplasia 10:797-803.

24.Van Slambrouck, S., Hilkens, J., Bisoffi, M., and Steelant, W.F. 2009. AsialoGM1 and integrin alpha2beta1 mediate prostate cancer progression. Int J Oncol 35:693-699.

25.Trerotola, M., Rathore, S., Goel, H.L., Li, J., Alberti, S., Piantelli, M., Adams, D., Jiang, Z., and Languino, L.R. CD133, Trop-2 and alpha2beta1 integrin surface receptors as markers of putative human prostate cancer stem cells. Am J Transl Res 2:135-144.

26.Fotheringham, J.A., Coalson, N.E., and Raab-Traub, N. Epstein-Barr Virus Latent Membrane Protein-2A Induces ITAM/Syk and Akt Dependent Epithelial Migration through alphaV-Integrin Membrane Translocation. J Virol.

27.Woollard, K.J., Fisch, C., Newby, R., and Griffiths, H.R. 2005. C-reactive protein mediates CD11b expression in monocytes through the non-receptor tyrosine kinase, Syk, and calcium mobilization but not through cytosolic peroxides. Inflammation Research 54:485-492.

28.Stoletov, K., Kato, H., Zardouzian, E., Kelber, J., Yang, J., Shattil, S., and Klemke, R. 2010. Visualizing extravasation dynamics of metastatic tumor cells. J Cell Sci 123:2332-2341.

29.Van den Hoogen, C., van der Horst, G., Cheung, H., Buijs, J.T., Pelger, R.C., and van der Pluijm, G. 2011. Integrin alphav expression is required for the acquisition of a metastatic stem/progenitor cell phenotype in human prostate cancer. Am J Pathol 179:2559-2568.

30.Baudot, A.D., Jeandel, P.Y., Mouska, X., Maurer, U., Tartare-Deckert, S., Raynaud, S.D., Cassuto, J.P., Ticchioni, M., and Deckert, M. 2009. The tyrosine kinase Syk regulates the survival of chronic lymphocytic leukemia B cells through PKCdelta and proteasome-dependent regulation of Mcl-1 expression. Oncogene 28:3261-3273.

31.Suljagic, M., Longo, P.G., Bennardo, S., Perlas, E., Leone, G., Laurenti, L., and Efremov, D.G. 2010. The Syk inhibitor fostamatinib disodium (R788) inhibits tumor growth in the Emu- TCL1 transgenic mouse model of CLL by blocking antigen-dependent B-cell receptor signaling. Blood 116:4894-4905.

32.Buchner, M., Baer, C., Prinz, G., Dierks, C., Burger, M., Zenz, T., Stilgenbauer, S., Jumaa, H., Veelken, H., and Zirlik, K. 2010. Spleen tyrosine kinase inhibition prevents chemokine- and integrin-mediated stromal protective effects in chronic lymphocytic leukemia. Blood 115:4497-4506.

33.Zhang, J., Benavente, C.A., McEvoy, J., Flores-Otero, J., Ding, L., Chen, X., Ulyanov, A., Wu, G., Wilson, M., Wang, J., et al. A novel retinoblastoma therapy from genomic and epigenetic analyses. Nature 481:329-334.

34.Zou, W., Reeve, J.L., Zhao, H., Ross, F.P., and Teitelbaum, S.L. 2009. Syk tyrosine 317 negatively regulates osteoclast function via the ubiquitin-protein isopeptide ligase activity of Cbl. J Biol Chem 284:18833-18839.

35.Yuan, Y., Mendez, R., Sahin, A., and Dai, J.L. 2001. Hypermethylation leads to silencing of the SYK gene in human breast cancer. Cancer research 61:5558-5561.

36.Wang, L., Duke, L., Zhang, P.S., Arlinghaus, R.B., Symmans, W.F., Sahin, A., Mendez, R., and Dai, J.L. 2003. Alternative splicing disrupts a nuclear localization signal in spleen tyrosine kinase that is required for invasion suppression in breast cancer. Cancer research 63:4724-4730.

CHAPTER 6

MST1R SUPPORTS PROSTATE CANCER INVASION, DISSEMINATION AND FORMATION OF BONE METASTASES

Veerander PS Ghotra [1], Shuning He [2], Geertje van der Horst [3], Steffen Nijhoff [4], Hans de Bont [1], Zuzanna Baranski [1], Annemarie Lekkerkerker [4], Richard Janssen [4], Gabri van der Pluijm[3], Guido Jenster [5], Geert JLH van Leenders [6], A. Marije Hoogland [6], Bob van de Water [1], B. Ewa Snaar-Jagalska [2] and Erik HJ Danen[1]

Submitted

[1]Division of Toxicology, Leiden Academic Center for Drug Research and [2]Department of Molecular cell Biology, Institute of Biology, Leiden University, Leiden, the Netherlands; [3]Division of Urology, Leiden University Medical Center, Leiden, The Netherlands; [4]Galapagos BV, Leiden, The Netherlands; [5]Department of Urology and [6]Department of Pathology, Erasmus University Medical Center, Rotterdam, The Netherlands

ABSTRACT

The receptor tyrosine kinase, MST1R has been implicated in prostate cancer growth and angiogenesis and, in this context; an important role has been attributed to MST1R expressed on tumor-associated macrophages. Here, we observed that MST1R expression in human prostate cancer cell lines correlates with androgen-independency and metastatic capacity. We expressed MST1R shRNAs in androgen-independent, metastatic PC3 cells. Bulk selected stable populations showed ~50% reduction in MST1R mRNA and protein surface expression. As a consequence, cell scattering in 2D and invasive outgrowth in 3D collagen matrices was attenuated, which could be restored by HGF stimulation of the MST1R-related MET receptor. PC3shMST1R cells were also blocked in their ability to disseminate in a zebrafish embryo xenotransplantation model. Furthermore, RNAi targeting MST1R prevented the formation of bone metastases following intracardiac inoculation in mice. Together, these findings demonstrate that down regulation of MST1R can inhibit prostate cancer invasion, dissemination and metastatic colonization.

INTRODUCTION

The macrophage stimulating 1 receptor (MST1R; RON; Met-related tyrosine kinase) is a receptor tyrosine kinase that has been implicated in various epithelial malignancies including breast, colon, ovarian, liver, and head and neck cancers (1-11). MST1R is also overexpressed in primary prostate cancer and at metastatic prostate cancer sites (12). Experiments using MST1R kinase-deficient mice have established a role for MST1R in prostate tumor growth and angiogenesis (13). Interestingly, this can be explained at least in part by a critical role for MST1R expression on macrophages in the tumor microenvironment (14). MST1R transgene expression in prostate epithelium and findings from in vitro experiments indicate that MST1R expressed on prostate cancer cells could contribute to tumor cell survival, production of angiogenic chemokines, and tumor growth (12, 15). Importantly, while localized prostate cancer has an almost 100% survival rate, the occurrence of metastases in bone and other distant sites lowers 5-year survival to ~30%(16). MST1R has not been implicated in prostate cancer progression. The MST1R-related MET receptor stimulates tumor growth and lymph node metastasis in a xenograft model using human PC3 prostate cancer cells (17) and HGF-MET signaling is an important target in prostate cancer progression (18). In this study, we took an RNAi-based approach to investigate the role of MST1R in several aspects of the prostate cancer metastatic cascade including cell migration, invasion, dissemination, and formation of bone metastases.

MATERIALS AND METHODS

Prostate cancer cell lines were obtained from ATCC and cultured according to the standard protocol. PC3-M-Pro4luc cells have been described previously (19). Lentiviral shRNA constructs targeting MST1R (TRCN000012148; TRCN000012150) were obtained from the MISSION library (Sigma-Aldrich). Stable shRNA expressing PC3 and PC3-M-Pro4luc cells were bulk selected by puromycin. Generation of extracellular matrix (ECM)-embedded tumor cell spheroids was performed as previously described (20). Spheroid outgrowth and collagen invasion was quantified using an automated Image pro 7-based plugin to calculate surface area of the spheroid, number of cells migrating into the collagen, and mean cumulative distance (MCD) travelled by these cells. Recombinant hepatocyte growth factor (HGF; Sigma) was used at 5 ng/ml. For zebrafish xenograft assays, CMDiI-labeled PC3 cells were injected in the yolk of 2-day-old fli-EGFP-casper em-

bryos and fixed 6 days post-implantation as described previously (21). The automated process for collection of confocal image stacks, generation of in-focus composite images, alignment and orientation of the images, and subsequent quantification of tumor cell dissemination was done as described previously (21). Dissemination is described as mean cumulative distance (MCD) reflecting cumulative distance from the primary injection site of all tumor cells in each embryo, averaged over all embryos. Experimental bone metastasis in mice was analyzed by ~weekly whole body bioluminescent imaging (BLI) of nude mice following intracardiac injection with PC3-M-Pro4luc cells as described (19). Metastatic lesions in bone were identified by immunohistochemistry. FACS and Western blot experiments were performed as described previously (22) using MET phospho-Tyr1349 (Cell Signaling) and tubulin (Sigma) antibodies. Data for all experiments are presented as mean ± SEM of at least 2 independent biological replicates. Student's t test (two-tailed) was used to compare groups.

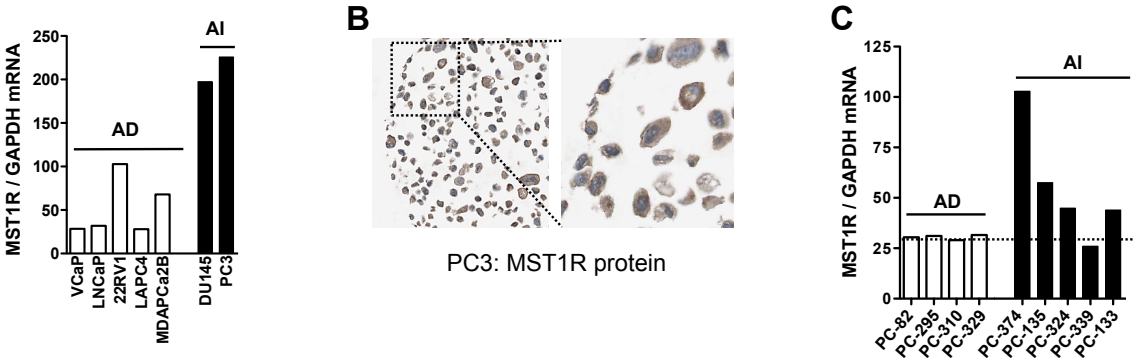

FIGURE 1. *MST1R expression on human prostate cancer cells*. A: MST1R mRNA expression determined by qPCR in panel of human prostate cancer cell lines. AD, androgen-dependent; AI, androgen independent. B: Immuno-histochemical staining showing MST1R expression in PC3 cells. Right panel shows zoom-in of area marked by dotted line in left panel. Adapted from www.proteinatlas.org. C: MST1R RNA expression determined by qPCR in series of human prostate cancer xenograft models.

RESULTS AND DISCUSSION

We evaluated MST1R mRNA expression in a panel of prostate cancer cell lines. MST1R levels in cells reported to be androgen-independent and metastatic in mice, including PC3 cells were 2-8 fold higher than levels found in androgen-dependent non-metastatic cells (Fig 1A). MST1R protein expression was also detected in PC3 cells (Fig 1B). Likewise, in a series of human prostate cancer xenografts representing various aspects of human prostate cancer progression (23), MST1R mRNA levels were higher in most androgen-independent xenografts as compared to androgen-dependent xenografts (Fig 1C).

Based on these expression data, we asked if MST1R plays a role in aspects of prostate cancer progression. To address this question, MST1R expression in PC3 cells was silenced using lentiviral shRNAs. In bulk puromycin-selected stable PC3 shRNA populations, two distinct shRNAs caused ~50% silencing MST1R expression (Fig 2A).

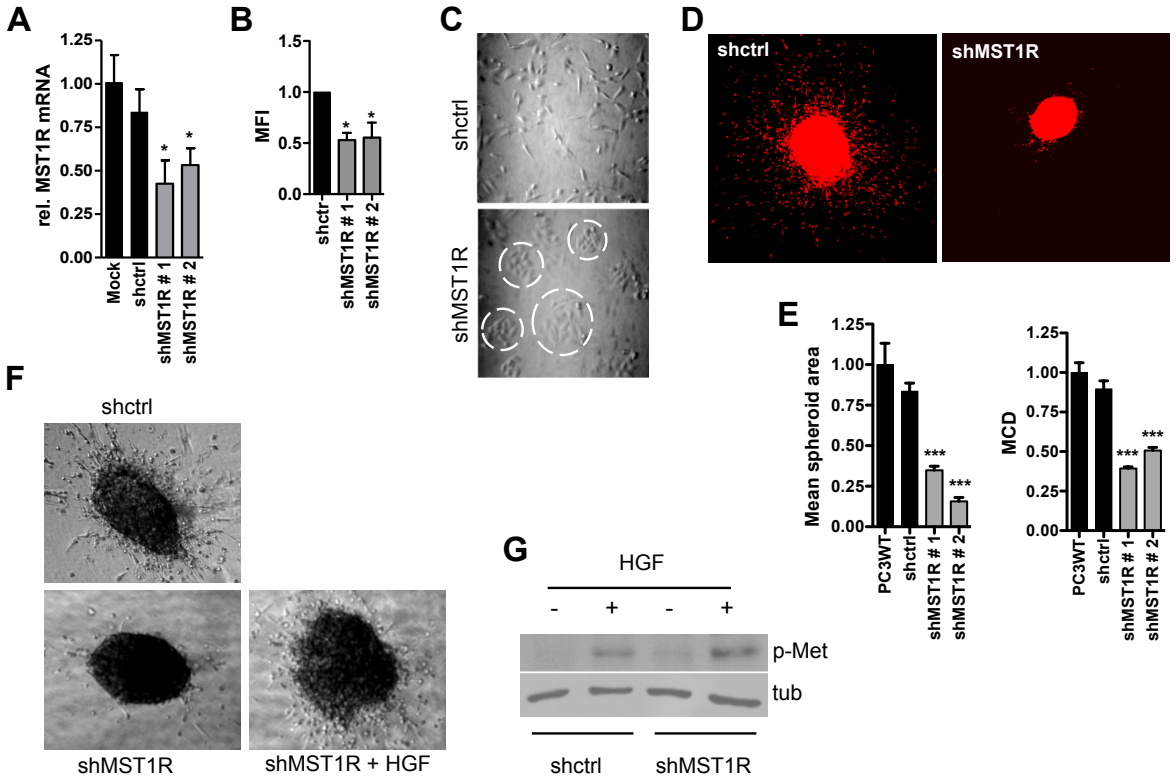

FIGURE 2.*MST1R expression supports invasive growth of human prostate cancer cells*. A: Relative MST1R mRNA expression determined by qPCR in PC3 cells bulk puromycin selected for expression of indicated lentiviral shRNAs. B: FACS analysis of MST1R surface expression on PC3 cells expressing indicated lentiviral shRNAs. MFI, mean fluorescence intesity. C: Microphotographs of 2D cultures of PC3 cells expressing indicated lentiviral shRNAs. Dotted circles indicate cell islands observed in PC3shMST1R cells. D,E: Representative images (D) and quantification (E) of spheroid outgrowth and ECM invasion (mean cummulative distance from spheroid center of migrating cells, MCD) for Phalloidin-stained PC3 cells expressing indicated shRNAs 6 days post-injection in collagen gels. F: Microphotographs of 3D collagen-embedded spheroids 6 days post-injection for PC3shctrl (upper) and PC3shMST1R cells in absence (lower, left) or presence of HGF (lower, right). G: Western blot showing MET phospho-Tyr1349 levels and tubulin (tub) loading control in PC3 cells expressing indicated shRNAs in absence or presence of HGF. Data are presented as mean ± s.e.m.; *p<0.05, ***p<0.001.

FACS analysis confirmed downregulation at the level of MST1R cell surface expression (Fig 2B). Interestingly, reduced expression of MST1R caused a conversion from a completely scattered phenotype to more cohesive growth in 2D culture with formation of multicellular islands (Fig 2C). Moreover, when these cells were grown as spheroids in 3D collagen matrices, wild type- and PC3shctr cells were invasive whereas the number of cells migrating into the collagen was strongly reduced in PC3shMST1R cells (Fig 2D). Quantification of spheroid area and cell migration in Phalloidin-stained 3D cultures demonstrated that MST1R silencing significantly inhibited expansion of spheroids and invasion of cells into the collagen (Fig 2E).

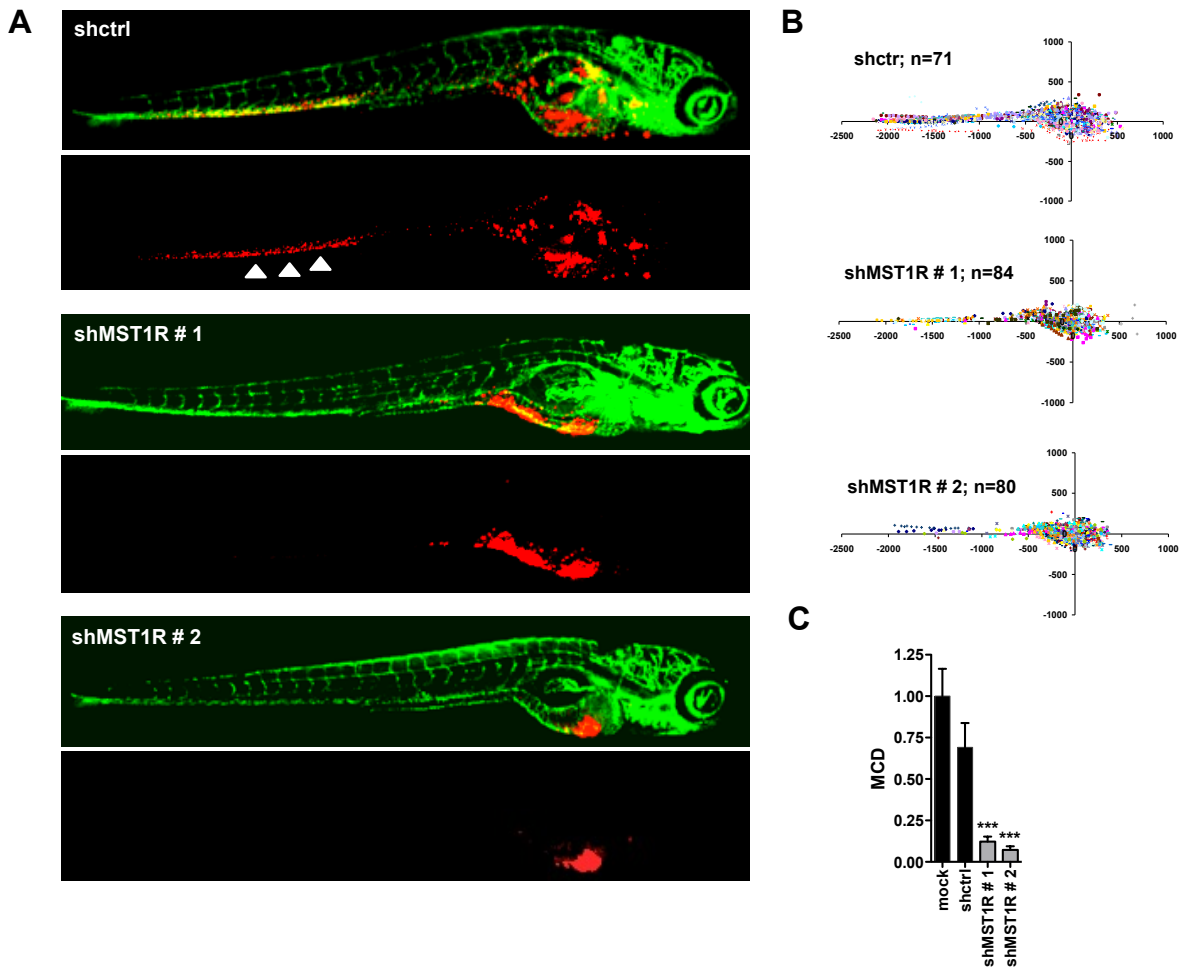

FIGURE 3. *MST1R expression on human prostate cancer cells supports dissemination in zebrafish xenotransplantation model*. A: Confocal microscopy images showing dissemination of PC3 cells expressing indicated MST1R shRNAs 6 days post implantation in yolk of Fli-GFP-Casper zebrafish embryos. Red, CM-DiI-labeled tumor cells; green, GFP-marked endothelial cells. Arrow heads indicate PC3 cells disseminated to tail region. B: Scatter plot representation of dissemination of PC3 cells expressing indicated MST1R shRNAs. Colors represent individual embryos. N=number of injected embryos from 2 biological replicates. C: Mean cumulative distance (MCD) determined from data represented in B. Data are presented as mean ± s.e.m. *p<0.05, ***p<0.001.

Scattering and invasion are stimulated by HGF binding to the MST1R-related MET receptor and this signaling axis is a candidate drug target to halt prostate cancer progression (18). Cross talk between MST1R and MET has been shown to support the transforming potential of oncogenic MET mutants (24). To test if the attenuated invasion caused by MST1R downregulation was due to inactivation of MET signaling PC3shMST1R were treated with HGF. HGF treatment could restore invasion of PC3shMST1R cells (Fig 2F). In agreement, MST1R silencing did not prevent MET phosphorylation in response to HGF (Fig 2G). Together, this indicates that the level of downregulation of MST1R in PC3shMST1R cells attenuates invasion without compromising HGF-MET signaling.

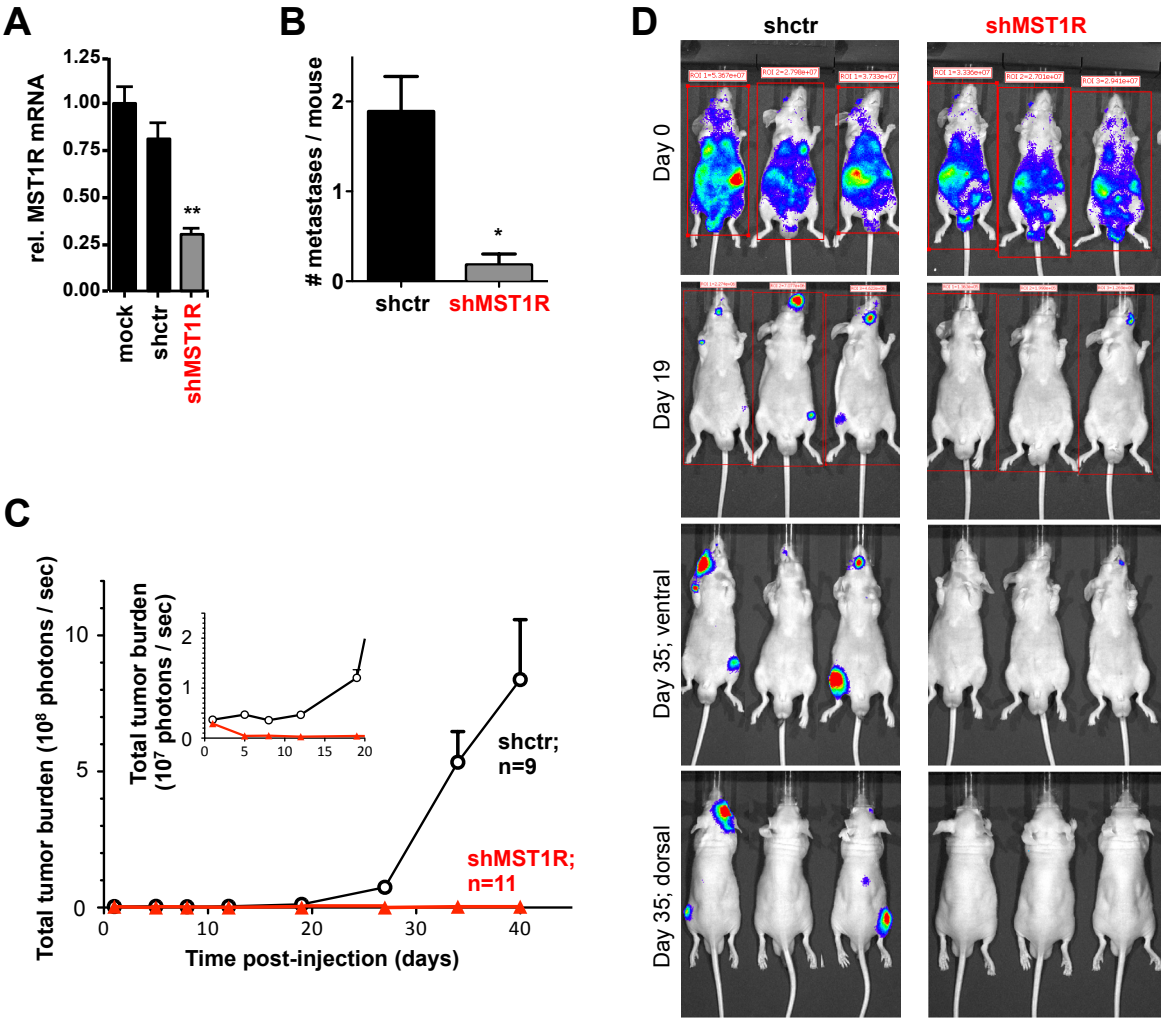

FIGURE 4. *MST1R expression on human prostate cancer cells supports metastatic colonization in mouse experimental bone metastasis model*. A: Relative MST1R RNA expression determined by qPCR in PC3-M-Pro4luc cells bulk puromycin selected for expression of indicated lentiviral shRNAs. B: Number of bone metastases per mouse determined by immunohistochemistry 40 days post intracardiac injection of 100,000 PC3-M-Pro4luc cells expressing indicated lentiviral shRNAs. C: Total tumor burden determined by whole body BLI at indicated time points post intracardiac injection of 100,000 PC3-M-Pro4luc cells expressing indicated lentiviral shRNAs. Inset shows tumor burden during the first 20 days. N=number of injected mice. Data are presented as mean ± s.e.m. *p<0.05, **p<0.005.

These in vitro results indicated that enhanced levels of MST1R as observed in prostate cancer cells not only regulate tumor growth but also stimulate cell migration/invasion of prostate cancer cells in extracellular matrix. To study effects on cell migration in vivo, we made use of zebrafish embryo xenografts. Here, a primary tumor is formed at the injection site and subsequent dissemination throughout the embryo is assessed 6 days post-injection. The small size and optical transparency of zebrafish embryos and the use of transgenic strains with a fluorescently marked vasculature allows automated confocal imaging and image analysis to quantify dissemination in large numbers of embryos (21). Injected PC3 cells and PC3 cells expressing con-

trol shRNA disseminated throughout the embryo with multiple tumor cell foci in the tail region (Fig 3A,B). By contrast, in agreement with the observed effect in PC3 migration/invasion in vitro, PC3shMST1R mostly remained close to the area of injection and very few tumor cell foci were observed in the tail. In two independent shMST1R lines, reduced expression of MST1R significantly impaired dissemination in this model (Fig 3A-C). Subsequently, we assessed if MST1R plays a role in later stages of prostate cancer metastasis that involve extravasation and homing and expanding in bone lesions. For this purpose, we silenced MST1R in the PC3-derived PC3-Pro4-luc cells (19) and analyzed stable bulk-selected shMST1R populations that had ~70% reduction in MST1R expression (Fig 4A) in a preclinical mouse model for bone metastasis (19). Following intracardiac injection of control or shMST1R cells whole animal BLI was used to measure outgrowth of metastatic lesions over time and immunohistochemistry of bone sections at the end of the experiment was used to determine the number of metastases. Mice injected with PC3 cells expressing a control shRNA showed on average ~ 2 bone metastases whereas very few metastatic lesions were detected in the bone of mice injected with PC3shMST1R cells (Fig 4B). In agreement, the total metastatic tumor burden determined by BLI was strongly suppressed as a consequence of the reduction in MST1R expression (Fig 4C,D).

In summary, our findings in 3D in vitro and preclinical in vivo models show that MST1R expression in human prostate cancer cells can support local invasion, dissemination, and formation of bone metastases. These results significantly extend earlier findings on the role of MST1R in prostate cancer formation. It has been previously established that MST1R supports prostate tumor growth and angiogenesis and this can involve MST1R expressed on prostate cancer cells as well as MST1R expressed on cells in the tumor microenvironment (13-15). Our current report also implicates MST1R expressed on prostate cancer cells in aspects of prostate cancer metastasis. Altogether, the data from several studies indicate that MST1R represents an attractive potential drug target for molecular targeted therapy.

ACKNOWLEDGEMENTS

This work was supported by grants from EU FP7 (HEALTH-F2-2008-201439) and Dutch Cancer Society (UL-2010-4670). We thank Mr. Hans de Bont for assistance with microscopy and Ms Lizette Haazen for assistance with qPCR.

AUTHOR CONTRIBUTIONS

VPSG, SH, SN, GvdH, and SB designed and performed experiments. GvdP, GJ, BvdW, BES-J, and EHJD analyzed and interpreted data. VPSG and EHJD wrote the manuscript.

CONFLICTS OF INTEREST

The authors declare no conflicts of interest.

REFERENCES

1. Chen Q, Seol DW, Carr B, Zarnegar R. Co-expression and regulation of Met and Ron proto-oncogenes in human hepatocellular carcinoma tissues and cell lines. Hepatology. 1997;26:59-66.

2. Lin HS, Berry GJ, Fee WE, Jr., Terris DJ, Sun Z. Identification of tyrosine kinases overexpressed in head and neck cancer. Archives of otolaryngology--head & neck surgery. 2004;130:311-6.

3. Maggiora P, Lorenzato A, Fracchioli S, Costa B, Castagnaro M, Arisio R, et al. The RON and MET oncogenes are co-expressed in human ovarian carcinomas and cooperate in activating invasiveness. Experimental cell research. 2003;288:382-9.

4. Moser C, Lang SA, Hackl C, Zhang H, Lundgren K, Hong V, et al. Oncogenic MST1R activity in pancreatic and gastric cancer represents a valid target of HSP90 inhibitors. Anticancer research. 2012;32:427-37.

5. Thangasamy A, Rogge J, Ammanamanchi S. Regulation of RON tyrosine kinase-mediated invasion of breast cancer cells. The Journal of biological chemistry. 2008;283:5335-43.

6. Thomas RM, Toney K, Fenoglio-Preiser C, Revelo-Penafiel MP, Hingorani SR, Tuveson DA, et al. The RON receptor tyrosine kinase mediates oncogenic phenotypes in pancreatic cancer cells and is increasingly expressed during pancreatic cancer progression. Cancer research. 2007;67:6075-82.

7. Wang MH, Kurtz AL, Chen Y. Identification of a novel splicing product of the RON receptor tyrosine kinase in human colorectal carcinoma cells. Carcinogenesis. 2000;21:1507-12.

8. Wang MH, Lee W, Luo YL, Weis MT, Yao HP. Altered expression of the RON receptor tyrosine kinase in various epithelial cancers and its contribution to tumorigenic phenotypes in thyroid cancer cells. The Journal of pathology. 2007;213:402-11.

9. Welm AL, Sneddon JB, Taylor C, Nuyten DS, van de Vijver MJ, Hasegawa BH, et al. The macrophage-stimulating protein pathway promotes metastasis in a mouse model for breast cancer and predicts poor prognosis in humans. Proceedings of the National Academy of Sciences of the United States of America. 2007;104:7570-5.

10. Willett CG, Wang MH, Emanuel RL, Graham SA, Smith DI, Shridhar V, et al. Macrophage-stimulating protein and its receptor in non-small-cell lung tumors: induction of receptor tyrosine phosphorylation and cell migration. American journal of respiratory cell and molecular biology. 1998;18:489-96.

11. Zhou D, Pan G, Zheng C, Zheng J, Yian L, Teng X. Expression of the RON receptor tyrosine kinase and its association with gastric carcinoma versus normal gastric tissues. BMC cancer. 2008;8:353.

12. Thobe MN, Gurusamy D, Pathrose P, Waltz SE. The Ron receptor tyrosine kinase positively regulates angiogenic chemokine production in prostate cancer cells. Oncogene. 2010;29:214-26.

13. Thobe MN, Gray JK, Gurusamy D, Paluch AM, Wagh PK, Pathrose P, et al. The Ron receptor promotes prostate tumor growth in the TRAMP mouse model. Oncogene. 2011;30:4990-8.

14. Gurusamy D, Gray JK, Pathrose P, Kulkarni RM, Finkleman FD, Waltz SE. Myeloid-specific expression of Ron receptor kinase promotes prostate tumor growth. Cancer Res. 2013;73:1752-63.

15. Gray JK, Paluch AM, Stuart WD, Waltz SE. Ron receptor overexpression in the murine prostate induces prostate intraepithelial neoplasia. Cancer letters. 2012;314:92-101.

16. Jin JK, Dayyani F, Gallick GE. Steps in prostate cancer progression that lead to bone metastasis. Int J Cancer. 2011;128:2545-61.

17. Kim SJ, Johnson M, Koterba K, Herynk MH, Uehara H, Gallick GE. Reduced c-Met expression by an adenovirus expressing a c-Met ribozyme inhibits tumorigenic growth and lymph node metastases of PC3-LN4 prostate tumor cells in an orthotopic nude mouse model. Clinical cancer research : an official journal of the American Association for Cancer Research. 2003;9:5161-70.

18. Varkaris A, Corn PG, Gaur S, Dayyani F, Logothetis CJ, Gallick GE. The role of HGF/c-Met signaling in prostate cancer progression and c-Met inhibitors in clinical trials. Expert opinion on investigational drugs. 2011;20:1677-84.

19. van den Hoogen C, van der Horst G, Cheung H, Buijs JT, Pelger RC, van der Pluijm G. Integrin alphav expression is required for the acquisition of a metastatic stem/progenitor cell phenotype in human prostate cancer. The American journal of pathology. 2011;179:2559-68.

20. Truong HH, de Sonneville J, Ghotra VP, Xiong J, Price L, Hogendoorn PC, et al. Automated microinjection of cell-polymer suspensions in 3D ECM scaffolds for high-throughput quantitative cancer invasion screens. Biomaterials. 2012;33:181-8.

21. Ghotra VP, He S, de Bont H, van der Ent W, Spaink HP, van de Water B, et al. Automated whole animal bio-imaging assay for human cancer dissemination. PloS one. 2012;7:e31281.

22. Danen EH, Sonneveld P, Brakebusch C, Fassler R, Sonnenberg A. The fibronectin-binding integrins alpha5beta1 and alphavbeta3 differentially modulate RhoA-GTP loading, organization of cell matrix adhesions, and fibronectin fibrillogenesis. J Cell Biol. 2002;159:1071-86.

23. van Weerden WM, de Ridder CM, Verdaasdonk CL, Romijn JC, van der Kwast TH, Schroder FH, et al. Development of seven new human prostate tumor xenograft models and their histopathological characterization. The American journal of pathology. 1996;149:1055-62.

24. Follenzi A, Bakovic S, Gual P, Stella MC, Longati P, Comoglio PM. Cross-talk between the proto-oncogenes Met and Ron. Oncogene. 2000;19:3041-9.

CHAPTER 7

SUMMARY AND DISCUSSION

The complexity of a biological process such as metastasis necessitates that with our current technology discrete steps of the problem are analyzed. We decided to focus our studies on androgen independent prostate cancer (AIPC), which is generally highly aggressive and metastatic. Reliable and well-characterized model systems of prostate cancer progression are of utmost importance to achieve the challenge of finding a cure especially for the AI stage of prostate cancer. The dream of molecular targeted therapies is that some day a patient's own cells will be rapidly tested in vitro with a palette of therapeutic agents to find the one best suited to the patient's specific needs (1). An obvious goal of tissue engineers and cancer modelers is to progress from good models of tissue complexity and function into models that can be standardized for drug screening purposes. In order to effectively hunt for targets in preclinical testing it is necessary to scale the reliable models for medium or high throughput screening (HTS) (1). Because of the technical challenges involved, there are few accomplished metastasis models that have the ability to support HTS (1).

In order to meet this challenge, we worked in the direction of developing new models that recapitulate key steps in the metastatic cascade. We developed a 3D culture and a xenograft model to study growth, invasion and dissemination. First, we developed a three-dimensional collagen matrix based spheroid assay of growth and invasion (*chapter 2*). This assay recapitulates the steps of growth and invasion of tumors at primary or metastatic sites. Collagen type 1 is one of the predominant matrix proteins in the bone, and hence the model provides an ideal environment to study the growth and invasion characteristics of the androgen independent metastatic prostate tumors. Furthermore, we adapted this model in 96 well plates and demonstrated the applicability of this model in high throughput screening platforms. We also applied this method to cell suspensions derived from resection specimens, which opens the possibility to test therapeutic strategies on freshly isolated material from individual patients. So far, sarcoma biopsies were used; it remains to be established whether this will also be successful for carcinomas, including prostate cancer. For the future, we would also like to adapt/expand this assay to study the complex interactions between tumor cells and stromal cells including for instance endothelial cells, which could be achieved by injecting these spheroids together in one matrix. This could provide us novel information regarding the process of tumor induced neoangiogenesis or vasculogenesis, which could be further useful for the development of novel anti-angiogenic therapies against cancer. In addition, we have used PC3 cells to study prostate cancer invasion in this in vitro model. A major challenge will be to modify the culture conditions such that also less aggressive prostate cancer cell lines could be studied in the same system for instance by modification of the ECM environment or inclusion of supportive stromal cells. Ultimately this could provide a 3D in vitro model that mimics more closely prostate cancer in patients.

Secondly, we turned our attention to the zebrafish, which is proving to be an excellent whole animal based model to study tumor development, invasion, and the dynamics of the metastasis cascade. Several research groups have demonstrated successful xenotransplantation of human cancer cells of different origin in zebrafish, and have carried out in vivo assessment of invasiveness, tumor induced angiogenesis (2-6), metastatic behavior (7-10) and response to anticancer therapies (2, 11-14). The small size, transparency and availability of various transgenic fluorescent zebrafish lines prompted us to couple this model to automated confocal imaging and image analysis (*chapter 3*). To the best of our knowledge, this assay represents the first ever semi-automated, quantitative whole organism based bio-imaging assay in a vertebrate that allows

analysis of dissemination of cancer cells in a high throughput manner. Further automation that is developed for the injection of embryos will further develop this pipeline into a fully automated system. With the continued development in the field of imaging technology and availability of novel transgenic zebrafish lines, It will also be extremely interesting to use our assay to xenotransplant cell lines expressing combinations of fluorescent markers allowing quantification of apoptosis, proliferation and dissemination. Furthermore, incorporation of specific transgenic zebrafish lines expressing fluorescently labeled immune cells or tissues into our automated assay will provide us valuable information regarding the tumor cell and microenvironmental interactions. There are also some outstanding questions on the use of zebrafish; what is the predictability of the zebrafish xenograft model for other (rodent) modes; to what extent do effects observed correlate with the effects of compounds seen in man; what is the predictability of the zebrafish with respect to the PK-PD (Pharmacokinetics-Pharmacodynamics) relationships(15)? These questions need to be urgently addressed to warrant use of this model in drug discovery/development pipelines.

In *chapter 5*, we expanded this assay further and xenotransplanted a panel of aggressive (AI) and non-aggressive (AD) prostate cancer cell lines. Prostate cancer cell lines, which are known to be androgen-independent and/or metastatic in mice (LNCaP-derived C4-2 and C4-2B; DU145 and PC3) showed enhanced dissemination in zebrafish embryos as compared to androgen-dependent non-metastatic cells (LNCaP). Our findings show that this assay closely reflects the results obtained in more expensive and much lower throughput assays such as rodent xenografts. Based on these data, zebrafish embryos provide a microenvironment that allows successful engraftment, proliferation and dissemination of AIPC cell lines. Therefore, this assay represents an ideal platform to screen for targets mediating invasion and dissemination of hormone refractory prostate cancer using RNA interference or compound screens.

Current treatment options for prostate cancer are often unsuccessful, and in *chapter 4* we discuss some strategies for improvement. However, there is clear need for new drug targets to widen the possibilities for treatment. Discovery of such new targets has been the major goal of our work. Therefore, we used our experimental models to address the following questions:

- Can we use them to identify critical new targets involved in aspects of prostate cancer metastasis?
- Are these targets validated in other models?
- Are these targets relevant for the human situation?

To answer these questions we devised an adenoviral based RNAi screen for mediators of prostate cancer dissemination using our automated whole animal based zebrafish model of xenotransplantation (*chapter 5*). Based on this screen, we identify SYK as a kinase supporting human prostate cancer dissemination. In line with zebrafish and 3D models, depletion of SYK also led to a strong reduction in metastatic colonization of androgen independent prostate carcinoma cells in a preclinical mouse model for prostate cancer bone metastasis. In the present xenotransplantation models, the study of human material grafted into the mouse has various limitations, including a compromised immune system, differences in species specificity of proteins and an inability to capture early events in tumorigenesis (16). The use of genetically engineered models (GEM) that mimic prostate cancer progression provides a possibility for further validation of candidate targets identified in our screen (17). Thus, a key next step in studying the role of SYK in prostate cancer pro-

gression would be to silence or delete the SYK gene in the TRAMP (transgenic adenocarcinoma mouse prostate) model that recapitulates the pathophysiological features of the prostate cancer progression in humans (18). SYK has been implicated in lymphoid malignancies and appears to play opposing roles in different solid tumors but has not been previously associated with prostate cancer (19). SYK is believed to act as an oncogene because of its ability to increase phosphorylated AKT, which may imply the involvement of PI3K (20, 21), which is a key molecule implicated in migration and chemotaxis of both tumor and endothelial cells (22). Phosphorylation of SYK at Tyr323 forms a docking site for the p85 subunit of PI3K (23). The effect of SYK depletion on PI3K or AKT activity has to be determined but our findings indicate that it is indeed the SYK kinase activity that supports prostate cancer invasion and dissemination: the effect of SYK knockdown on metastatic colonization is reversed by wild type but not kinase dead SYK expression; pharmacological inactivation of SYK using R-406 and BAY-61- 3606 recapitulated the effect of silencing the SYK gene in vitro and in zebrafish model of xenotransplantation.

It will be important to study the effect of SYK inhibition also in the mouse model used by us and other preclinical mouse models mentioned above. We found that SYK regulates surface expression of adhesion receptors at the posttranslational level. This is a potential underlying mechanism for the support of prostate cancer dissemination by SYK: decreased expression of two of these candidate targets of SYK, integrin alpha-2 and CD44 leads to similar defects as depletion of SYK. It has been previously shown that SYK can regulate turnover or transport of adhesion receptors in other cell types (23,24) through a mechanism requiring ITAM-mediated SYK and AKT activation and inducing membrane translocation or stabilization of adhesion receptors. Future experiments should further unravel the mechanism of action of SYK in this respect. SYK acts as an oncogene in lymphomas, chronic leukemias, gastric cancers, and – based on our findings – in prostate cancer. Paradoxically it appears to be a tumor suppressor in breast cancer : downregulation of SYK levels correlate with growth and invasion in the latter case. Importantly, the SYK gene undergoes alternative splicing and the apparent opposite roles of SYK in different cancers may be related to this (25). Most studies have not distinguished between global and splice isoform–specific increases in SYK expression. It is possible that differential expression of SYK (L) and SYK (S) may contribute to these disparate observations in different cancers. It will be important to extend our own studies to identifying which isoforms are expressed and upregulated with progression (25).

Another gene that was identified in the RNAi screen was MST1R. This MET-related receptor tyrosine kinase has been previously implicated in prostate cancer growth and angiogenesis. Its function in prostate cancer growth at least in part can be explained by a need for MST1R in cancer-associated macrophages (26). Nevertheless, two studies indicate that this receptor also plays a role on prostate cancer cells themselves (27, 28). In *chapter 6*, we show that downregulation of MST1R leads to a phenotype that is also observed when MET (the receptor for HGF) is downregulated in different cancer cell types: cells appear less scattered and form epithelial islands. We show for the first time that MET and MST1R both regulate prostate cancer cell invasion/migration in 3D collagen, and MST1R downregulation also inhibits dissemination in the zebrafish model. An increasing number of basic, translational and clinical studies have shown the importance of MET in prostate cancer progression. MET is overexpressed in primary prostate cancers, and its expression is further increased in bone metastases and is associated with the development of castrate-resistant disease. Be-

cause of its importance as a therapeutic target, MET inhibitors have reached clinical trials for advanced, castrate-resistant prostate cancer (29). A robust pipeline of high-quality inhibitors targeting different aspects of MET activation is already being explored in phase II, III clinical trials across multiple tumor types. The best-known example is the ARQ-197, which has already reached the late phase of clinical development in various tumors including prostate cancer (30,31).

In the screen that was the basis for *chapter 5*, two MET shRNAs did not significantly affect PC3 dissemination. Since levels of knockdown were not analyzed in this screen, this does not exclude a role for MET in PC3 dissemination in this model. In fact, based on the literature, effective stable knockdown of MET may well interfere with dissemination similar to silencing of MST1R. Notably, there is also evidence for extensive cross talk between MET and MST1R (32). To test if the attenuated invasion caused by MST1R downregulation was due to inactivation of MET signaling, PC3shMST1R were treated with HGF. The fact that HGF treatment restored invasion of PC3shMST1R cells shows that MET signaling was intact.

In agreement, MST1R silencing did not prevent MET phosphorylation in response to HGF. Whether MST1R and MET signaling act in parallel and HGF-stimulated MET activity compensates for the loss of MST1R, or whether HGF-induced MET activation resulted in transphosphorylation of MST1R in our experiments as reported earlier (33, 34) remains to be established. Importantly, as observed for SYK, MST1R is confirmed in the mouse model as an important player in the later stages of prostate cancer metastasis perhaps playing a role in extravasation or outgrowth in the bone metastatic niche. Moreover, MST1R expression correlates with androgen-independence / metastatic potential in a panel of cell lines indicating that it may serve as another potential target in prostate cancer progression. As discussed above for SYK, further studies in the different prostate cancer mouse models will be required to further implicate MST1R in prostate cancer progression and metastasis. Our current study, in combination with work by others on its role in tumor growth, warrants investment in this direction.

In conclusion, the results from this thesis have contributed small pieces of knowledge to our overall understanding of the problem of prostate cancer metastasis. We have developed novel fluorescence bio-imaging based automated models to screen for novel candidate targets involved in prostate cancer metastasis. Utilizing these models and adopting a functional genomics based approach; we identified SYK as a novel regulator of prostate cancer progression. We also identified functional involvement of MST1R in regulating the progression of prostate cancer. For both of these targets, there is supporting human clinical data to validate our results in prostate cancer. Although much further insight is required in the mechanism of action of these kinases as well as in their RNA expression levels, splicing, protein levels, and activity in human prostate cancers, this is reassuring: it shows that results obtained in these models may be applicable to humans.

REFERENCES

1. Kimlin LC, Casagrande G, Virador VM.In Vitro Three-Dimensional (3D) Models in Cancer Research: An Update Mol Carcinog. 2013 Mar;52(3):167-82

2. Haldi M, Ton C, Seng WL, McGrath P. Human melanoma cells transplanted into zebrafish proliferate, migrate,produce melanin, form masses and stimulate angiogenesis in zebrafish. Angiogenesis. 2006;9:139-51.

3. Nicoli S, Presta M. The zebrafish/tumor xenograft angiogenesis assay. Nature protocols. 2007;2:2918-23.

4. Nicoli S, Ribatti D, Cotelli F, Presta M. Mammalian tumor xenografts induce neovascularization in zebrafish embryos. Cancer research. 2007;67:2927-31.

5. Stoletov K, Montel V, Lester RD, Gonias SL, Klemke R. High-resolution imaging of the dynamic tumor cell vascular interface in transparent zebrafish. Proceedings of the National Academy of Sciences of the United States of America. 2007;104:17406-11.

6. Vlecken DH, Bagowski CP. LIMK1 and LIMK2 are important for metastatic behavior and tumor cell-induced angiogenesis of pancreatic cancer cells. Zebrafish. 2009;6:433-9.

7.Lee LM, Seftor EA, Bonde G, Cornell RA, Hendrix MJ. The fate of human malignant melanoma cells transplanted into zebrafish embryos: assessment of migration and cell division in the absence of tumor formation. Developmental dynamics : an official publication of the American Association of Anatomists.2005;233:1560-70.

8.Marques IJ, Weiss FU, Vlecken DH, Nitsche C, Bakkers J, Lagendijk AK, et al. Metastatic behaviour of primary human tumors in a zebrafish xenotransplantation model. BMC cancer. 2009;9:128.

9. Topczewska JM, Postovit LM, Margaryan NV, Sam A, Hess AR, Wheaton WW, et al. Embryonic and tumorigenic pathways converge via Nodal signaling: role in melanoma aggressiveness. Nature medicine. 2006;12:925-32.

10.Zhao H, Tang C, Cui K, Ang BT, Wong ST. A screening platform for glioma growth and invasion using bio-lumines cence imaging. Laboratory investigation. Journal of neurosurgery. 2009;111:238-46.

11. Corkery DP, Dellaire G, Berman JN. Leukaemia xenotransplantation in zebrafish--chemotherapy response as say in vivo. British journal of haematology. 2011;153:786-9.

12. Geiger GA, Fu W, Kao GD. Temozolomide-mediated radiosensitization of human glioma cells in a zebrafish embryonic system. Cancer research. 2008;68:3396-404.

13. Lally BE, Geiger GA, Kridel S, Arcury-Quandt AE, Robbins ME, Kock ND, et al. Identification and biological evaluation of a novel and potent small molecule radiation sensitizer via an unbiased screen of a chemical library.

14. Lara R, Mauri FA, Taylor H, Derua R, Shia A, Gray C, et al. An siRNA screen identifies RSK1 as a key modula- tor of lung cancer metastasis. Oncogene. 2011;30:3513-21.

15. Zon LI, Peterson RT. In vivo drug discovery in the zebrafish.Nat Rev Drug Discov. 2005 Jan;4(1):35-44.

16. Chauchereau A. Experimental models for the development of new medical treatments in prostate cancer. Eur J Cancer. 2011;47 Suppl 3:S200-14.

17. Pienta KJ, Abate-Shen C, Agus DB, Attar RM, Chung LW, Greenberg NM, et al. The current state of preclinical prostate cancer animal models. The Prostate. 2008;68:629-39.

18. Gingrich JR, Greenberg NM. A transgenic mouse prostate cancer model. Toxicologic pathology. 1996;24:502-4.

19. Coopman PJ, Mueller SC. The Syk tyrosine kinase: a new negative regulator in tumor growth and progression.Cancer letters. 2006;241:159-73.

20. Law CL, Chandran KA, Sidorenko SP, Clark EA. Phospholipase C-gamma1 interacts with conserved phosphoty rosyl residues in the linker region of Syk and is a substrate for Syk. Molecular and cellular biology. 1996;16:1305-15.

21. Moon KD, Post CB, Durden DL, Zhou Q, De P, Harrison ML, et al. Molecular basis for a direct interaction between the Syk protein-tyrosine kinase and phosphoinositide 3-kinase. The Journal of biological chemistry.2005;280:1543-51.

22.Brader S, Eccles SA. Phosphoinositide 3-kinase signalling pathways in tumor progression, invasion and angiogenesis.Tumori. 2004;90:2-8.

23. Fotheringham JA, Coalson NE, Raab-Traub N. Epstein-Barr virus latent membrane protein-2A induces ITAM/ Syk- and Akt-dependent epithelial migration through alphav-integrin membrane translocation. Journal of virology.2012;86:10308-20.

24. Woollard KJ, Fisch C, Newby R, Griffiths HR. C-reactive protein mediates CD11b expression in monocytes through the non-receptor tyrosine kinase, Syk, and calcium mobilization but not through cytosolic peroxides.Inflammation research : official journal of the European Histamine Research Society [et al]. 2005;54:485-92.

25. Prinos P, Garneau D, Lucier JF, Gendron D, Couture S, Boivin M, et al. Alternative splicing of SYK regulates mitosis and cell survival. Nature structural & molecular biology. 2011;18:673-9.

26. Gurusamy D, Gray JK, Pathrose P, Kulkarni RM, Finkleman FD, Waltz SE. Myeloid-specific expression of Ron receptor kinase promotes prostate tumor growth. Cancer research. 2013;73:1752-63.

27. Thobe MN, Gurusamy D, Pathrose P, Waltz SE. The Ron receptor tyrosine kinase positively regulates angiogenic chemokine production in prostate cancer cells. Oncogene. 2010;29:214-26.

28. Thobe MN, Gray JK, Gurusamy D, Paluch AM, Wagh PK, Pathrose P, et al. The Ron receptor promotes pros tate tumor growth in the TRAMP mouse model. Oncogene. 2011;30:4990-8.

29. Varkaris A, Corn PG, Gaur S, Dayyani F, Logothetis CJ, Gallick GE.The role of HGF/c-Met signaling in-prostate cancer progression and c-Met inhibitors in clinical trials. Expert opinion on investigational drugs. 2011;20:1677-84.

30. Sharma N, Adjei AA. In the clinic: ongoing clinical trials evaluating c-MET-inhibiting drugs. Therapeutic advances in medical oncology. 2011;3:S37-50.

31. Gherardi E, Birchmeier W, Birchmeier C, Vande Woude G. Targeting MET in cancer: rationale and progress.Nature reviews Cancer. 2012;12:89-103.

32. Wagh PK, Peace BE, Waltz SE. Met-related receptor tyrosine kinase Ron in tumor growth and metastasis. Advances in cancer research. 2008;100:1-33.

33. Benvenuti S, Lazzari L, Arnesano A, Li Chiavi G, Gentile A, Comoglio PM. Ron kinase transphosphorylation sustains MET oncogene addiction. Cancer research. 2011;71:1945-55.

34. Follenzi A, Bakovic S, Gual P, Stella MC, Longati P, Comoglio PM. Cross-talk between the proto-oncogenes Met and Ron. Oncogene. 2000;19:3041-9.

NEDERLANDSE SAMENVATTING

Metastasering is een complex biologisch proces, dat stapsgewijs geanalyseerd moet worden met behulp van de huidige technologie. We hebben besloten om onze studies te richten op androgeen-onafhankelijke (AI) prostaatkanker, die over het algemeen zeer agressief is. Een betrouwbaar en goed gekarakteriseerd modelsysteem van prostaatkanker progressie is van groot belang om een behandeling voor de androgeen-onafhankelijk staat te ontwikkelen. Om effectief nieuwe geneesmiddelen te maken, is het nodig om betrouwbare modellen op te schalen voor medium of high throughput screening (HTS). Gezien de technische uitdagingen zijn er weinig modellen die de mogelijkheid voor HTS ondersteunen.

Om deze uitdaging aan te gaan , hebben wij gewerkt aan het ontwikkelen van nieuwe modellen die de belangrijkste stappen in de progressie van kanker recapituleren. We hebben 3D sferoïde en een xenograft-model ontwikkeld om groei , invasie en disseminatie van kanker cellen te bestuderen. Eerst hebben wij een 3D collageen matrix sferoïde assay van groei en invasie ontwikkeld (*hoofdstuk 2*). Deze test recapituleert de stappen van groei en invasie van tumoren op de primaire of metastatische sites. Collageen type 1 is een van de belangrijkste extracellulaire matrix (ECM) eiwitten in het bot , en is een ideale omgeving om de groei en invasie kenmerken van de androgeen-onafhankelijke metastaserende prostaatkanker te bestuderen. Dit model hebben wij toegepast in 96 wells platen waardoor het toepasbaar is voor high throughput screening. Vervolgens is dit model toegepast voor celsuspensies verkregen uit resectiepreparaten. Het laatste opent de mogelijkheid om therapeutische strategieën op vers geïsoleerde materiaal van individuele patiënten te testen . Tot zover werden sarcoom biopten gebruikt , het is nog onbekend of deze ook succesvol zijn voor carcinomen, waaronder prostaatkanker. Voor de toekomst zouden wij graag deze assay willen uitbreiden/ toepassen om complexe interacties tussen tumorcellen en stromale cellen te bestuderen, bijvoorbeeld door injectie van combinaties van kanker -, endotheel, fibroblastcellen. Dit zou ons nieuwe informatie kunnen opleveren over het proces van tumor geïnduceerde neo-angiogenese of vasculogenese, dit kan vervolgens weer van belang zijn voor de ontwikkeling van nieuwe anti - angiogene therapieën tegen kanker. Wij hebben vooral gebruik gemaakt van PC3 cellen om prostaatkanker invasie in het in-vitro model te bestuderen. Een grote uitdaging zal zijn om de kweekomstandigheden zodanig aan te passen dat ook minder agressieve prostaatkanker cellijnen kunnen worden bestudeerd in hetzelfde systeem, bijvoorbeeld door wijziging van de ECM omgeving.

Ten tweede, richtten wij onze aandacht op de zebravis. Deze blijkt een goed diermodel te zijn om de ontwikkeling van tumoren, de invasie, en de dynamiek van de metastaseringscascade te bestuderen. Verschillende onderzoeksgroepen hebben succesvol xenotransplantatie van menselijke kankercellen van verschillende oorsprongen in de zebravis uitgevoerd om deze processen te bestuderen zoals invasie; tumor geïn-

duceerde angiogenese, experimentele metastasering en de respons op anti-kanker therapieën. Het kleine formaat, transparantie en de beschikbaarheid van verschillende transgene zebravis fluorescerende lijnen hebben geleid tot koppeling van dit model aan geautomatiseerde confocale beeldvorming en beeldanalyse (*hoofdstuk 3*). Tot zo ver bekend, is dit de eerste semiautomatische bio-imaging assay gebaseerd op het hele organisme dat de analyse van de disseminatie van kankercellen in een high throughput manier mogelijk maakt. De volgende stap is de ontwikkeling van geautomatiseerde injectie van de cellen in het embryo zodat het een volledig geautomatiseerd systeem wordt. Door de voortdurende ontwikkeling op het gebied van imaging technologie en de beschikbaarheid van nieuwe transgene zebravis lijnen, zal het ook zeer interessant zijn om onze test te gebruiken voor kankercellijnen waarin combinaties van fluorescente markers worden gebruikt in kwantificering van apoptose, proliferatie en disseminatie. In onze assay kunnen ook specifieke transgene zebravis lijnen gebruikt worden die fluorescent gelabelde immuuncellen of andere celtypen bevatten. Dit zal ons waardevolle informatie over de tumorcel en de micro-omgeving interacties opleveren. Er zijn enkele belangrijke openstaande vragen over het gebruik van de zebravis: wat is de voorspelbaarheid van het model voor gedrag in zoogdiermodellen; in welke mate correleren de effecten met de effecten in de mens; wat is de voorspelbaarheid van de zebravis met betrekking tot de PK - PD (Farmacokinetiek - Farmacodynamiek) relaties ? Deze vragen moeten dringend worden beantwoordt om de inzetbaarheid van dit geautomatiseerde in vivo model in de geneesmiddelindustrie te realiseren.

In *hoofdstuk 5*, is het zebravis xenotransplantatie model toegepast op een een panel van agressieve (AI) en minder agressieve (androgeen afhankelijk; AD) prostaatkanker cellijnen. AI cellen toonden meer verspreiding in zebravis embryo's ten opzichte van AD cellen (LNCaP). Onze bevindingen tonen aan dat deze assay correleert met de resultaten van duurdere en low throughput assays zoals muismodellen. Op basis van deze gegevens, kunnen wij concluderen dat zebravis embryo's een passende omgeving leveren voor de succesvolle implantatie, proliferatie en verspreiding van AI cellijnen. Daarom representeert deze test een ideaal platform voor het screenen van genen die zijn betrokken bij de invasie en disseminatie van AI prostaat kanker met behulp van RNA interferentie. Huidige behandelingsopties voor prostaatkanker zijn vaak niet succesvol en in *hoofdstuk 4* bespreken we een aantal huidige strategieën voor verbetering. Echter, er is duidelijk behoefte aan nieuwe drug targets om de mogelijkheden voor behandeling te verruimen.

De ontwikkelde experimentele modellen zijn dan ook gebruikt om de volgende vragen te beantwoorden :

- Kunnen wij onze modellen gebruiken om kritische targets te identificeren en valideren die betrokken zijn bij prostaatkanker metastasering?
- Kunnen we deze targets valideren in andere modellen?
- Zijn deze targets relevant voor de menselijke situatie?

Om deze vragen te beantwoorden hebben wij een adenovirale RNAi screen uitgevoerd in het zebravis xenotransplantatie model om nieuwe targets voor prostaat kanker progressie te identificeren en valideren (*hoofdstuk 5*). Op basis van deze screen hebben wij het SYK kinase geïdentificeerd die betrokken is bij disseminatie van de AI prostaatkankercellen. In lijn met de zebravis en 3D modellen leidt downregulatie van SYK ook tot een sterke vermindering van metastatische kolonisatie in een preklinisch muismodel voor prostaatkanker bot metastasering. Dit model heeft belemmeringen zoals een gecomprimeerd immuunsys-

teem, mogelijke effecten van muis-humaan combinatie, en het onvermogen om de eerste stappen van tumorgroei, invasie, en disseminatie te bestuderen. Het gebruik van genetisch gemanipuleerde modellen (GEM) die de progressie van prostaatkanker recapituleert biedt de mogelijkheid voor verdere validatie van de kandidaat- targetgenen geïdentificeerd in onze screen. De volgende stap is bijvoorbeeld om de rol van SYK in prostaatkanker progressie te bestuderen door het SYK gen uit te schakelen in het TRAMP model dat de pathofysiologische kenmerken bij het vorderen van prostaatkanker in de mens recapituleert . De betrokkenheid van SYK is al aangetoond bij lymfoïde maligniteiten en lijkt tegengestelde rollen te spelen in verschillende solide tumoren. Tot zover bekend is, is SYK niet eerder verbonden aan prostaatkanker.

Het effect van SYK depletie op bekende downstream targets als PI3K of AKT activiteit moet worden bepaald. Maar uit onze bevindingen blijkt wel al dat SYK kinase activiteit de prostaatkanker invasie, dissemination en metastatische kolonisatie ondersteunt : Het effect van SYK downregulatie op metastatische kolonisatie wordt teniet gedaan door expressie van wild type SYK maar niet door een “kinase-dode” mutant. Inderdaad, recapituleert farmacologische remming van SYK activiteit met R-406 en BAY-61-3606 het effect van de SYK downregulatie in vitro en in het zebravis xenotransplantatie model. Het zal belangrijk zijn om het effect van farmacologische remming van SYK activiteit ook te bestuderen in het muismodel zoals gebruikt door ons en de andere bovengenoemde preklinische muismodellen. Verder hebben wij ook gevonden dat SYK de oppervlakte-expressie van adhesie receptoren, zoals CD44 en α2β1 integrine reguleert op het post translationele niveau. Dit zou een mogelijk onderliggende mechanisme zijn voor de rol van SYK in de disseminatie van prostaatkanker. siRNA downregulatie van het integrine of CD44 leidt eveneens tot verminderde invasie of bot kolonisatie. Het is eerder aangetoond in andere celtypen dat SYK het transport en stabilisatie van adhesie receptoren door ITAM - gemedieerde SYK en AKT activatie- reguleert. Toekomstige experimenten moeten verder het mechanisme van de werking van SYK ontrafelen. SYK fungeert in prostaatkanker mogelijk als een oncogen, net als bij verschillende andere maligniteiten zoals lymfomen, chronische leukemie en maagkanker. In tegenstelling lijkt SYK op een tumor suppressor in borstkanker, waar downregulatie van SYK is gecorreleerd met groei en invasie. Belangrijk zou kunnen zijn dat het SYK gen alternatieve splicing ondergaat. De meeste studies hebben geen onderscheid gemaakt tussen globale en splice-specifieke SYK expressie. Het is mogelijk dat differentiële expressie van SYK(L) en SYK(S) de zo verschillende functies in verschillende vormen van kanker verklaart. Het zal belangrijk zijn om onze eigen studies uit te breiden met de identificatie van de SYK isovormen.

Een ander gen dat wij hebben geïdentificeerd in onze screen is MST1R. Deze MET- gerelateerde receptor tyrosine kinase is al eerder aangetoond voor betrokkenheid bij groei en tumor geïnduceerd angiogenese bij prostaatkanker. De functie van MST1R in groei van prostaat tumor kan onder andere ondersteunt worden door MST1R in kanker - geassocieerde macrofagen. Twee studies laten zien dat deze receptor ook een rol speelt in de prostaatkankercellen. In *hoofdstuk 6* laten wij zien dat downregulatie van MST1R leidt tot een fenotype dat ook wordt waargenomen wanneer MET (de receptor voor HGF) down gereguleerd wordt in verschillende typen kankercellen. Cellen lijken minder verspreid en vormen epitheliale eilanden. Deze rol voor MST1R in invasie en migratie van prostaatkanker cellen is nieuw. Naast migratie in 3D collageen matrix bevordert MST1R de disseminatie van prostaatkanker cellen in het zebravis embryo xenotransplantatie model en in de muis xenograft. Fundamenteel, translationeel en klinisch onderzoek heeft het belang van

MET aangetoond bij prostaatkanker progressie. MET komt verhoogd voor bij primaire prostaatkanker, en de MET expressie wordt verder verhoogd in bot metastasen en wordt geassocieerd met de ontwikkeling van castratie resistente prostaatkanker. Vanwege het therapeutische belang, werden MET remmers al gebruikt in klinische studies voor behandeling van geavanceerde castratie-resistente prostaatkanker. Een robuuste pijplijn van MET inhibitoren gericht op verschillende aspecten van de MET activering wordt al onderzocht in fase II en fase III klinische studies. Het bekendste voorbeeld is de ARQ-197, dat reeds de late fase van klinische ontwikkeling in verschillende tumoren heeft bereikt, waaronder prostaatkanker. Overigens bevatte de in hoofdstuk 5 beschreven screen twee MET shRNAs. Die vertoonden geen significant effect op de dissseminatie van de PC3 cellen. Aangezien het niveau van knockdown niet is geanalyseerd in de screen kunnen we over de “non-hits” geen uitspraak doen en betekent dit zeker niet dat een rol voor MET is uitgesloten in de disseminatie van de PC3 cellen in dit model. In feite zou gebaseerd op de literatuur, effectieve stabiele knockdown van MET een hetzelfde effect moeten hebben op disseminatie van prostaatkanker cellen als de MST1R knockdown. Er is ook bewijs voor een functionele interactie tussen MET en MST1R. Ons onderzoek wijst er tot dusver niet op dat MST1R downregulatie een effect op MET signalering heeft maar in het licht van de beschreven cross-fosforylatie zou dit zou verder onderzocht kunnen worden. Belangrijk is dat MST1R, net als SYK, wordt bevestigd in het muismodel. Bovendien laten AI lijnen een hogere expressie zien van MST1R. Zoals hierboven genoemd voor SYK, zullen verdere studies in de verschillende prostaatkanker muismodellen van belang zijn om MST1R te betrekken bij prostaatkanker progressie. Onze huidige studie waarin MST1R in migratie, invasie van prostaatkanker cellen wordt geïmpliceerd is een eerste stap in deze richting.

Tot slot hebben de resultaten van dit proefschrift bijgedragen aan ons algemeen begrip van het probleem van prostaatkanker metastase. We hebben nieuwe op fluorescentie bio-imaging gebaseerde geautomatiseerde modellen ontwikkeld om te detecteren welke kandidaat genen betrokken zijn bij prostaatkanker metastasering. Gebruikmakend van deze modellen konden we SYK en MST1R identificeren als nieuwe regulatoren van prostaatkanker progressie. Voor beide potentiele drug-targets hebben we een eerste stap gezet voor validatie in humane prostaatkanker. Hoewel dit sterk moet worden uitgebreid en verder onderzoek nodig is naar hun werkingsmechanisme en regulatie van RNA expressie/ splicing/ eiwit niveaus, zijn de resultaten bemoedigend dat het mogelijk targets zijn met klinische relevantie.

ABBREVIATIONS

AR	Androgen receptor
DHT	Dihydrotestosterone
PSA	Prostate specific antigen
AIPC	Androgen independent prostate cancer
3D	Three dimensional
CS	Cell spheroids
ECM	Extracellular matrix
2D	Two dimensional
ZF	Zebrafish
MCD	Mean cumulative distance
RT	Radiotherapy

LIST OF PUBLICATIONS

Ghotra VPS, Puigvert JC, Danen EH.The cancer stem cell microenvironment and anti-cancer therapy. Int J Radiat Biol. 2009 Nov;85(11):955-62.

Le Devedec SE, Yan K, de Bont H, **Ghotra VPS**, Truong H, Danen EH, Verbeek F, Van de Water B .System microscopy approaches to understand cancer cell migration and metastasis. Cell Mol Life Sci. 2010 Oct; 67(19) : 3219-40.

Truong H, de Sonneville J, **Ghotra VPS**, Xiong J, Price L, Hogendoorn PC, Spaink HH, Van de Water B, Danen EH. Automated microinjection of cell-polymer suspensions in 3D ECM scaffolds for high-throughput quantitative cancer invasion screens. Biomaterials. 2012 Jan; 33(1) : 181-8.

Ghotra VPS, He S, De Bont H, Van der Ent W, Spaink HP, Van de Water B, Snaar-Jagalska BE, Danen EH. Automated whole animal bio-imaging assay for human cancer dissemination. PLoS One. 2012;7(2):e31281.

He S, Lamers GE, Beenakker JW, Cui C, **Ghotra VPS**, Danen EH, Meijer AH, Spaink HP, Snaar-Jagalska BE. Neutrophil-mediated experimental metastasis is enhanced by VEGFR inhibition in a zebrafish xenograft model. J Pathol. 2012 Aug; 227(4): 431-45

Ghotra VPS, Geldof AA, Danen EH.Targeted radiosensitization in prostate cancer. Curr Pharm Des. 2013;19(15):2819-28.

Truong H, Xiong J, **Ghotra VPS**, Nirmala E, Haazen L, Le Devedec S, He S, Snaar-Jagalska E, Amiet A, Vreugdenhil E, Meerman JH, Van de Water B, Danen EH. Integrin regulation of TGF beta/miR200/ZEB signaling network controls breast cancer migration strategy and metastasis. *Submitted*

Ghotra VPS, He S, Van der horst G, Nijhoff S, de Bont H, Lekkerkerker A, Janssen R, Jenster G, Leenders G.J.H.L. van, Hoogland AM, Baranski Z, Van de water B, Van der Pluijm G,Snaar-Jagalska BE, Danen EH. siRNA screen identifies SYK as a candidate player in prostate cancer progression. *Submitted*

Ghotra VPS, He S, Van der horst G, Nijhoff S, de Bont H, Baranski Z, Jenster G, Van de water B, Van der Pluijm G,Snaar-Jagalska BE, Danen EH. MST1R supports prostate cancer invasion, dissemination, and formation of bone metastases. *Submitted*

CURRICULUM VITAE

Veerander PS Ghotra was born on December 12,1979 in Mukerian, India. After completing the pre-university education, he started his bachelor studies in medicine and surgery at the government medical college Patiala (India) in 1998, from which he graduated in 2004. In 2006 he began a research master in oncology offered by the Vrije University in Amsterdam. This master program exposed him to the exciting challenges in the field of oncological research. To gain further expertise in this area, he started his PhD studies in the division of toxicology in 2008 under supervision of Dr. Erik Danen. The aim of his project described in this thesis, was to develop novel models to study tumor progression and to identify novel candidate metastasis genes that could serve as novel potential drug targets for treatment of prostate cancer. Veerander is highly interested in understanding the dynamics of the prostate cancer metastatic cascade, ranging from local invasion to metastatic colonization. Since September 2012, he is doing Master in medicine at the university of Maastricht. His ambition is to become an expert in the field of urological oncology, and to translate scientific knowledge for the benefit of prostate cancer patients.